# Self-Assembly of Colloidal Spheres into One, Two, and Three Dimensional Structures

Utrecht University

Cover design: Yong Guo

Printed by: ProefschriftMaken | Proefschriftmaken.nl

ISBN: 978-94-629-5697-1

# Self-Assembly of Colloidal Spheres into One, Two, and Three Dimensional Structures

Zelf-assemblage van Één-, Twee- en Driedimensionale Structuren uit Colloïdale Bollen

(met een samenvatting in het Nederlands)

## Proefschrift

ter verkrijging van de graad van doctor aan de
Universiteit Utrecht op gezag van de rector magnificus,
prof. dr. G.J. van der Zwaan, ingevolge het besluit van het
college voor promoties in het openbaar te verdedigen
op woensdag 27 september 2017 des middags te 2.30 uur

door

**Yong Guo**

geboren op 6 april 1987 te Zhejiang Province, China

**Promotor:** Prof. dr. W. K. Kegel

The research described in this thesis was financially supported by the China Scholarship Council (CSC) under project number of 201306200056.

# Contents

Chapter 1

# Introduction

## 1.1 Colloids

Colloidal particles are objects with at least one dimension in the order of 1 nm to 1000 nm and that are dispersed in a continuous medium [1, 2]. The most important consideration behind this definition is that these particles are much larger than the surrounding medium molecules while much smaller compare to macroscopic objects. Therefore, the colloidal world exists in between the microscopic (atoms and molecules) and macroscopic world (visible with naked eye). Colloidal systems are ubiquitous in our daily life, examples are fog (water droplets dispersed in air), milk (a dispersion of fine droplets of fat in an aqueous phase), and paints (fine solid particles dispersed in a liquid medium).

The unique dimensions of colloids (1 nm to 1000 nm, especially with size larger than hundred nm), on the one hand, allow them to be visualized and studied *in situ* by microscopy, such as electron microscopy and optical microscopy; on the other hand, they still display thermal motion like atoms or molecules, so called Brownian motion [1, 2]. Consequently, colloids can serve as excellent models to study the phase and crystallization behaviors of their atomic and molecular counterparts [3–7].

Besides model systems for atoms or molecules, colloids can also act as the building blocks to assemble into sophisticated functional super-structures that have no molecular analog and have great potential applications in the areas of photonics, plasmonics, sensing, catalysis and solar cells [8–15].

## 1.2 Colloidal synthesis

The extensive applications of colloids as model systems for atoms or molecules and as building blocks for assembling into super-structures stimulate the development of new approaches for preparing colloids [16–20]. Herein, we will briefly introduce two methods that are commonly used to prepare monodisperse polymer colloids, namely emulsion polymerization and dispersion polymerization. We will mainly focus on the regulation of the size, shape, surface charge and functionalities of the polymer colloids because the control over these parameters is crucial to better implement and even broaden the potential applications of the polymer colloids. For example, by introducing shape anisotropicity, virus-like microcapsules can be spontaneously assembled [21].

Emulsion polymerization is a type of radical polymerization and its initial mixture is inhomogeneous. The mixture typically consists of water as the continuous phase, hydrophobic monomer droplets stabilized by surfactant, and monomer-swollen micelles. A characteristic of emulsion polymerization is that the polymerization takes place in monomer-swollen micelles [22, 23]. After polymerization, the monomer-swollen micelles turn into polymer particles. The polymer particles continue to grow by polymerizing the monomers that diffuse from the oil droplets across the continuous phase into the particles.

In contrast to emulsion polymerization, the initial mixture for a dispersion polymerization is a homogeneous solution of monomer, initiator and stabilizer in a solvent, typically aqueous alcohol mixtures. Upon initiating the polymerization, polymers start to grow in the continuous phase. Once they reach a critical molecular weight the polymers are no longer soluble and precipitate out of the solution. Subsequently, these precipitated polymers form particle nuclei *via* aggregating with other polymers and stabilized by attachment of stabilizers present in the reaction mixtures. After nucleation, both monomers and stabilizers are transferred to the primary particles until maximum conversion and hence particle sizes are reached [24–26].

An important difference between emulsion polymerization and dispersion polymerization is that emulsion polymerization can be easily extended to synthesize cross-linked spherical particles while that is problematic in dispersion polymerization (**Chapter 2**). However, both methods allow to prepare 'clean' particles, i.e., emulsifier-free or stabilizer-free particles (**Chapter 5**). The 'clean' particles are required in some

applications where the presence of emulsifiers or stabilizers is not desired [21, 27].

By using emulsion polymerization, particles with sizes in the range of several tens of nanometers to several hundreds of nanometers can be synthesized. While dispersion polymerization allows for the preparation of particles in the micrometers size regime. For both polymerization method, the dimensions of the particles are readily tunable with monomer concentration, type and concentration of initiator and stabilizer/emulsifier, reaction temperature and solvent [16, 25, 26]. Therefore, particles with sizes range from several ten nanometers up to several ten micrometers can be easily obtained by appropriately choosing the polymerization method and tuning the experimental conditions.

Spherical particles are typically formed after polymerization due to the minimization of the surface energy. However, non-spherical particles can also be synthesized under some conditions. One method is the asymmetrical shrinkage of surface layer by increasing the cross-linking density of the surface layer. For example, by the delayed addition of cross-linker, the shell of the growing particles is cross-linked. When the cross-linked shell thickness over the particle radius is sufficient small, buckling is generated, eventually dimple particles are formed *via* either emulsion polymerization [28, 29] or dispersion polymerization (**Chapter 2**) [30, 31]. Another method relies on the internal phase separation of a monomer-swollen, cross-linked polymer particle. Upon swelling of the cross-linked seed particles with monomer, an elastic stress is induced. This elastic stress can be released by heating, which results in a contraction of the polymer network, finally leads to the formation of a liquid monomer protrusion on the particle. Subsequent polymerization of the protrusion allows for the preparation of dumbbell particles as well as Mickey Mouse shaped particles [32–35]. Furthermore, hollow and yolk-shell particles can be prepared by etching the partially cross-linked particles.

Particle charge not only is vital for particles stabilization, but also plays a significant role in particles aggregation behavior (**Chapter 3 and 5**). In the framework of DLVO theory, the total interactions between particles are the result of attractive van der Waals interaction and repulsive electrostatic interaction [2]. The repulsive electrostatic interaction is an important stabilizing mechanism for particles and it is determined by the surface charge density of the particles as well as the ionic strength in the solvent. Introduction of charge on the particles can be achieved by employing charged

initiator [36, 37], functional monomer [38, 39] and emulsifier [40] or stabilizer [41], therefore negatively charged, positively charged and even amphoteric particles can be synthesized by the selection of suitable aforementioned ingredients. Recently, van Ravensteijn et al. [42] reported a robust way to continuously tune the particle surface charge, which is achieved by introducing positive charges *via* the Menschutkin reaction of tertiary amine with chlorine groups on the negatively charged particles. Another way to introduce or tune the surface charges is by adsorption of polyelectrolytes [43].

Surface functionality is another key parameter that enable to widen the potential applications of colloids. Functional groups can be introduced on the colloids by either polymerizing functional co-monomers together with monomer or using initiators bearing functional groups (**Chapter 2**) [42, 44]. The incorporated functional groups provide a chemical handle for further surface modification. For example, chlorinated particles can be synthesized by copolymerizing of vinylbenzyl chloride with styrene *via* emulsion polymerization, and the surface chlorine groups on these particles can serve as an initiator to graft a polymer layer *via* an atom transfer radical polymerization reaction (**Chapter 4**). Therefore, the hydrophobicity and the charge density of particles can be easily tuned *via* chemical modification of functional groups decorated particles. Furthermore, the presence of functional groups on the particles also makes it possible for the immobilization of assembled super-structures.

## 1.3 Colloidal (self-)assembly

Self-assembly is a spontaneous process in which a disordered system of pre-existing building blocks forms an ordered structure without human intervention. It is ubiquitous in nature and can take place on all length scales, from the atomistic to the macroscopic world. Examples include the formation of virus capsids from proteins, lipid bilayers from phospholipids, and the collective motion of flocks of birds. In the above examples, the building blocks are proteins, phospholipids and birds, respectively.

Colloidal (self-)assembly has been gaining increasing attention in recent years [12, 45–49]. On the one hand, colloidal particles are excellent model systems to mimic the atomic/molecular world owing to the similarities to the atomic/molecular systems. For example, self-assembly of colloidal spheres provides valuable insight into the phase transition behavior of atoms and molecules [3, 4]. On the other hand,

colloidal (self-)assembly is a versatile and powerful strategy to construct sophisticated functional materials, which have great potential applications in the areas of materials science, sensing and biomedical engineering [50–53]. For instance, two-dimensional photonic crystals for molecular recognition and chemical sensing applications have been developed by the self-assembly of particle monolayers on the substrate and subsequent post-treatment [11].

The successful assembly of colloids into desired structures depends on many parameters, such as the particles shapes, compositions, surface functionalities, sizes and polydispersity; the ability to balance the attractive and repulsive interactions between particles and their surroundings. By carefully taking these parameters into account, a large number of strategies have been developed to assemble colloids into desired structures [12, 13, 19, 49, 54–59]. The widely employed assembly approaches include external force driven assembly (gravitational [4], electric [60], magnetic [61], optical [62] and shear [63] force), interfacial force driven assembly (horizontal deposition [64], vertical deposition [65] and liquid interface mediated [66]), physical confinement assembly (patterned surface [67], Langmuir-Blodgett trough [68] and emulsion [69]), template assisted assembly (layer-by-layer [70], copolymer matrix [71], surfactant [72] and liquid crystal [73]), de-stabilization induced assembly (introduction of depletion attraction [74] and reduction of electrostatic repulsion [75]), and anisotropic re-arrangement of the surface layer [76, 77].

The scope of colloidal (self-)assembly has been broadened in recent years, a variety of super-structures have been developed through (self-)assembly of colloids with various interactions and shapes by the aforementioned approaches, such as colloidal molecules [78], raspberry-like clusters [79], one-dimensional [80, 81], two-dimensional [82, 83] and three-dimensional [84, 85] colloidal crystals. The final structure of the assembly is mainly governed by the shape of the colloids and the interparticle interactions. For example, colloidal spheres with hard interactions, i.e. no attraction between the particles, can self-assemble into hexagonal crystal, while colloidal rods and platelets can self-assemble into liquid crystal, such as nematic phase and smectic phase [86].

In this thesis, we are trying to gain more insight into self-assembly mechanisms and develop new strategies to assemble spherical polymer colloids into super-structures, such as one, two and three dimensional assemblies.

## 1.4 Scope of this thesis

The work presented here focuses on the synthesis of anisotropic colloids and the self-assembly of spherical colloids.

In **Chapter 2**, we show that dimple particles with a single cavity can be synthesized by a one-pot dispersion polymerization method which involves the delayed addition of cross-linker into a reaction mixture. The size of the formed cavity can be tuned either by the delay time after which cross-linker is added, or by the concentration of the cross-linker. Furthermore, this method can be extended to synthesize functional dimple particles by introducing co-monomers during the delayed addition step. Interestingly, hollow dumbbell particles can be synthesized by using the dimple particles as the seeds and these hollow dumbbell particles align perpendicular to the applied AC electric field with their solid parts in closest contact.

In **Chapter 3**, we report the spontaneous formation of one-dimensional aggregates of aqueous dispersions of spherical colloidal particles. The one-dimensional aggregates resemble a so-called Bernal spiral. A Bernal spiral consists of three twisting strands of particles and each particle is in contact with six neighboring particles. The observations can be explained by a combination of short-range hydrophobic attraction and relatively longer-range electrostatic repulsion.

In **Chapter 4**, we describe a facile method to prepare two-dimensional free-floating colloidal crystal monolayers (CCM) from isotropic colloids as well as from anisotropic colloids. The influence of the experimental conditions on the CCM formation is systematically studied. A possible mechanism of the CCM formation is proposed, which is similar to the mechanism of the vertical deposition involving the deformation of the interface and the generation of capillary attraction. A unique feature of this method is that the prepared CCM can freely float in the dispersion, which is achieved by using an appropriate extracting solvent that can release the formed CCM from the wall into the continuous phase.

In **Chapter 5**, we present an example of pH reversible three-dimensional assembly (encapsulation) of oppositely charged colloids with a vast size difference. The assembly process is regulated by pH responsive polyelectrolytes present in solution. The influence of these polyelectrolytes on the encapsulation behavior with respect to the coverage, the pH-dependence and the reversibility is systematically investigated.

# Bibliography

[1] R. J. Hunter. *Foundations of colloid science, 2nd ed.* Oxford University Press, Oxford, 2001.

[2] D. H. Everett. *Basic principles of colloid science.* Royal Society of Chemistry, 1988.

[3] V. J. Anderson and H. N. W. Lekkerkerker. Insights into phase transition kinetics from colloid science. *Nature*, 416:811–815, 2002.

[4] P. N. Pusey and W. van Megen. Phase behaviour of concentrated suspensions of nearly hard colloidal spheres. *Nature*, 320:340–342, 1986.

[5] P. Schall, I. Cohen, D. A. Weitz, and F. Spaepen. Visualizing dislocation nucleation by indenting colloidal crystals. *Nature*, 440:319–323, 2006.

[6] A. Yethiraj and A. van Blaaderen. A colloidal model system with an interaction tunable from hard sphere to soft and dipolar. *Nature*, 421:513–517, 2003.

[7] K. N. Pham, A. M. Puertas, J. Bergenholtz, S. U. Egelhaaf, A. Moussaïd, P. N. Pusey, A. B. Schofield, M. E. Cates, M. Fuchs, and W. C. K. Poon. Multiple glassy states in a simple model system. *Science*, 296:104–106, 2002.

[8] H. Gao, W. Zhou, and T. W. Odom. Plasmonic crystals: a platform to catalog resonances from ultraviolet to near-infrared wavelengths in a plasmonic library. *Advanced Functional Materials*, 20:529–539, 2010.

[9] S. C. Yang, D. J. Yang, J. Kim, J. M. Hong, H. G. Kim, I. D. Kim, and H. Lee. Hollow $TiO_2$ hemispheres obtained by colloidal templating for application in dye-sensitized solar cells. *Advanced Materials*, 20:1059–1064, 2008.

[10] Z. Zhang, C. Geng, Z. Hao, T. Wei, and Q. Yan. Recent advancement on micro-/nano-spherical lens photolithography based on monolayer colloidal crystals. *Advances in Colloid and Interface Science*, 228:105–122, 2016.

[11] J.-T. Zhang, L. Wang, J. Luo, A. Tikhonov, N. Kornienko, and S. A. Asher. 2-D array photonic crystal sensing motif. *Journal of the American Chemical Society*, 133:9152–9155, 2011.

[12] F. Li, D. P. Josephson, and A. Stein. Colloidal assembly: the road from particles to colloidal molecules and crystals. *Angewandte Chemie International Edition*, 50:360–388, 2011.

[13] L. Xu, W. Ma, L. Wang, C. Xu, H. Kuang, and N. A. Kotov. Nanoparticle assemblies: dimensional transformation of nanomaterials and scalability. *Chemical Society Reviews*, 42:3114–3126, 2013.

[14] X. Ye and L. Qi. Two-dimensionally patterned nanostructures based on monolayer colloidal crystals: controllable fabrication, assembly, and applications. *Nano Today*, 6:608–631, 2011.

[15] S. Glotzer and M. Solomon. Anisotropy of building blocks and their assembly into complex structures. *Nature Materials*, 6:557–562, 2007.

[16] R. Arshady. Suspension, emulsion, and dispersion polymerization: a methodological survey. *Colloid and Polymer Science*, 270:717–732, 1992.

[17] M. Okubo. *Polymer particles*. Springer Berlin Heidelberg, 2005.

[18] M. Niederberger. Nonaqueous solgel routes to metal oxide nanoparticles. *Accounts of Chemical Research*, 40:793–800, 2007.

[19] E. Duguet, A. Desert, A. Perro, and S. Ravaine. Design and elaboration of colloidal molecules: an overview. *Chemical Society Reviews*, 40:941–960, 2011.

[20] J. Hu, S. Zhou, Y. Sun, X. Fang, and L. Wu. Fabrication, properties and applications of janus particles. *Chemical Society Reviews*, 41:4356–4378, 2012.

[21] C. H. J. Evers, J. A. Luiken, P. G. Bolhuis, and W. K. Kegel. Self-assembly of microcapsules *via* colloidal bond hybridization and anisotropy. *Nature*, 534:364–368, 2016.

[22] W. D. Harkins. A general theory of the mechanism of emulsion polymerization1. *Journal of the American Chemical Society*, 69:1428–1444, 1947.

[23] C. S. Chern. Emulsion polymerization mechanisms and kinetics. *Progress in Polymer Science*, 31:443–486, 2006.

[24] Y. Almog, S. Reich, and M. Levy. Monodisperse polymeric spheres in the micron size range by a single step process. *British Polymer Journal*, 14:131–136, 1982.

[25] K. P. Lok and C. K. Ober. Particle-size control in dispersion polymerization of polystyrene. *Canadian Journal of Chemistry-Revue Canadienne De Chimie*, 63:209–216, 1985.

[26] C. M. Tseng, Y. Y. Lu, M. S. El-Aasser, and J. W. Vanderhoff. Uniform polymer particles by dispersion polymerization in alcohol. *Journal of Polymer Science Part A: Polymer Chemistry*, 24:2995–3007, 1986.

[27] B. Vincent, C. A. Young, and T. F. Tadros. Adsorption of small, positive particles onto large, negative particles in the presence of polymer. part 1.-adsorption isotherms. *Journal of the Chemical Society, Faraday Transactions 1: Physical Chemistry in Condensed Phases*, 76:665–673, 1980.

[28] L. Xu, H. Li, X. Jiang, J. Wang, L. Li, Y. Song, and L. Jiang. Synthesis of amphiphilic mushroom cap-shaped colloidal particles towards fabrication of anisotropic colloidal crystals. *Macromolecular Rapid Communications*, 31:1422–1426, 2010.

[29] Y. Huang, J. Wang, J. Zhou, L. Xu, Z. Li, Y. Zhang, J. Wang, Y. Song, and L. Jiang. Controllable synthesis of latex particles with multicavity structures. *Macromolecules*, 44:2404–2409, 2011.

[30] Z. Cheng, F. Luo, Z. Zhang, and Y.-q. Ma. Syntheses and applications of concave and convex colloids with precisely controlled shapes. *Soft Matter*, 9:11392–11397, 2013.

[31] B. Peng and A. Imhof. Surface morphology control of cross-linked polymer particles *via* dispersion polymerization. *Soft Matter*, 11:3589–3598, 2015.

[32] J.-W. Kim, R. J. Larsen, and D. A. Weitz. Synthesis of nonspherical colloidal particles with anisotropic properties. *Journal of the American Chemical Society*, 128:14374–14377, 2006.

[33] B. G. P. van Ravensteijn, M. Kamp, A. van Blaaderen, and W. K. Kegel. General route toward chemically anisotropic colloids. *Chemistry of Materials*, 25:4348–4353, 2013.

[34] H. R. Sheu, M. S. El-Aasser, and J. W. Vanderhoff. Uniform nonspherical latex particles as model interpenetrating polymer networks. *Journal of Polymer Science Part A: Polymer Chemistry*, 28:653–667, 1990.

[35] J. R. Wolters, G. Avvisati, F. Hagemans, T. Vissers, D. J. Kraft, M. Dijkstra, and W. K. Kegel. Self-assembly of "mickey mouse" shaped colloids into tube-like structures: experiments and simulations. *Soft Matter*, 11:1067–1077, 2015.

[36] J. W. Goodwin, J. Hearn, C. C. Ho, and R. H. Ottewill. Studies on the preparation and characterisation of monodisperse polystyrene laticee. *Colloid and Polymer Science*, 252:464–471, 1974.

[37] J. W. Goodwin, R. H. Ottewill, and R. Pelton. Studies on the preparation and characterization of monodisperse polystyrene latices v.: the preparation of cationic latices. *Colloid and Polymer Science*, 257:61–69, 1979.

[38] A. Homola and R. O. James. Preparation and characterization of amphoteric polystyrene latices. *Journal of Colloid and Interface Science*, 59:123–134, 1977.

[39] P. H. Wang and C. Y. Pan. Preparation of styrene/acrylic acid copolymer microspheres: polymerization mechanism and carboxyl group distribution. *Colloid and Polymer Science*, 280:152–159, 2002.

[40] C. Graillat, B. Dumont, P. Depraetere, V. Vintenon, and C. Pichot. Stability behavior of polystyrene latexes covered with zwitterionic sulfobetaine-type emulsifiers. *Langmuir*, 7:872–877, 1991.

[41] A. Tuncel, R. Kahraman, and E. Pişkin. Monosize polystyrene microbeads by dispersion polymerization. *Journal of Applied Polymer Science*, 50:303–319, 1993.

[42] B. G. P. van Ravensteijn and W. K. Kegel. Colloids with continuously tunable surface charge. *Langmuir*, 30:10590–10599, 2014.

[43] R. Messina, C. Holm, and K. Kremer. Polyelectrolyte multilayering on a charged sphere. *Langmuir*, 19:4473–4482, 2003.

[44] T. Delair, C. Pichot, and B. Mandrand. Synthesis and characterization of cationic latex particles bearing sulfhydryl groups and their use in the immobilization of Fab antibody fragments (1). *Colloid and Polymer Science*, 272:72–81, 1994.

[45] S. Jiang, Q. Chen, M. Tripathy, E. Luijten, K. Schweizer, and S. Granick. Janus particle synthesis and assembly. *Advanced Materials*, 22:1060–1071, 2010.

[46] O. D. Velev and S. Gupta. Materials fabricated by micro- and nanoparticle assembly the challenging path from science to engineering. *Advanced Materials*, 21:1897–1905, 2009.

[47] J. Zhang, Y. Li, X. Zhang, and B. Yang. Colloidal self-assembly meets nanofabrication: from two-dimensional colloidal crystals to nanostructure arrays. *Advanced Materials*, 22:4249–4269, 2010.

[48] N. Vogel, M. Retsch, C.-A. Fustin, A. del Campo, and U. Jonas. Advances in colloidal assembly: the design of structure and hierarchy in two and three dimensions. *Chemical Reviews*, 115:6265–6311, 2015.

[49] H. Cong, B. Yu, J. Tang, Z. Li, and X. Liu. Current status and future developments in preparation and application of colloidal crystals. *Chemical Society Reviews*, 42:7774–7800, 2013.

[50] J. F. Galisteo-López, M. Ibisate, R. Sapienza, L. S. Froufe-Pérez, Á. Blanco, and C. López. Self-assembled photonic structures. *Advanced Materials*, 23:30–69, 2011.

[51] C. Fenzl, T. Hirsch, and O. S. Wolfbeis. Photonic crystals for chemical sensing and biosensing. *Angewandte Chemie International Edition*, 53:3318–3335, 2014.

[52] J. P. Camden, J. A. Dieringer, J. Zhao, and R. P. Van Duyne. Controlled plasmonic nanostructures for surface-enhanced spectroscopy and sensing. *Accounts of Chemical Research*, 41:1653–1661, 2008.

[53] J. N. Anker, W. P. Hall, O. Lyandres, N. C. Shah, J. Zhao, and R. P. Van Duyne. Biosensing with plasmonic nanosensors. *Nat Mater*, 7:442–453, 2008.

[54] Y. Xia, B. Gates, Y. Yin, and Y. Lu. Monodispersed colloidal spheres: old materials with new applications. *Advanced Materials*, 12:693–713, 2000.

[55] T. Wang and J. L. Keddie. Design and fabrication of colloidal polymer nanocomposites. *Advances in Colloid and Interface Science*, 147148:319–332, 2009.

[56] M. A. Boles, M. Engel, and D. V. Talapin. Self-assembly of colloidal nanocrystals: from intricate structures to functional materials. *Chemical Reviews*, 116:11220–11289, 2016.

[57] G. von Freymann, V. Kitaev, B. V. Lotsch, and G. A. Ozin. Bottom-up assembly of photonic crystals. *Chemical Society Reviews*, 42:2528–2554, 2013.

[58] J. Zhang, Z. Sun, and B. Yang. Self-assembly of photonic crystals from polymer colloids. *Current Opinion in Colloid and Interface Science*, 14:103–114, 2009.

[59] K. C. Barick and D. Bahadur. Self-assembly of colloidal nanoscale particles: fabrication, properties and applications. *Journal of Nanoscience and Nanotechnology*, 10:668–689, 2010.

[60] K.-Q. Zhang and X. Y. Liu. *In situ* observation of colloidal monolayer nucleation driven by an alternating electric field. *Nature*, 429:739–743, 2004.

[61] D. Zerrouki, J. Baudry, D. Pine, P. Chaikin, and J. Bibette. Chiral colloidal clusters. *Nature*, 455:380–382, 2008.

[62] M. Righini, A. S. Zelenina, C. Girard, and R. Quidant. Parallel and selective trapping in a patterned plasmonic landscape. *Nat Phys*, 3:477–480, 2007.

[63] A. Mihi, M. Ocaa, and H. Mguez. Oriented colloidal-crystal thin films by spin-coating microspheres dispersed in volatile media. *Advanced Materials*, 18:2244–2249, 2006.

[64] N. Denkov, O. Velev, P. Kralchevski, I. Ivanov, H. Yoshimura, and K. Nagayama. Mechanism of formation of two-dimensional crystals from latex particles on substrates. *Langmuir*, 8:3183–3190, 1992.

[65] A. S. Dimitrov and K. Nagayama. Continuous convective assembling of fine particles into two-dimensional arrays on solid surfaces. *Langmuir*, 12:1303–1311, 1996.

[66] M. Kondo, K. Shinozaki, L. Bergstroem, and N. Mizutani. Preparation of colloidal monolayers of alkoxylated silica particles at the air-liquid interface. *Langmuir*, 11:394–397, 1995.

[67] N. N. Khanh and K. B. Yoon. Facile organization of colloidal particles into large, perfect one- and two-dimensional arrays by dry manual assembly on patterned substrates. *Journal of the American Chemical Society*, 131:14228–14230, 2009.

[68] B. van Duffel, R. H. A. Ras, F. C. De Schryver, and R. A. Schoonheydt. Langmuir-Blodgett deposition and optical diffraction of two-dimensional opal. *Journal of Materials Chemistry*, 11:3333–3336, 2001.

[69] Z. Tang, N. A. Kotov, and M. Giersig. Spontaneous organization of single CdTe nanoparticles into luminescent nanowires. *Science*, 297:237–240, 2002.

[70] P. Podsiadlo, M. Michel, J. Lee, E. Verploegen, N. Wong Shi Kam, V. Ball, J. Lee, Y. Qi, A. J. Hart, P. T. Hammond, and N. A. Kotov. Exponential growth of LBL films with incorporated inorganic sheets. *Nano Letters*, 8:1762–1770, 2008.

[71] Y. Zhao, K. Thorkelsson, A. J. Mastroianni, T. Schilling, J. M. Luther, B. J. Rancatore, K. Matsunaga, H. Jinnai, Y. Wu, D. Poulsen, J. M. J. Frechet, A. Paul Alivisatos, and T. Xu. Small-molecule-directed nanoparticle assembly towards stimuli-responsive nanocomposites. *Nat Mater*, 8:979–985, 2009.

[72] L. Ramos, T. C. Lubensky, N. Dan, P. Nelson, and D. A. Weitz. Surfactant-mediated two-dimensional crystallization of colloidal crystals. *Science*, 286:2325–2328, 1999.

[73] U. Ognysta, A. Nych, V. Nazarenko, M. Škarabot, and I. Muševič. Design of 2D binary colloidal crystals in a nematic liquid crystal. *Langmuir*, 25:12092–12100, 2009.

[74] D. J. Kraft, R. Ni, F. Smallenburg, M. Hermes, K. Yoon, D. A. Weitz, A. van Blaaderen, J. Groenewold, M. Dijkstra, and W. K. Kegel. Surface roughness

directed self-assembly of patchy particles into colloidal micelles. *Proceedings of the National Academy of Sciences*, 109:10787–10792, 2012.

[75] P. M. Johnson, C. M. van Kats, and A. van Blaaderen. Synthesis of colloidal silica dumbbells. *Langmuir*, 21:11510–11517, 2005.

[76] H. Wang, L. Chen, X. Shen, L. Zhu, J. He, and H. Chen. Unconventional chain-growth mode in the assembly of colloidal gold nanoparticles. *Angewandte Chemie International Edition*, 51:8021–8025, 2012.

[77] M. S. Nikolic, C. Olsson, A. Salcher, A. Kornowski, A. Rank, R. Schubert, A. Fromsdorf, H. Weller, and S. Forster. Micelle and vesicle formation of amphiphilic nanoparticles. *Angewandte Chemie-International Edition*, 48:2752–2754, 2009.

[78] D. J. Kraft, W. S. Vlug, C. M. van Kats, A. van Blaaderen, A. Imhof, and W. K. Kegel. Self-assembly of colloids with liquid protrusions. *Journal of the American Chemical Society*, 131:1182–1186, 2009.

[79] Y. Lan, Y. Wu, A. Karas, and O. A. Scherman. Photoresponsive hybrid raspberry-like colloids based on cucurbit[8]uril hostguest interactions. *Angewandte Chemie International Edition*, 53:2166–2169, 2014.

[80] A. D. Dinsmore, M. F. Hsu, M. G. Nikolaides, M. Marquez, A. R. Bausch, and D. A. Weitz. Colloidosomes: selectively permeable capsules composed of colloidal particles. *Science*, 298:1006–1009, 2002.

[81] K. Liu, Z. Nie, N. Zhao, W. Li, M. Rubinstein, and E. Kumacheva. Step-growth polymerization of inorganic nanoparticles. *Science*, 329:197–200, 2010.

[82] Z. Tang, Z. Zhang, Y. Wang, S. C. Glotzer, and N. A. Kotov. Self-assembly of CdTe nanocrystals into free-floating sheets. *Science*, 314:274–278, 2006.

[83] M. P. Boneschanscher, W. H. Evers, J. J. Geuchies, T. Altantzis, B. Goris, F. T. Rabouw, S. A. P. van Rossum, H. S. J. van der Zant, L. D. A. Siebbeles, G. Van Tendeloo, I. Swart, J. Hilhorst, A. V. Petukhov, S. Bals, and D. Vanmaekelbergh. Long-range orientation and atomic attachment of nanocrystals in 2D honeycomb superlattices. *Science*, 344:1377–1380, 2014.

[84] A. M. Kalsin, M. Fialkowski, M. Paszewski, S. K. Smoukov, K. J. M. Bishop, and B. A. Grzybowski. Electrostatic self-assembly of binary nanoparticle crystals with a diamond-like lattice. *Science*, 312:420–424, 2006.

[85] M. E. Leunissen, C. G. Christova, A.-P. Hynninen, C. P. Royall, A. I. Campbell, A. Imhof, M. Dijkstra, R. van Roij, and A. van Blaaderen. Ionic colloidal crystals of oppositely charged particles. *Nature*, 437:235–240, 2005.

[86] F. M. van der Kooij, K. Kassapidou, and H. N. W. Lekkerkerker. Liquid crystal phase transitions in suspensions of polydisperse plate-like particles. *Nature*, 406:868–871, 2000.

Chapter 2

# Cavity Size Control, Surface Functionalization and Applications of Dimple Particle

ABSTRACT

Monodisperse, micron-sized dimple polystyrene particles with a single cavity are synthesized by a facile one-pot dispersion polymerization method. The procedure involves the delayed addition of cross-linker into the reaction mixture. The size of the cavity can be easily tuned either by changing the delayed time after which the cross-linker is added or by the concentration of the cross-linker. More importantly, by introducing functional co-monomers together with cross-linker during the delayed addition step, dimple particles with various surface functionalities are readily synthesized. As examples, dimple particles with chlorine groups, epoxide groups and thermoresponsive groups on their surfaces are synthesized by introducing co-monomers vinylbenzyl chloride (VBC), glycidyl methacrylate (GMA) and *N*-isopropylacrylamide (NIPAM), respectively. Afterwards, two applications of the synthesized dimple particles are conducted: as locks to assemble with shape complementary spheres which act as keys to form lock-key assembly *via* depletion interaction, and as seeds to synthesize hollow dumbbell particles. Eventually, the assembly behavior of the hollow dumbbell particles in an AC electric field is preliminarily studied.

## 2.1 Introduction

Colloidal particles with anisotropic shape and composition are getting increasingly more attentions due to their potential applications in many fields, such as colloidal assemblies [1, 2], photonic crystals [3], drug delivery [4], and self-propelling systems [5, 6]. Various shapes of particles, including dumbbell particles [7, 8], Mickey Mouse particles [9], patchy particles [10, 11], cubic particles [12], ellipsoidal particles [13], and dimple particles [14–18] are therefore designed and synthesized. Much effort has been devoted to synthesize dimple particles which have potential applications in lock-key assembly [16, 19], Pickering emulsion [17], and red blood cell imitation [20, 21]. For example, Okubo et al. [14] prepared dimple particles by utilizing a dynamic swelling method, which required several steps including seeds synthesis, seeds swelling by stepwise adding of bad solvent of monomer into the seeds/monomer mixture, and, finally, seeds polymerization. Sacanna et al. [16] synthesized dimple particles with well-defined cavities through polymerization-induced buckling of monodisperse silicon oil droplets. However, tedious purification steps were required to remove secondarily nucleated particles. Huang et al. [15] and Xu et al. [22] synthesized dimple particles with a diameter below 400 nm by a modified emulsion polymerization. This procedure involved the delayed addition of cross-linker into the reaction mixture. At constant delayed addition time, slow addition resulted in dimple particles with a single cavity, while fast addition generated dimple particles with multiple cavities. However, its inherently relatively small size because of the emulsion polymerization method limits applications, for example, as a model system to study lock-key interaction *in situ* by optical microscopy. To synthesize larger dimple particles, a modified dispersion polymerization was introduced by Cheng et al. [17]. Dispersion polymerization is widely used to synthesize monodisperse particles with sizes in the micrometer regime. Under their experimental conditions, micron-sized dimple particles with multiple cavities were obtained, while additional swelling/polymerization steps were required to obtain dimple particles with a single cavity.

However, most previous work focused on the preparation of dimple particles with multiple cavities, and only relatively few work has been reported on dimple particles with a single cavity, not to mention on the control of the cavity size systematically. Moreover, to the best of our knowledge no articles described the preparation of dimple

particles with various surface functionalities. While the control of the cavity size and the surface functionalities of the dimple particles are still highly desired, such as, for studying lock and key interaction in more precise and controllable way, for covalent immobilization of lock and key structures, and for preparation of chemically anisotropic dumbbell particles.

In this chapter, we present a facile and versatile route to synthesize monodisperse, micron-sized dimple particles with a single cavity by a modified one-pot dispersion polymerization method. The procedure involves the delayed addition of cross-linker into the reaction mixture. The desired dimple particles are formed in high yield and purity without significantly secondary nucleation. The influence on the cavity size of dimple particles is investigated in detail in terms of the delayed addition time and the concentration of the cross-linker. More importantly, we extend this method to synthesize dimple particles with various surface functionalities. This is achieved by introducing additional functional co-monomers together with cross-linker during the delayed addition step. As examples, vinylbenzyl chloride (VBC), glycidyl methacrylate (GMA) and *N*-isopropylacrylamide (NIPAM) are chosen as the functional co-monomers to obtain dimple particles with various surface functionalities. The accessibility of the surface functional groups on the dimple particles is demonstrated by making the surface functional groups react with a fluorescent molecule. Furthermore, the dimple particles (as locks) can assemble with shape complementary spheres (as keys) to form a lock-key assembly *via* depletion interaction. Finally, we show that the dimple particles can be used as seeds to synthesize hollow dumbbell particles whose assembly behavior in an AC electric field is also studied.

## 2.2 Experimental Section

### 2.2.1 Materials

Styrene (St, 99%), divinylbenzene (DVB, 55% mixture of isomers, tech. grade), 4-vinylbenzyl chloride (VBC, $\geq$ 90%, tech. grade), *N*-isopropylacrylamide (NIPAM, 97%), fluoresceinamine (for fluorescence, mixture of isomers, $\geq$ 75%), dimethylformamide (DMF, $\geq$ 99%) polyvinylpyrrolidone (PVP, K30, $M_w$ = 40,000 g/mol), polyvinyl alcohol (PVA, $M_w$ = 85-124 kg/mol, 87-89% hydrolyzed), polyethylene gly-

col (PEO, $M_w$ = 600,000 g/mol), sodium chloride (NaCl, ACS reagent, $\geq$ 99.5%) were obtained from Sigma-Aldrich. Azobis(isobutyronitrile) (AIBN, 98%) was purchased from Acros Organics. Glycidyl methacrylate (GMA, $\geq$ 97.0%) was purchased from Fluka Analytical. 2,2'-Azobis(2,4-dimethylvaleronitrile) (V65) was purchased from Wako chemicals GmbH. Ethanol (p.a., ACS reagent) was purchased from Merck. All of the chemicals were used as received. The water used throughout all of the synthesis was purified using a Milli-Q water purification system.

### 2.2.2 Synthesis of polystyrene dimple particles

5 g PVP, 126 mL ethanol, 0.136 g AIBN, and 14 mL water were charged into a 250 mL three-neck round bottom flask. Dissolution of PVP and AIBN was aided by sonication of the mixture for about 1 min. Subsequently, 10 mL St was added. The transparent mixture was constantly stirred with a magnetic stirrer under nitrogen flow, and the flask was immersed in a 70 °C water bath to initiate polymerization. After 1.5 h of polymerization, a premixed solution containing 0.3 mL DVB, 2.5 mL St and 5 mL ethanol was added dropwise, where the total addition time was approximately 30 min. The reaction was allowed to proceed for another 22.5 h. The final product was washed with ethanol and water twice, respectively, and stored in water.

To monitor the particle formation in time, 300 $\mu$L of sample was withdrawn from the reaction mixture at 0.1 h, 0.25 h, 0.5 h, 1 h, 2 h, 4 h, 8 h, 10 h, 23 h, 24 h of polymerization. 150 $\mu$L of that was used to measure the solid content; the remainder of the aliquot was used to measure size by TEM. The monomer conversion was measured gravimetrically. For TEM measurement, samples were washed with ethanol and water twice respectively.

### 2.2.3 Particle etching experiments in DMF

Typically, 15 $\mu$L of the dimple particle dispersion (solid content = 18%) was centrifuged, washed with DMF three times, and re-dispersed in 1 mL DMF. The dispersion was stirred for 24 h at 80 °C using an oil bath. After the etching procedure, the sample was centrifuged and washed with DMF three times, with water three times. Finally, the particles were stored in water.

### 2.2.4 Synthesis of dimple polystyrene particles with various surface functionalities

The preparation procedure is essentially the same as in the previous **subsection 2.2.2**, except that a premixed solution containing 1.5 mL VBC (or 1.5 mL GMA, or 1.2 g NIPAM), 1.5 mL St, 0.36 mL DVB and 5 ml ethanol was added dropwise after 1.5 h of polymerization. The final products were washed with ethanol and water twice, respectively, and stored in water.

### 2.2.5 Synthesis of hollow dumbbell polystyrene particles

The seed particles for the synthesis of the hollow dumbbell particles were prepared by using essentially the same method in **subsection 2.2.2**, except that no water was added, and the delayed addition time of the cross-linker was 4 h after the start of polymerization. By doing so, larger dimple particles with thinner shells were obtained.

For the preparation of dumbbell particles, 15.4 mg V65, 11.3 $\mu$L DVB, 750 $\mu$L St, and 9 mL 1 wt % aqueous PVA solution were mixed in an elongated 25 mL vial and emulsified at 8000 rpm for 6 min by using an IKA T-25 Ultra Turrax with an S25N 10G dispersing tool. Subsequently, 2.5 mL seeds dispersion (solid content = 3.5%) was added and the vial was placed on a roller-table for 24 h. After that, the vial was immersed into an oil bath of 70 °C to polymerize for 24 h. The final product was washed with ethanol and water twice, respectively, and stored in water.

The procedure for etching the dumbbell particles is as follows. 100 $\mu$L of the dumbbell particles dispersion (solid content $\approx$ 2%) was centrifuged, washed with DMF three times, and re-dispersed in 1 mL DMF. The dispersion was stirred for 6 h at room temperature. Subsequently, the dispersion was washed with DMF three times and finally stored in DMF. As a caution we would like to stress that the etching procedure should not be too harsh like in **subsection 2.2.3**. Also, sonication should be avoided during the washing steps. Otherwise, the two lobes of the dumbbell particles break apart, as shown in **Appendix 1**.

### 2.2.6 Covalent attachment of fluoresceinamine to chlorinated dimple particles

A 55 $\mu$L aliquot of chlorinated dimple particles dispersion (solid content = 18%) was centrifuged and washed with DMF three times. After the washing steps, the colloids were re-dispersed in 1 mL DMF. Subsequently, 3.5 mg fluoresceinamine was added to the dispersion, and the dispersion was heated for 24 h at 90 °C, where sample was wrapped in an aluminum foil to avoid dye bleaching. The particles were sequentially washed with DMF and ethanol to remove excess dye. Finally the labeled particles were stored in water and covered by an aluminum foil.

### 2.2.7 Lock and key assembly process

Typically, 10 $\mu$L lock colloids dispersion (solid content = 0.5%), 10 $\mu$L key colloids dispersion (solid content = 1%), 30 $\mu$L 2 g/L aqueous PEO solution, 20 $\mu$L 100 mM aqueous NaCl solution and 130 $\mu$L water were mixed, and the sample was placed on a roller-table for 1 h before observation with optical microscopy.

### 2.2.8 Assembly of hollow dumbbell particles in an AC electric field

Hollow dumbbell particles were dispersed in DMF with the solid content of approximately 0.2%. The particles dispersion was filled into a home-made capillary and the two ends of the capillary were sealed using Bison kombi snel-rapide. Subsequently, an AC electric field (40 V/mm, frequency of 1 MHz) was applied for 30 min. The preparation of the home-made capillary was as follows: Two copper wires (diameter = 0.05 mm) were passed through a capillary (4.5 cm × 1 mm × 0.1 mm) and closely put to the two sides of the capillary separately. Subsequently, the capillary was placed on a microscope slide (Menzel-Gläser) and fixated using tape.

### 2.2.9 Characterization

Transmission electron microscopy pictures were taken with a Philips Tecnai 10 electron microscope typically operating at 100 kV. The samples were prepared by drying a

drop of diluted aqueous dispersion on top of polymer-coated copper grids.

Scanning electron microscopy images were taken with a Philips SEM XL FEG 30 typically operating at 5 - 10 kV. The dried samples of particles were sputter coated with 6 nm platinum prior to imaging.

IR spectra were obtained using a PerkinElmer Frontier FT-IR/FIR spectrometer. The attenuated total reflectance (ATR) mode was used. Measurements were carried out on powders obtained by drying the particle dispersion.

Confocal microscopy pictures were taken with a Nikon TE 2000U laser scanning confocal microscope equipped with a Nikon C1 scanning head in combination with an Ar-ion laser (488 NM, Spectra Physics), a HeNe laser (543.5 nm, Melles Griot) and an oil immersion lens (100× Nikon Plan Apc, NA 1.4).

Optical microscopy (OM) images were taken with a Nikon Ti-E inverted microscope. The microscope was equipped with a Nikon TIRF NA 1.49 100× oil immersion objective, intermediate magnification of 1.5×, and a Hamamatsu ORCA Flash camera.

## 2.3 Results and Discussion

### 2.3.1 Influence of the adding time of cross-linker

To select the suitable addition time of DVB, the time-dependent evolution of the particle size and the monomer conversion of a dispersion polymerization of solely styrene is studied first. As seen in Figure 2.1, after 0.1 h, particles have already formed. Macroscopically, the onset of particles formation is evident from the appearance of turbidity in the initially transparent reaction mixture. After about 6 h of polymerization, the particle size as well as the styrene conversion levels off, indicating the maximum achievable particle dimensions are reached (under the employed reaction conditions). In between 0.1 h and 6 h, a steep increase in the particle diameter and the monomer conversion is observed. Therefore, DVB is added 0.1 h, 1.5 h and 6 h after the polymerization reaction has started in order to investigate the influence of the addition time on the resulting particles geometry and morphology. All other experimental conditions are kept constant. As seen in Figure 2.2, when DVB is added after 0.1 h (PS-0.1h), microspheres with a rough surface are obtained, and no cavity is observed (Figure 2.2a and 2.2d). When DVB is added 1.5 h after the start of the

polymerization (PS-1.5h), as seen in Figure 2.2b and 2.2e, the low contrast region in the TEM images indicating the presence of a cavity, and the cavity has a diameter of approximately 500 nm. Delaying DVB addition even further to 6 h (PS-6h), leads to the formation of dimple particles with a cavity diameter of approximately 360 nm, much smaller compared to PS-1.5h, as depicted in Figure 2.2c and 2.2f.

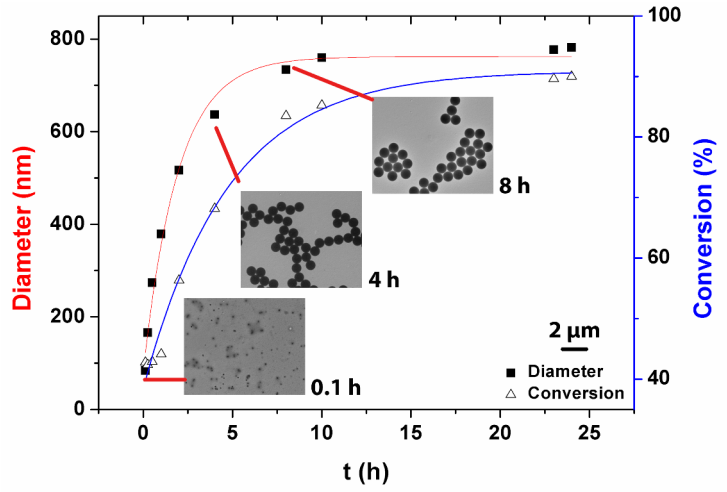


Figure 2.1. Time-dependent size evolution of polystyrene particles and monomer conversion during dispersion polymerization. Inset: TEM images of samples withdrawn from the reaction mixture after 0.1 h, 4 h and 8 h of polymerization. Scale bar: 2 $\mu$m for all images.

It is well-established that during dispersion polymerization, the monomer concentration in the growing particles is very low and decreases further as the polymerization proceeds [23]. Thus, the growing particles are composed of a relatively dense PS core and a thin outer layer with a relatively low polymer density. The outer layer is preferentially swollen with monomer that is present in the reaction mixture. When DVB is added to the reaction mixture, we speculate it will be trapped in the swollen thin outer layer [24]. Therefore we hypothesize that the polymerization of DVB leads to the formation of cross-linked shell, while the core remains linear. With the polymerization proceeding, the thickness of the shell grows as well as its cross-linking density, which eventually leads to the buckling of the cross-linked shell. The tendency of the

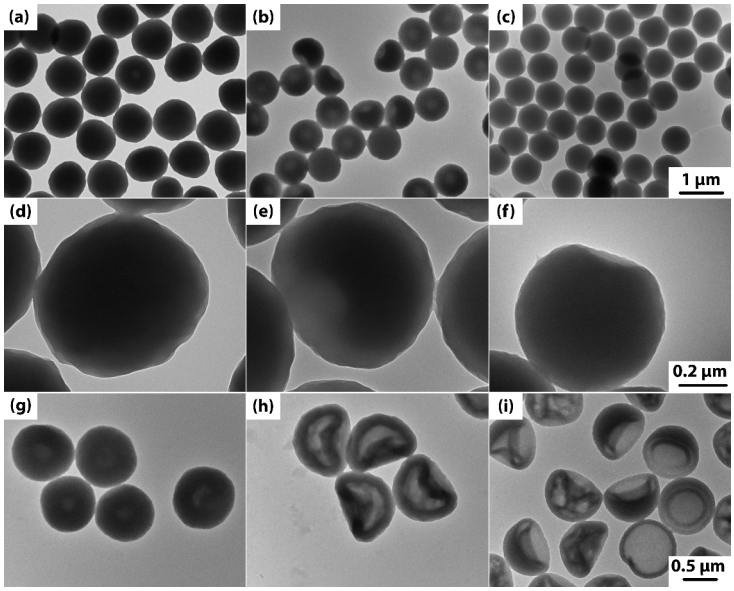


Figure 2.2. TEM images of polystyrene particles with different delayed addition time of cross-linker divinylbenzene (DVB): (a) 0.1 h, (b) 1.5 h and (c) 6 h, and (d), (e), (f) are their corresponding high magnification images; (g), (h), (i) are their corresponding images after etched with DMF, respectively. Scale bars: top panels, 1 $\mu$m; middle panels, 200 nm; bottom panels, 500 nm.

cross-linked shell to buckle increases with the inverse ratio of the shell thickness over the particle radius [25]. At an addition time of DVB of 0.1 h after polymerization starts, as shown in Figure 2.1, the size of the growing particles is relatively small, approximately one tenth of the final particle size. Thus, the ratio of the shell thickness over the particle radius is relatively large, and no dimple is observed but the particle surface is rough. Further delaying the addition time of DVB to 1.5 h and 6 h result in a decrease of the ratio of the shell thickness over the particle radius, and buckling is indeed being observed. As shown in Figure 2.2b and 2.2c, both of these delayed addition of DVB generate cavities. Furthermore, in the case of PS-1.5h (Figure 2.2b and 2.2e), as polymerization proceeds, the size of the whole particle grows, but the size of the cavity grows even faster. As seen in Figure 2.3c, the $L/D$ ($L$ is the diameter of the cavity and $D$ is the diameter of the whole dimple particle) value increases with

time, and the dimple particles obtained after 24 h of polymerization show much larger cavities than the one obtained after 3.25 h of polymerization (Figure 2.3a and 2.3b). This observation is consistent with the observation that growth was heavily restricted along the axial direction of the cavity, but continued at angles to the axial direction of the cavity [24]. On the other hand, in the case of PS-6h (Figure 2.2c and 2.2f), the size of the growing particles after 6 h of polymerization nearly reaches the final size as seen from Figure 2.1. Probably because of that, the size of the cavity hardly grows since the overall size of the particles only increases to a limited extent, and eventually, dimple particles with smaller cavity are obtained compared to the case of PS-1.5h (Figure 2.2b and 2.2e). In this scenario, one would expect that the as-synthesized particles should have core-shell structure with linear PS core and cross-linked PS shell regardless of the presence of a dimple, since it was assumed that DVB does not reach the particle core. Moreover, the thickness of the cross-linked shell should decrease, or the size of the linear core should increase, when DVB is added after a longer delayed time. To verify the core-shell morphology, PS-0.1h, PS-1.5h and PS-6h are treated with DMF for 24 h at 80 °C. DMF is capable of dissolving linear polystyrene, but does not dissolve cross-linked polystyrene. Subsequently, the dissolved linear polystyrene is washed away by centrifugation/redispersion of the dispersion with DMF for three times. Afterwards, the washed particles are transferred into water and TEM samples are prepared by drying under atmospheric conditions. The treated particles are named as PS-0.1h-DMF, PS-1.5h-DMF and PS-6h-DMF, and their TEM images are shown in Figure 2.2g, 2.2h and 2.2i, respectively. Based on the low contrast of the inner region of the colloids we conclude that all of them are hollow. In agreement with the hypothesized core-shell morphology, these results prove that the cores are all linear, while the shells are all cross-linked. Furthermore, the trends observed in the shell thickness and the core size is also consistent with our hypothesis: the thickness of the shell decreases and the size of the core increases when the delayed time after which DVB is added is prolonged. For example, the thickness of the shell decreases from 278 nm (PS-0.1h-DMF), 158 nm (PS-1.5h-DMF) to 50 nm (PS-6h-DMF) when the addition time of DVB is later. These results demonstrate that the addition time of DVB is indeed important for the dimple formation, and the size of the cavity on the dimple particles can be readily tuned by changing the delayed time between the start of the polymerization and the addition of the cross-linker.

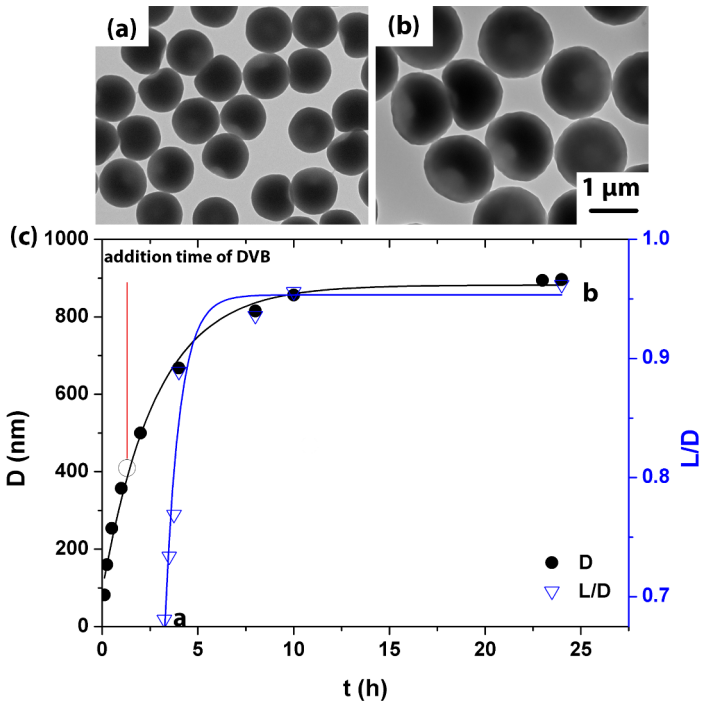


Figure 2.3. TEM images of PS-1.5h at (a) 3.25 h and (b) 24 h from the start of the dispersion polymerization, respectively; (c) Time evolution of the diameter ($D$) of PS-1.5h and the ratio of the cavity diameter to the particle diameter ($L/D$) of PS-1.5h. Scale bar: 1 $\mu$m for both images.

### 2.3.2 Influence of the cross-linking density

From the previous discussion, we conclude that the addition time of cross-linker has significant influence on the particles geometry and morphology. Next, we investigate the influence of the total DVB concentration on the resulting particles geometry and morphology. Therefore particles with cross-linking densities ranging from 0.6% to 10.8% are prepared. The addition time of DVB is fixed at 1.5 h after the polymerization starts. The results are summarized in Figure 2.4. When the concentration of cross-linker is too low (0.6%), no dimple is found on the particles. Instead, the particles have a hemisphere-like structure, as shown in Figure 2.4a. When the cross-linking density ranges from 1.2% to 10.8%, with the increase of the cross-linking density,

the diameter of the cavity decreases from 500 nm to 350 nm until to no cavity, as shown in Figure 2.4b, 2.4c and 2.4d, respectively. To understand the influence of the cross-linking density on the morphology of the particles, the particles are again treated with DMF to etch away the linear core. As depicted in Figure 2.5, the ratio of the shell thickness over the particle radius increases with increasing cross-linking density, resulting in a decreased tendency to buckle the particles. Therefore, dimple particles with smaller cavities are observed with increasing cross-linking density. These results demonstrate that the cavity size of the dimple particles can also be tuned by adjusting the cross-linking density.

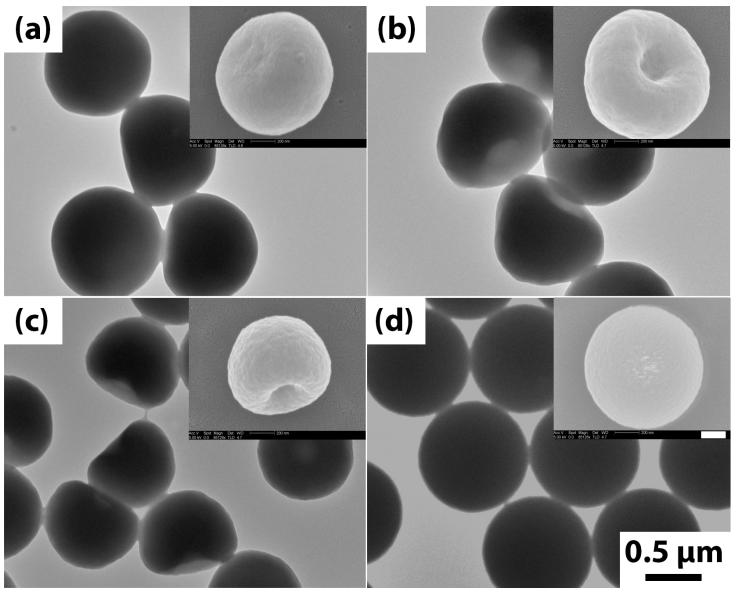


Figure 2.4. TEM images of particles synthesized using cross-linking densities of (a) 0.6%, (b) 1.2%, (c) 4.6% and (d) 10.8%, respectively. The addition time of the cross-linker is fixed at 1.5 h after the polymerization started. The total addition time is approximately 30 min. Scale bar: 0.5 $\mu$m. Inset: the corresponding SEM images. Scale bar: 200 nm.

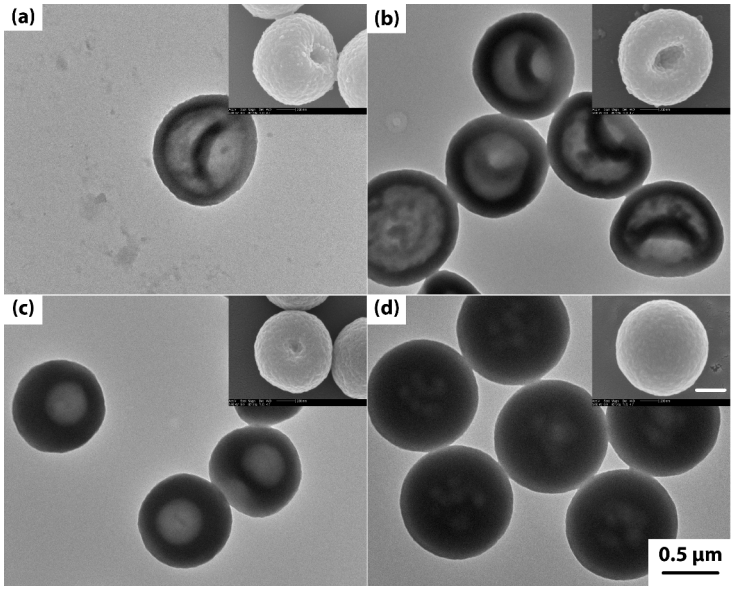


Figure 2.5. TEM images of particles synthesized under different cross-linking density after treated with DMF, which is (a) 0.6%, (b) 1.2%, (c) 4.6% and (d) 10.8%, respectively. Scale bars: 0.5 $\mu$m. Inset: the corresponding SEM images. Scale bars: 200 nm.

### 2.3.3 Synthesis of dimple particles with various surface functionalities

Owing to their special shape, the synthetic dimple particles have been attempted to mimic the red blood cell (RBC). Up to now, the common approach is to mimic the shape and mechanical properties of the RBC [20, 21]. Considering the complex surface functionalities of the RBC, it will be greatly beneficial to mimic the RBC if the synthetic dimple particles bear functional groups on their surfaces which allow for the further modifications. Therefore we extend our method to prepare surface chemical functionalized dimple particles. The procedure is rather straightforward, the only difference with the method that used to synthesize non-functionalized dimple particles is that the additional functional co-monomers is added to the polymerization mixture together with DVB during the delayed addition process. As examples, dimple particles

with chlorine groups (PS-PVBC), epoxide groups (PS-PGMA) and thermoresponsive groups (PS-PNIPAM) on their surfaces are synthesized by introducing co-monomer VBC, GMA and NIPAM, respectively. The results are shown in Figure 2.6. Clearly, all of the resulting particles have dimple shapes, indicating that the introduction of the functional co-monomers has no significant influence on the dimple formation and properties. The incorporation of functional groups is confirmed by infrared (IR) spectroscopy, as shown in Figure 2.6d. Compared to the IR spectrum of the non-functionalized polystyrene particles, the spectra of the PS-PVBC, PS-PGMA and PS-PNIPAM show a new signal at 1266 $cm^{-1}$, 1730 $cm^{-1}$, and 1676 $cm^{-1}$, which correspond to the $CH_2$-Cl stretching vibration, the carbonyl stretching vibration from ester groups and the carbonyl stretching vibration from amide groups, respectively. To further confirm that the functional groups are indeed present on the surface and are accessible to other chemicals, as an example, the chlorine modified dimple particles PS-PVBC are selected and treated with dye fluoresceinamine. This dye carries a primary amine group that can react with benzyl chloride functionalities immobilized on the surface of the dimple particles. The resulting dye-labeled particles are imaged by confocal microscopy. As seen from Figure 2.7, the green signals originating from the fluorescence of the attached dye is homogeneously distributed over the particle surface, indicating that the initial chlorine groups also are homogeneously distributed over the particle surface. Additionally, these chlorine groups are reactive towards further surface modifications, for example, being a initiator to graft a polymer layer on the particle surface *via* atom transfer radical polymerization reaction (**Chapter 3**).

### 2.3.4 Lock-key assembly *via* depletion interaction

The dimple particles can be used as the building blocks and assemble with particles of complementary shape to form lock-key assembly *via* depletion interaction. Depletion interaction is an effective attraction that arises between large particles that are suspended in a solution of depletant, which can be polymers or smaller colloidal particles [26]. The strength of the depletion interaction is proportional to the concentration of the depletant. The lock-key assembly is favored because it maximizes the free volume of the depletant by overlapping of the exclude volume of particles and hence results in the strongest depletion attraction. Up to now, most lock-key experiments accomplished

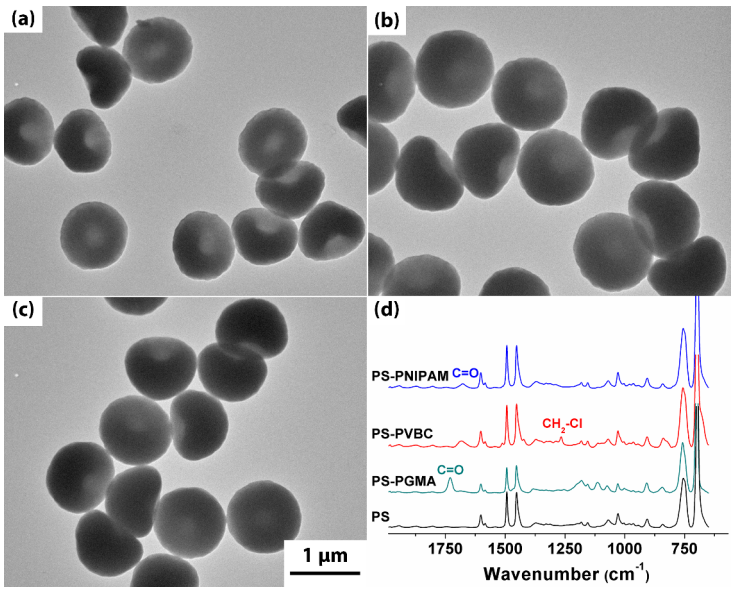


Figure 2.6. TEM images of surface functionalized dimple particles (a) PS-PVBC, (b) PS-PGMA and (c) PS-PNIPAM. (d) FTIR spectra of PS-PNIPAM, PS-PVBC, PS-PGMA and non-functionalized PS particles (from top to bottom). Scale bars: 1 $\mu$m for all the TEM images.

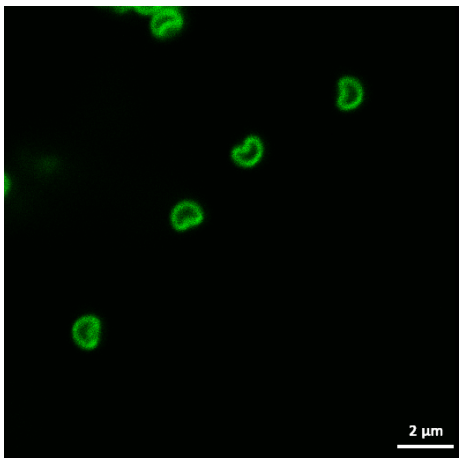


Figure 2.7. Confocal microscopy image of surface functionalized dimple particles PS-PVBC after surface modification with fluoresceinamine. Scale bars: 2 $\mu$m.

were based on charged lock and key [16, 19, 27]. Sacanna et al. [19] showed that both locks and keys with a coated hydrophilic polymer layer on their surfaces can also form lock-key assembly *via* depletion attraction. By using self-consistent field theory, Egorov et al. found that the lock-key assembly by using sterically stabilized locks and keys can be formed, provided that the length of the depletant chains is longer than that of the stabilizer chains [28]. Herein we experimentally show that the sterically stabilized locks and keys can assemble to form lock-key assembly *via* depletion interaction. In our experiments, both locks and keys used are stabilized by PVP with molecular weight of 40,000 g/mol. The nonadsorbing polymer PEO with a molecular weight of 600,000 g/mol and a concentration ranges from 0.3 to 0.9 g/L is used as the depletant to induce the depletion interaction. Figure 2.8 shows two examples of the lock-key assemblies. Clearly, lock-key assemblies are formed in both cases.

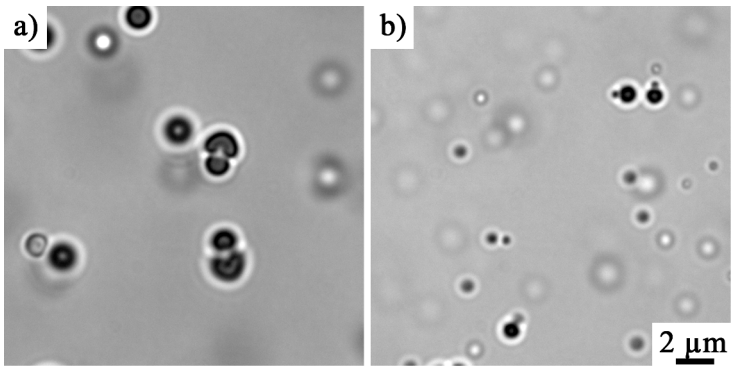


Figure 2.8. Two examples of self-assembled lock-key assemblies in the presence of depletant PEO ($M_w$ = 600,000 g/mol). (a) Lock with cavity diameter of 1.1 $\mu$m and key with diameter of 1.2 $\mu$m; (b) Lock with cavity diameter of 0.47 $\mu$m and key with diameter of 0.46 $\mu$m. Scale bars: 2 $\mu$m for both images.

### 2.3.5 Assembly of hollow dumbbell particles in an AC electric field

The dimple particles can be used as seeds to synthesize hollow dumbbell particles. As depicted in Figure 2.9, firstly, the dimple particles are swollen by styrene monomer and the cross-linker DVB. After heating and polymerization, dumbbell particles are formed

due to the phase separation of the swelling reagents and the seeds [29]. Subsequently, the dumbbell particles are etched with DMF, the dissolution of linear polystyrene in the seed part results in the formation of hollow dumbbell particles with one lobe hollow and the other lobe solid. As shown in Figure 2.10a, dumbbells with similar sizes of the lobes are obtained, and one of the lobes clearly is hollow. In the following we term the solid lobe 'head' and the hollow lobe 'tail'.

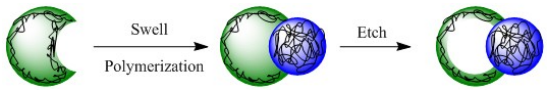


Figure 2.9. Schematic illustrations for the preparation of hollow dumbbell particles.

In an external AC electric field colloids acquire a dipole moment that is parallel to the electric field. In that case assembly into chains can occur [30–34]. Therefore, the obtained hollow dumbbell particles are dispersed in DMF and an electric field (40 V/mm, frequency of 1 MHz) is applied. Interestingly, in DMF (Figure 2.10b), the differences in contrast between two lobes are remarkable, the head is smaller and darker than the tail, which is ascribed to the different density of the head and the tail. These contrast differences of the lobes are advantageous, and distinguish the heads from the tails in the assemblies. As can be seen in Figure 2.10b, in an AC electric field, most particles chains have the heads in closest contact, indicating that the dipole interactions between the heads are stronger than that of head-to-tail and tail-to-tail. Overall, approximately 80% of the hollow dumbbell particles are aligned perpendicular to the electric field. Sometimes, helix structures are found, as marked in Figure 2.10b. The low yield of helix structures can be ascribed to the following reasons. First, the size difference between the two lobes is not large enough, in other words, the tail is not large enough to provide sufficient steric barrier effect; second, the etching process is not fully complete, some particles kept intact after etching (Figure 2.10a); finally, the assembly conditions (the concentration of the hollow dumbbell particles, the strength of the electric field, the time of the electric field that applied) should be optimized [33]. Regardless of these problems, the preliminary results are still promising. We are still working on optimizing our system and trying to assemble better helix-like structures. Furthermore, as shown before, the dimple particles can be functionalized by reactive functional groups, which makes it possible to fix the formed helix-like chains.

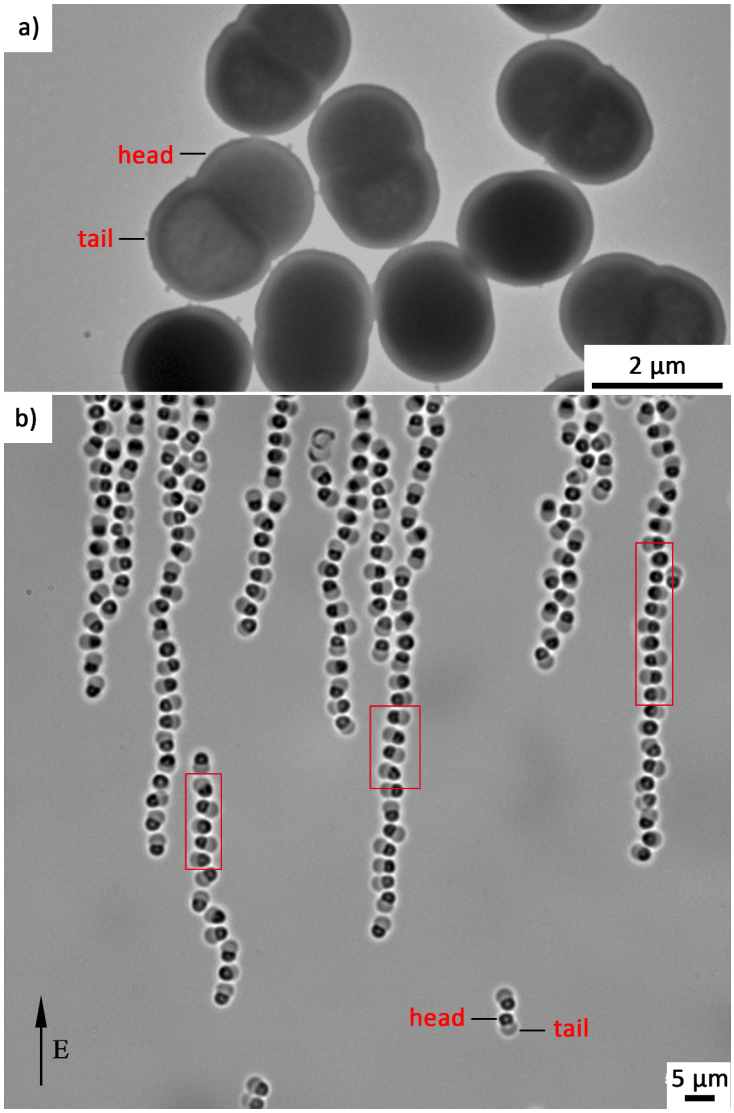


Figure 2.10. (a) TEM image of the hollow dumbbell particles. (b) Optical micrograph of the hollow dumbbell particles in DMF in an AC electric field. Scale bars: 2 $\mu$m for (a) and 5 $\mu$m for (b).

## 2.4 Conclusion

We present a facile synthesis procedure towards monodisperse micron-sized dimple particles with a single cavity which relies on the delayed addition of cross-linker during a modified dispersion polymerization. The size of the cavity is readily tunable by the variation of the delayed addition time as well as the concentration of cross-linker. Furthermore, we show that this method can be readily extended to synthesize dimple particles with various surface functionalities. This is achieved by introducing additional functional co-monomers together with cross-linker during the delayed addition step. As examples, vinylbenzyl chloride (VBC), glycidyl methacrylate (GMA) and *N*-isopropylacrylamide (NIPAM) are chosen as the functional co-monomers to obtain the dimple particles with various surface functionalities. The functional groups are accessible which is confirmed by their reaction with a dye, leading to fluorescent particles. Furthermore, the dimple particles can be used as locks and assemble with shape complementary spheres that act as keys to form lock-key assembly *via* depletion interaction. Finally, we show that hollow dumbbell particles can be synthesized by using the dimple particles as seed particles and these hollow dumbbell particles align perpendicular to the applied AC electric field.

## Acknowledgements

I would like to thank Bas van Ravensteijn for the initial idea of assembly of hollow dumbbell particles in an AC electric field and Pepijn Moerman for operating the electric field and for useful discussion.

# Appendix 1

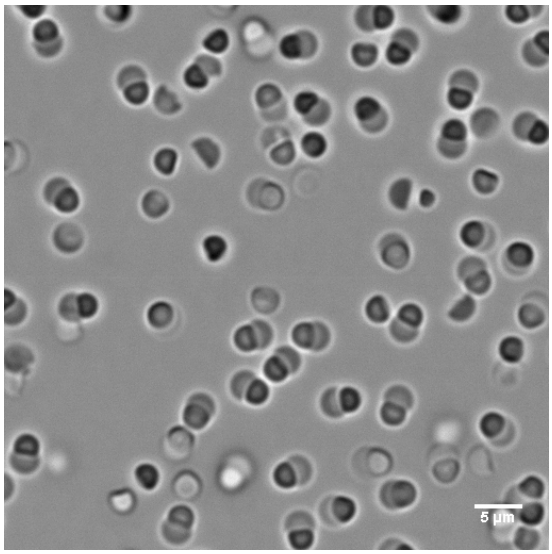


Figure 2.11. Optical micrograph of dumbbell particles after treated in DMF at 80 °C for 15 h. Clearly, some dumbbell particles are broken apart. Scale bar: 5 $\mu$m.

# Bibliography

[1] S. C. Glotzer and M. J. Solomon. Anisotropy of building blocks and their assembly into complex structures. *Nat Mater*, 6:557–562, 2007.

[2] Q. Chen, S. C. Bae, and S. Granick. Directed self-assembly of a colloidal kagome lattice. *Nature*, 469:381–384, 2011.

[3] Y. Lu, Y. D. Yin, and Y. N. Xia. Three-dimensional photonic crystals with non-spherical colloids as building blocks. *Advanced Materials*, 13:415–420, 2001.

[4] J.-B. Fan, Y. Song, H. Li, J.-P. Jia, X. Guo, and L. Jiang. Controllable drug release and effective intracellular accumulation highlighted by anisotropic biodegradable PLGE nanoparticles. *Journal of Materials Chemistry B*, 2:3911–3914, 2014.

[5] W. F. Paxton, K. C. Kistler, C. C. Olmeda, A. Sen, S. K. St. Angelo, Y. Cao, T. E. Mallouk, P. E. Lammert, and V. H. Crespi. Catalytic nanomotors: autonomous movement of striped nanorods. *Journal of the American Chemical Society*, 126:13424–13431, 2004.

[6] H. H. Wensink, V. Kantsler, R. E. Goldstein, and J. Dunkel. Controlling active self-assembly through broken particle-shape symmetry. *Physical Review E*, 89:010302, 2014.

[7] B. G. P. van Ravensteijn, M. Kamp, A. van Blaaderen, and W. K. Kegel. General route toward chemically anisotropic colloids. *Chemistry of Materials*, 25:4348–4353, 2013.

[8] J.-W. Kim, R. J. Larsen, and D. A. Weitz. Synthesis of nonspherical colloidal particles with anisotropic properties. *Journal of the American Chemical Society*, 128:14374–14377, 2006.

[9] J. R. Wolters, G. Avvisati, F. Hagemans, T. Vissers, D. J. Kraft, M. Dijkstra, and W. K. Kegel. Self-assembly of "mickey mouse" shaped colloids into tube-like structures: experiments and simulations. *Soft Matter*, 11:1067–1077, 2015.

[10] D. J. Kraft, W. S. Vlug, C. M. van Kats, A. van Blaaderen, A. Imhof, and W. K. Kegel. Self-assembly of colloids with liquid protrusions. *Journal of the American Chemical Society*, 131:1182–1186, 2009.

[11] A. B. Pawar and I. Kretzschmar. Fabrication, assembly, and application of patchy particles. *Macromolecular Rapid Communications*, 31:150–168, 2010.

[12] L. Rossi, S. Sacanna, W. T. M. Irvine, P. M. Chaikin, D. J. Pine, and A. P. Philipse. Cubic crystals from cubic colloids. *Soft Matter*, 7:4139–4142, 2011.

[13] Z. Zhang, P. Pfleiderer, A. B. Schofield, C. Clasen, and J. Vermant. Synthesis and directed self-assembly of patterned anisometric polymeric particles. *Journal of the American Chemical Society*, 133:392–395, 2011.

[14] M. Okubo and H. Minami. Studies on suspension and emulsion part CXCIV - production of micron-sized monodispersed anomalous polymer particles having red blood corpuscle shape. *Macromolecular Symposia*, 150:201–210, 2000.

[15] Y. Huang, J. Wang, J. Zhou, L. Xu, Z. Li, Y. Zhang, J. Wang, Y. Song, and L. Jiang. Controllable synthesis of latex particles with multicavity structures. *Macromolecules*, 44:2404–2409, 2011.

[16] S. Sacanna, W. T. M. Irvine, L. Rossi, and D. J. Pine. Lock and key colloids through polymerization-induced buckling of monodisperse silicon oil droplets. *Soft Matter*, 7:1631–1634, 2011.

[17] Z. Cheng, F. Luo, Z. Zhang, and Y.-q. Ma. Syntheses and applications of concave and convex colloids with precisely controlled shapes. *Soft Matter*, 9:11392–11397, 2013.

[18] C. I. Zoldesi, C. A. van Walree, and A. Imhof. Deformable hollow hybrid silica/siloxane colloids by emulsion templating. *Langmuir*, 22:4343–4352, 2006.

[19] S. Sacanna, W. T. M. Irvine, P. M. Chaikin, and D. J. Pine. Lock and key colloids. *Nature*, 464:575–578, 2010.

[20] N. Doshi, A. S. Zahr, S. Bhaskar, J. Lahann, and S. Mitragotri. Red blood cell-mimicking synthetic biomaterial particles. *Proceedings of the National Academy of Sciences*, 106:21495–21499, 2009.

[21] S. She, Q. Li, B. Shan, W. Tong, and C. Gao. Fabrication of red-blood-cell-like polyelectrolyte microcapsules and their deformation and recovery behavior through a microcapillary. *Advanced Materials*, 25:5814–5818, 2013.

[22] L. Xu, H. Li, X. Jiang, J. Wang, L. Li, Y. Song, and L. Jiang. Synthesis of amphiphilic mushroom cap-shaped colloidal particles towards fabrication of anisotropic colloidal crystals. *Macromolecular Rapid Communications*, 31:1422–1426, 2010.

[23] Y. Y. Lu, M. S. El-Aasser, and J. W. Vanderhoff. Dispersion polymerization of styrene in ethanol: Monomer partitioning behavior and locus of polymerization. *Journal of Polymer Science Part B: Polymer Physics*, 26:1187–1203, 1988.

[24] B. Thomson, A. Rudin, and G. Lajoie. Dispersion copolymerization of styrene and divinylbenzene .2. effect of crosslinker on particle morphology. *Journal of Applied Polymer Science*, 59:2009–2028, 1996.

[25] B. Peng and A. Imhof. Surface morphology control of cross-linked polymer particles *via* dispersion polymerization. *Soft Matter*, 11:3589–3598, 2015.

[26] H. N. W. Lekkerkerker and R. Tuinier. *Colloids and the Depletion Interaction*. Springer Netherlands, 2011.

[27] Y. Wang, Y. Wang, X. Zheng, G.-R. Yi, S. Sacanna, D. J. Pine, and M. Weck. Three-dimensional lock and key colloids. *Journal of the American Chemical Society*, 136:6866–6869, 2014.

[28] S. A. Egorov. Sterically stabilized lock and key colloids: A self-consistent field theory study. *The Journal of Chemical Physics*, 134:194901, 2011.

[29] H. R. Sheu, M. S. El-Aasser, and J. W. Vanderhoff. Phase separation in polystyrene latex interpenetrating polymer networks. *Journal of Polymer Science Part A: Polymer Chemistry*, 28:629–651, 1990.

[30] H. R. Vutukuri, A. F. Demirörs, B. Peng, P. D. J. vanOostrum, A. Imhof, and A. vanBlaaderen. Colloidal analogues of charged and uncharged polymer chains with tunable stiffness. *Angewandte Chemie International Edition*, 51:11249–11253, 2012.

[31] A. van Blaaderen, M. Dijkstra, R. van Roij, A. Imhof, M. Kamp, B. W. Kwaadgras, T. Vissers, and B. Liu. Manipulating the self assembly of colloids in electric fields. *The European Physical Journal Special Topics*, 222:2895–2909, 2013.

[32] B. Peng, H. R. Vutukuri, A. van Blaaderen, and A. Imhof. Synthesis of fluorescent monodisperse non-spherical dumbbell-like model colloids. *Journal of Materials Chemistry*, 22:21893–21900, 2012.

[33] S. Frank, V. Hanumantha Rao, I. Arnout, B. Alfons van, and D. Marjolein. Self-assembly of colloidal particles into strings in a homogeneous external electric or magnetic field. *Journal of Physics: Condensed Matter*, 24:464113, 2012.

[34] M. Kamp, N. A. Elbers, T. Troppenz, A. Imhof, M. Dijkstra, R. van Roij, and A. van Blaaderen. Electric-field-induced lock-and-key interactions between colloidal spheres and bowls. *Chemistry of Materials*, 28:1040–1048, 2016.

Chapter 3

# Self-Assembly of One-Dimensional Aggregates from Spherical Colloids with Electrostatic Repulsion and Hydrophobic Attraction

ABSTRACT

We report the spontaneous formation of one-dimensional aggregates of aqueous dispersions of spherical colloidal particles. The one-dimensional aggregates resemble the structure of a so-called Bernal spiral. The observations can in principle be explained by a combination of short-range hydrophobic attraction and relatively longer-range electrostatic repulsion between the colloids. The hydrophobic attraction originates from the slightly hydrophobic layer grafted on the colloids surface. As far as we are aware, this is the first experimental observation of such structure in aqueous colloidal dispersions. Considering that several proteins can also spontaneously form one-dimensional assemblies, our system could be a model system to study the microscopic mechanism of protein aggregation.

## 3.1 Introduction

The assembly of colloids is not only an important process towards the development of functional materials for practical applications such as in the areas of photonics, sensing and catalysis, but also gives fundamental insight in, for example, phase behavior of atoms and molecules [1–6]. A significant challenge in this area is to spontaneously assemble the colloids into well-defined and sophisticated super-structures. The structures of the assemblies are in principle determined by the particles shape and the interparticle interactions. By altering the particles shape, i.e., introducing a shape anisotropy on the particles, assemblies with various super-structures can be formed, such as colloidal micelles [7], microcapsules [8], free-standing monolayers [9] and colloidal chains [10]. For spherical particles, the super-structures can be achieved by introducing patches on the particles that are attractive or repulsive towards patches present on the other particles. By introducing these patches, the interactions between the particles become directional, which eventually result in the formation of the super-structures, like colloidal kagome lattice [11], supracolloidal helices [12, 13], and colloidal molecules [14].

In order to obtain super-structures from spherical colloids with isotropic shape and surface functionality, several other strategies have been developed, such as by using the dipolar-dipolar interaction which is intrinsically anisotropic [15–17], or *via* the anisotropic re-arrangement of the surface layer [18–20]. By following these strategies, elongated colloidal chains can be formed. Another elegant approach to assemble isotropic colloids into the elongated colloidal chains is by delicately tuning the balance of short-range attraction and long-range repulsion among the colloids. Theory [21] and simulation [22, 23] studies have shown that elongated colloidal chains can be formed when short-range attraction is complemented by a long-range repulsion and these two interactions are elaborately balanced. This was also confirmed experimentally [24, 25], where electrostatic interaction and depletion interaction were applied as the long-range repulsion and the short-range attraction, respectively. However, a mixture of cyclohecyl bromide and *cis*-decalin was used as the solvent.

Proteins consist of one or more long chains of amino acid residues and contain both positive and negative charges (referred to as 'amphoteric'), hydrophobic moieties, and are flexible which allow them to deform upon assemble (deformable). By a combination

of these characteristics, proteins can self-assemble into a variety of structures such as microcapsules and linear chains [26–29].

In this chapter, inspired by proteins, we design and synthesize a type of colloids that bear all of the above characteristics of proteins: deformability (D), amphotericity (A) and hydrophobicity (H), which are named as CPS-DAH. We find that these colloids CPS-DAH can self-assemble into one-dimensional aggregates in aqueous conditions, similar to some proteins [26, 28–30]. To gain insight into the influence of each of these characteristics on the formation of one-dimensional aggregates, we first design and synthesize a series of control colloids with one or two of the above characteristics. By comparing the assembly results of these control colloids with the one-dimensional aggregates, we comprehend the importance of the overall charges and the hydrophobic layer, while the deformability is not prerequisite. Second, we conduct two additional experiments to further investigate the influence of the electrostatic repulsion and the hydrophobic attraction on the one-dimensional aggregates formation. In the first experiment, we study the influence of the electrostatic repulsion by addition of salt. In the second experiment, we systematically tune the magnitude of the electrostatic repulsion and hydrophobic attraction. Lastly, based on the above results, we hypothesize that the delicate balance of the short-range hydrophobic attraction and the relatively longer-range electrostatic repulsion is responsible for the formation of the one-dimensional aggregates.

## 3.2 Experimental Section

### 3.2.1 Materials

Styrene (St, 99%), divinylbenzene (DVB, 55% mixture of isomers, tech. grade), 4-vinylbenzyl chloride (VBC, $\geq$ 90%, tech. grade), dimethylformamide (DMF, $\geq$ 99%), acetonitrile (MeCN, GC, $\geq$ 99.5%), *t*-butyl acrylate (tBA, 98%), copper bromide (Cu(I)Br, 98%), 2,2'-bipyridyl (Bpy, Reagentplus, 99%), *N*,*N*,*N*',*N*'*N*"-pentamethyldiethylenetriamine (PMDETA, 99%), *n*-butylamine (Bu-$NH_2$, 99.5%), *N*,*N*-dimethyldodecylamine (DMDA, 97%), fluorescein sodium salt (used as fluorescent tracer), rhodamine B (for fluorescence), trifluoroacetic acid (TFA, Reagentplus, 99%) were obtained from Sigma-Aldrich. Sodium dodecyl sulfate (SDS) from BDH was

used. Tetrahydrofuran (THF, for analysis, ACS), dimethyl sulfoxide (DMSO, 99.7%), sodium bisulfite ($NaHSO_3$, ACS reagent) and potassium persulfate (KPS, > 99% for analysis) were purchased from Acros Organics. Ethanol (p.a., ACS reagent) was purchased from Merck. Methanol (exceeds ACS specifications) was obtained from J.T. Baker. Triethylamine (TEA, puriss. p.a.; $\geq$ 99.5%) was obtained from Fluka. All chemicals were used as received. The water used throughout all of the synthesis was purified using a Milli-Q water purification system.

### 3.2.2 Synthesis of negatively charged chlorinated polystyrene colloids (CPS-Cl)

CPS-Cl colloids were kindly provided by Bas van Ravensteijn and were synthesized by seeds emulsion polymerization. A 500 mL round-bottom flask equipped with a stir bar was placed in an oil bath of 80 °C. 200 mL water was charged into the reactor and allowed to reach the bath temperature. 21.15 g styrene, 0.635 g DVB, and 0.125 g SDS dissolved in 25 mL water were added, followed by 25 mL rinse water. The complete mixture was allowed to heat up to the temperature of the bath. Polymerization was initiated by addition of 0.78 g KPS dissolved in 37.5 mL water. Reaction was allowed to continue for 24 hours. The obtained particles were used as seeds for the preparation of CPS-Cl. 25 mL of the above crude emulsion and 10 mL of water were introduced into a 50 mL three-neck round-bottom flask equipped with a magnetic stir bar. This emulsion was bubbled with nitrogen for 30 minutes at room temperature. Subsequently, 1 mL VBC mixed with 20 $\mu$L DVB was injected while the flask remained under inert atmosphere. The seeds were swollen for 1 hour, after which the temperature was raised to 60 °C. When this temperature was reached, the initiator solution of 0.04 g KPS, 0.03 g sodium bisulfite and 2.5 mL water was injected. After 4 hours the reaction was stopped. The final product was washed with ethanol and water twice respectively. Finally, the particles were stored in water.

### 3.2.3 Synthesis of deformable amphoteric hydrophobic colloids (CPS-DAH)

Typically, 14 mg BPy and 6.5 mg Cu(I)Br were added in a small, oven-dried Schlenk flask, after which the flask was carefully degassed by evacuation and refilling with nitrogen three times. In another oven-dried Schlenk flask, 1 mL DMF and 73 $\mu$L tBA were added, and the flask was subjected to the same degassing process. Subsequently, the mixture of monomer and solvent was carefully transferred into the flask containing BPy and Cu(I)Br by a syringe equipped with a long needle, followed by an additional degassing cycle. Subsequently, 1 mL degassed CPS-Cl dispersion in DMF (solid content = 1%) was injected into the above dispersion by a syringe also equipped with a long needle. Upon mixing, the mixture became dark brown. After a final degassing process, the reaction flask was placed in an oil bath of 90 °C for 24 h. The ATRP reaction was quenched by exposing the dispersion to air. The product was washed several times with methanol, 50 mM aqueous $NaHSO_3$ solution and water sequentially, and finally the particles were dispersed in water.

The ATRP reactions were monitored in time by withdrawing samples from the reaction mixture. The samples were directly quenched, washed, and subsequently analyzed by IR spectroscopy and DLS measurements.

### 3.2.4 Synthesis of amphoteric colloids (CPS-A)

35 $\mu$L TEA was injected into 1 mL aqueous CPS-Cl dispersion (solid content = 1%). The mixture was stirred for 24 h at room temperature. The product was washed three times with ethanol and water sequentially, and finally the particles were dispersed in water.

### 3.2.5 Synthesis of deformable amphoteric colloids (CPS-DA)

1 mL aqueous CPS-Cl dispersion (solid content = 1%) was centrifuged and washed with DMF three times and finally dispersed in 1 mL DMF. The CPS-Cl dispersed in DMF was stirred for 24 h at 90 °C. The product was washed three times with DMF and water sequentially, and finally the particles were dispersed in water.

### 3.2.6 Synthesis of deformable colloids (CPS-D)

1 mL aqueous CPS-Cl dispersion (solid content = 1%) was centrifuged and washed with THF three times and finally dispersed in 1 mL THF. The CPS-Cl dispersed in THF was stirred for 24 h at room temperature. The product was washed three times with THF and water sequentially, and finally the particles were dispersed in water.

### 3.2.7 Synthesis of hydrophobic colloids (CPS-H)

The synthesis procedure of CPS-H is essentially the same as described for CPS-DAH (**subsection 3.2.2**), except that the acetonitrile/water mixture (v/v = 8:2) was used as the solvent instead of DMF. Additionally, the reaction temperature was kept at 60 °C to minimize the evaporation of acetonitrile.

### 3.2.8 Synthesis of amphoteric hydrophobic colloids CPS-AH

The synthesis of CPS-AH is also essentially the same as that for CPS-DAH (**subsection 3.2.2**), except that the ethanol/water mixture (v/v = 7:3) was used as the solvent instead of DMF, PMDETA was used as the ligand instead of BPy, and the reaction temperature was kept at 60 °C.

### 3.2.9 Synthesis of colloids CPS-$C_4N$

100 $\mu$L Bu-$NH_2$ was added into 1 mL ethanolic CPS-Cl dispersion (solid content = 1%). The mixture was stirred for 24 h at room temperature. The product was washed three times with ethanol and water sequentially, and finally the particles were dispersed in water.

### 3.2.10 Synthesis of colloids CPS-$C_{12}N$

20 $\mu$L DMDA was added into 2 mL ethanolic CPS-Cl dispersion (solid content = 1%). The mixture was stirred for 24 h at room temperature. During the reaction, aliquots of 100 $\mu$L dispersion were withdrawn from the reaction system at 5 min, 45 min, 60 min, 90 min, 150 min, 180 min and 480 min. The samples were washed three times with ethanol and water sequentially, and finally the particles were dispersed in water.

### 3.2.11 Hydrolysis experiments of hydrophobic layer on colloids CPS-DAH

Typically, 0.5 mL aqueous CPS-DAH dispersion (solid content = 1%) was centrifuged and the supernatant was discarded. The particles were redispersed in 2 mL TFA/water mixture (v/v = 9:1) and stirred for 24 h at room temperature. The product was washed ten times with methanol/water mixture (v/v = 7:3) and water sequentially, and finally the particles were dispersed in water.

### 3.2.12 Procedure for colloids assembly

Typically, the aqueous CPS-DAH dispersion (the solid content is approximately 0.5%) was first sonicated for approximately 30 min to destroy the possible clusters. Subsequently, the sample was centrifuged at 2100 $g$ for 2 h. After centrifugation, the sample was redispersed by manual shaking. Subsequently, 5 $\mu$L of the dispersion was placed on a home-made microscopy cell (for details see the **Characterization subsection**). The samples were directly observed with optical microscopy.

### 3.2.13 Characterization

Transmission electron microscope (TEM) pictures were taken with a Philips Tecnai 10 electron microscope typically operating at 100 kV. The samples were prepared by drying a drop of diluted aqueous dispersion on top of polymer-coated copper grid. In order to freeze-dry TEM samples, 1 $\mu$L dispersion was brought on a polymer coated copper grid. The grid was vitrified in liquid nitrogen and mounted onto a cryo transfer unit which was brought under vacuum of approximately $10^{-4}$ Pa. Temperature was increased to $-90\,^{\circ}$C at $5\,^{\circ}$C/min and kept constant for roughly six hours under vacuum to allow the water to sublimate.

Scanning electron microscopy (SEM) images were taken with a Philips SEM XL FEG 30 typically operating at 5 - 10 kV. The freeze-dried samples of particles were sputter coated with 6 nm platinum prior to imaging.

Energy dispersive X-ray (EDX) spectra were recorded on a TechnaiF20 from FEI with an acceleration voltage of 200 kV. The microscope was equipped with an EDX system from EDAX using Emispec software in STEM mode.

Infrared (IR) spectra were obtained using a PerkinElmer Frontier FT-IR/FIR spectrometer. The attenuated total reflectance (ATR) mode was used. Measurements were carried out on powders obtained by drying the particles dispersion. All the IR spectra were normalized with respect to the polystyrene signal (695 $cm^{-1}$).

Optical microscopy (OM) images were taken with a Nikon Ti-E inverted microscope. The microscope was equipped with a Nikon TIRF NA 1.49 100× oil immersion objective, intermediate magnification of 1.5×, and a Hamamatsu ORCA Flash camera. The used microscopy cell was constructed as follows: all glass slides were cleaned with water, ethanol and Kimtech precision wipes before use. Two coverslip glasses (VWR, #0, 22 × 22 mm) were placed at a distance of approximately 15 mm from each other on a microscope slide (Menzel-Gläser) and fixated using tape. Subsequently, a drop of dispersion was injected in between the coverslips. The sample cell was then closed by taping an additional coverslip (Menzel-Gläser, #1.5, 22 × 22 mm) on top of the two immobilized coverslips. The sample was monitored through the coverslip side of the sample cell.

Confocal microscopy pictures were taken with a Nikon TE 2000U laser scanning confocal microscope equipped with a Nikon C1 scanning head in combination with an Ar-ion laser (488 NM, Spectra Physics), a HeNe laser (543.5 nm, Melles Griot) and an oil immersion lens (100× Nikon Plan Apc, NA 1.4).

The hydrodynamic diameters of the particles were measured using dynamic light scatting (DLS). Measurements were performed on a Malvern Zetasizer Nano instrument. The measurements were taken in seven runs of 15 individual acquisitions at a scattering angle of 173°. The data was analyzed using the cumulant method.

Zeta ($\zeta$) potentials were determined by laser Doppler electrophoresis using the same instrument as used for DLS. Highly diluted, aqueous samples were prepared at various pH values. The radii of particles ($R$) were approximately 200 nm, while the Debye length ($\kappa^{-1}$) is on the order of 100 nm under the conditions at which the electrophoresis measurements were conducted (Milli-Q water). Hence, $\kappa R > 1$, justifying the use of the Smoluchowski limit of the Henry equation to convert the measured electrophoretic mobilites into the reported $\zeta$ potentials [31].

## 3.3 Results and Discussion

### 3.3.1 Synthesis of deformable amphoteric hydrophobic colloids CPS-DAH

In the following we abbreviate deformable, amphoteric and hydrophobic characteristics as D, A and H, respectively. Colloids with all of these three characteristics are named as CPS-DAH, where CPS refers to cross-linked polystyrene. CPS-DAH colloids are synthesized by using chlorinated colloids CPS-Cl (**Appendix 3.1**) as seeds. The preparation involves three processes: the growth of a hydrophobic layer on the seeds *via* an atom transfer radical polymerization (ATRP) reaction, the charge reversal through a Menschutkin reaction, and the formation of a yolk-shell structure by an etching process. These three processes occur simultaneously when dimethylformamide (DMF) is used.

The first role of DMF is that as the solvent for the ATRP reaction used in order to grow a hydrophobic poly(*tert*-butyl acrylate) (PtBA) layer on the surface of the colloids CPS-Cl. ATRP is a commonly employed controlled living radical polymerization method, by which we can easily tune the thickness of the polymer layer that grows onto the colloids *via* tuning the reaction time or the initial monomer concentration during the ATRP process (**Appendix 3.2**) [32–34]. The growth of PtBA layer on the surface of the colloids CPS-Cl is confirmed by Infrared (IR) spectroscopy. Figure 3.1a shows the IR spectra of CPS-Cl and CPS-DAH. Evidently, compared to the spectrum obtained for CPS-Cl, the spectrum of CPS-DAH contains an additional signal at 1726 $cm^{-1}$. This signal corresponds to the C=O stretching vibration of the ester groups of the incorporated tBA, indicating the hydrophobic PtBA layer is grafted onto the colloids [35]. However, since the presence of the Menschutkin reaction which will be discussed in the following paragraph, it is difficult to quantify the grafting density of the hydrophobic polymers and thereafter estimate the hydrophobicity of the colloids. Nevertheless, the observation that the colloids CPS-DAH are well dispersed in water indicates that the colloids are not very hydrophobic. Thus we regard CPS-DAH as being mildly hydrophobic.

The second role of DMF is to alter the surface charge of the colloids by reacting with the benzyl chloride functionalities that are immobilized on the colloids. Van Ravensteijn

et al. reported that the thermal degradation of DMF at elevated temperature generates dimethylamine which can react with benzyl chloride groups [36]. This type of reaction is called Menschutkin reaction and can lead to the formation of a positively charged quaternary amine. In the experimental conditions performed here, sufficient amount of quaternary amines are generated which finally reverse the charge of the colloids. This is confirmed by measuring the $\zeta$ potential of the prepared CPS-DAH. Compared to the $\zeta$ potential of CPS-Cl (-37.9 $\pm$ 3.9 mV), a value of 30 $\pm$ 4 mV is determined for CPS-DAH. This indicates that the charge of the colloids is reversed. However, the experimental conditions in our reaction are not completely the same as that for van Ravensteijn et al.'s situation. A key difference that might also contribute the charge reversal of the colloids is that Cu(I)Br is present in our system, whose complex with the ligand 2,2'-bipyridyl acts as the catalyst for ATRP reaction. The possible adsorption of copper ions onto the colloids might reverse the colloid charge. However, the copper ions adsorption scenario is excluded by energy dispersive X-ray (EDX) measurements (**Appendix 3.3**). Furthermore, even though the overall $\zeta$ potential of CPS-DAH is positive as shown before, the negative charges originating from sulfate groups are still present, therefore we regard CPS-DAH as being amphoteric.

The final role of DMF is that as an etching agent to create a yolk-shell structure of the colloids. A yolk-shell structure refers to a movable yolk inside a hollow shell [37]. DMF is a good solvent for linear polystyrene, dissolution of the linear polystyrene part of CPS-DAH in DMF results in the formation of the yolk-shell structure (**Appendix 3.4**) [38]. Figure 3.1b shows a representative TEM image of the colloids CPS-DAH which displays a yolk-shell structure. The TEM samples are prepared by drying the aqueous colloidal dispersion under atmospheric conditions, unless stated otherwise. The diameters of the whole colloids are 415 $\pm$ 7 nm and the diameters of their inner cores are 251 $\pm$ 8 nm. The colloids have a thin shell with thickness of approximately 45 nm, and the shell slightly shrink and deform which can be ascribed to the drying process of the TEM sample preparation. This shell consists of two parts: an inner layer which originating from the seeds CPS-Cl and an outer layer which is the grafted hydrophobic polymer layer. The thickness of the hydrophobic polymer is approximately 6 nm. Considering the shell is thin and can be deformed, we regard here the colloids with a yolk-shell structure as being deformable.

Figure 3.1c is a schematic illustration of the colloids CPS-DAH that summarizes

all the characteristics discussed before, which are deformability, amphotericity and hydrophobicity, and the corresponding apparatuses that are used to confirm these characteristics.

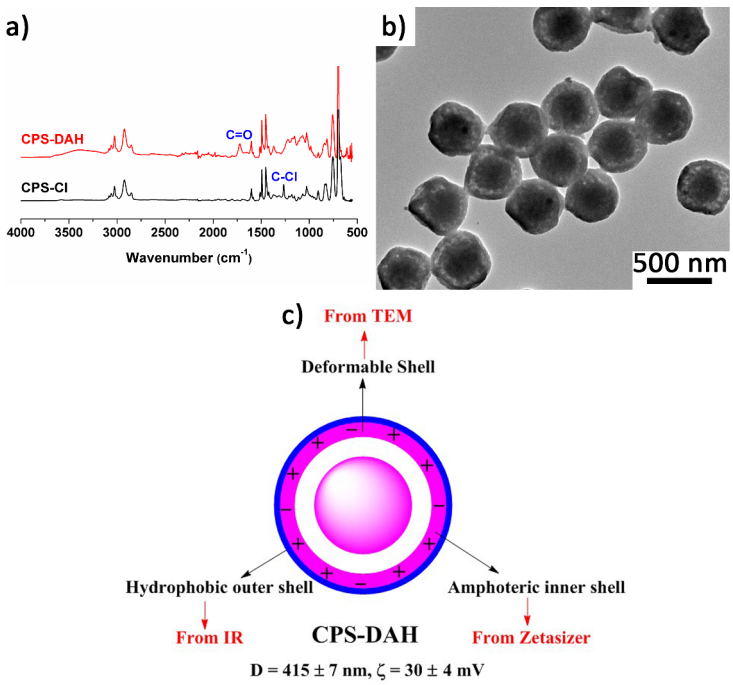


Figure 3.1. (a) Infrared spectra of deformable, amphoteric and hydrophobic colloids CPS-DAH (top, red) and chlorinated colloids CPS-Cl (bottom, black). (b) TEM image of CPS-DAH, the TEM sample was prepared by drying the aqueous colloidal dispersion under atmospheric conditions. (c) schematic illustration of the CPS-DAH that summarizing all the characteristics: Deformability, Amphotericity and Hydrophobicity, and these characteristics are abbreviate as DAH. Scheme also shows the corresponding apparatuses that are used to confirm these characteristics. Scale bar: 500 nm.

### 3.3.2 Assembly and characterization of one-dimensional aggregates

#### 3.3.2.1 Sedimentation induced assembly of Bernal spiral-like structure

Before starting the assembly process, the aqueous CPS-DAH dispersion of approximately 0.5% volume fraction is first sonicated for approximately 30 min to ensure all colloids are well dispersed. Figure 3.2a shows an optical micrograph of the initial aqueous CPS-DAH dispersion, clearly the particles are well dispersed, random aggregates are barely observed. Subsequently, the sample shown in Figure 3.2a is kept at rest for one week. During this period particles gradually sediment due to gravity and finally are concentrated at the bottom. Afterwards, the sample is redispersed by manual shaking and observed with optical microscopy again. As shown in Figure 3.2b, intriguingly, one-dimensional aggregates are formed. These elongated colloidal assemblies are relatively monodisperse in diameter while polydisperse in length. Their diameters are approximately 2 $\mu$m, and their lengths vary between 10 $\mu$m up to 50 $\mu$m. Subsequently, the sample shown in Figure 3.2b is placed in a sonication bath for 15 min to study the stability of the one-dimensional aggregates under sonication. After sonication, the one-dimensional aggregates are still present but with reduced length (Figure 3.2c). To further confirm the one-dimensional nature of the aggregates and obtain more details, the sample is characterized using scanning electron microscopy (SEM). The SEM samples of the assemblies are prepared by a freeze-drying process such that the shrinkage and collapse of the assemblies are prevented [39]. Figure 3.2d and 3.2e show that the one-dimensional assemblies are indeed formed. In the assemblies, the particles are slightly deformed compared to the non-aggregated ones (Figure 3.2e), which might be ascribed to the interparticle forces during the formation process of the one-dimensional aggregates. We observe that the colloids are close-packed and most colloids have six nearest neighbors. Due to the deformation of the colloids, the structure of the aggregates is not perfectly ordered. However, this one-dimensional structure observed here is reminiscent of a so-called Bernal spiral (Figure 3.2f). A Bernal spiral consists of three twisting strands of particles and each particle is in contact with six neighboring particles [12].

The spontaneous formation of the Bernal spiral-like structure is further confirmed by following experiments. The dispersion with the aggregates is slowly centrifuged to

remove the Bernal spiral-like aggregates, and the supernatant containing the separated particles is carefully collected. As shown in Figure 3.17a (**Appendix 3.5**), the colloids are well dispersed and no Bernal spiral-like aggregates are observed. After being kept at rest for one month, once more, the Bernal spiral-like aggregates are formed (Figure 3.17b).

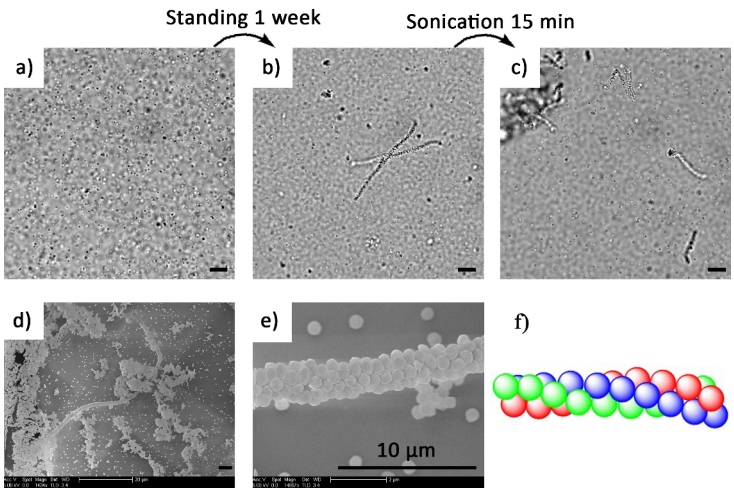


Figure 3.2. (a-c) Optical micrographs of (a) initial CPS-DAH dispersion, (b) sample a after being kept for one week, and (c) sample b after sonicating for 15 min. (d) Low and (e) high magnification of SEM images of the one dimensional colloidal assemblies of CPS-DAH. The SEM samples were prepared by freeze-drying process. (f) Scheme of a Bernal spiral. Scale bars: 10 $\mu$m for all images.

#### 3.3.2.2 Centrifugation induced assembly of tube-like structure

Our results indicate that the densification of colloids CPS-DAH by sedimentation results in the formation of the one-dimensional aggregates. Therefore, in the next step, we employ centrifugation to concentrate the colloids. After centrifugation, the sample is redispersed by manual shaking and observed with optical microscopy again. Surprisingly, except the similar Bernal spiral-like structures as shown in Figure 3.2b, several tube-like structures are also observed (Figure 3.3a and 3.3b). These tube-like assemblies are relatively polydisperse both in diameter and length, their diameters are in the range of 2 to 4 $\mu$m, and their lengths vary between 20 $\mu$m up to

100 $\mu$m. Furthermore, no aggregation between the one-dimensional aggregates after centrifugation are observed, implying the repulsions between the one-dimensional aggregates are sufficiently large. From the optical micrographs, the hollow structure of the aggregates is not obvious. Therefore, confocal microscopy is used in order to visualize the hollow structure of the aggregates. To do so, a small amount of dye is added into the dispersion. After mixing, the samples are imaged with confocal microscopy. Two types of water soluble dyes are used, negatively charged fluorescein sodium salt (Figure 3.3c) and positively charged rhodamine B (Figure 3.3d). Clearly, both samples show the hollow structure of the assemblies with a wall thickness of approximately one colloidal diameter. The hollow structure is further confirmed by scanning the samples in different $z$-values using confocal microscopy (**Appendix 3.6**). The formed one-dimensional aggregates by centrifugation are also robust against sonication, only their lengths are reduced after sonication for 1.5 hour, similar phenomenon to the aggregates obtained by sedimentation. Furthermore, the fact that both negatively charged and positively charged dyes can adsorb on the CPS-DAH indicates that the particles are indeed amphoteric. Additionally, by tuning the composition and the concentration of the initial monomers during the ATRP process, we synthesize CPS-DAH with grafted hydrophobic polymer layer of different thickness and composition. **Appendix 3.7** shows several additional assembly results of these colloids after centrifugation, the tube-like aggregates are found in all samples.

Further experiments show that only for the colloids CPS-DAH regardless of the thickness and composition of the grafted hydrophobic polymer layer, by using centrifugation, Bernal spiral-like aggregates as well as tube-like aggregates are formed. For the rest of colloids (the control colloids in the following subsections, including CPS-AH, CPS-$C_4$N and CPS-$C_{12}$N), centrifugation can only accelerate the formation of the Bernal spiral-like aggregates, no tube-like aggregates are observed.

Regardless of the assembly methods (sedimentation or centrifugation) and the assembly structures (Bernal spiral-like or tube-like), we observe that the formed one-dimensional aggregates are quite stable. No attachment of the colloids on or detachment of the colloids from the aggregates are observed during an observation time of approximately 1 hour, suggesting that these one-dimensional aggregates are irreversibly formed.

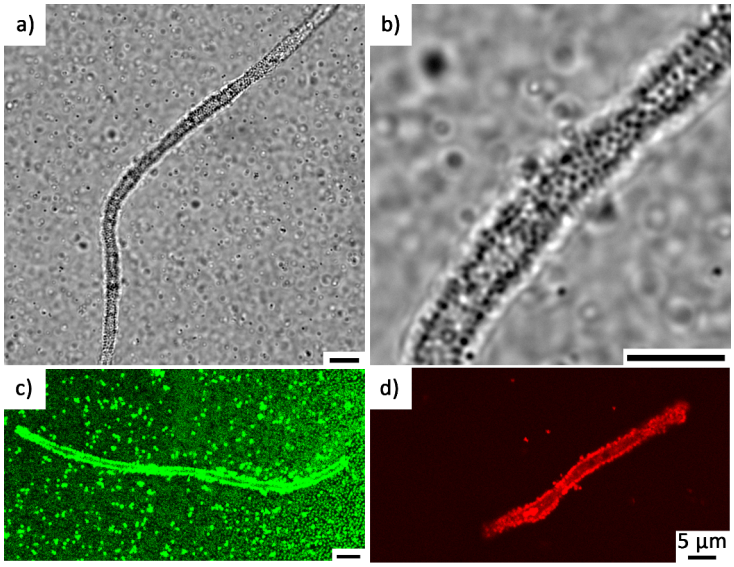


Figure 3.3. (a) Low and (b) high magnification of optical micrographs of the tube-like colloidal assemblies of CPS-DAH, (c) fluorescein sodium salt and (d) rhodamine B dyed confocal micrographs of the tube-like colloidal assemblies of CPS-DAH. Scale bars: 5 $\mu$m for all images.

### 3.3.3 Synthesis of control colloids

We conclude from the previous sections that deformable, amphoteric and hydrophobic colloids CPS-DAH self-assemble into one-dimensional colloidal aggregates. To gain insight into what characteristics are responsible for the formation of the one-dimensional assemblies and thereafter propose a possible mechanism, a series of control colloids with one or two of the above characteristics are designed and synthesized.

#### 3.3.3.1 Synthesis of deformable amphoteric colloids CPS-DA

To synthesize CPS-DA, CPS-Cl are dispersed in DMF and heated to 90 °C for 24 h. As discussed before, under these conditions, DMF will etch the linear polystyrene part of CPS-Cl to generate the yolk-shell structure, as well as react with benzyl chloride groups to reverse the charge of the colloids. Figure 3.4a shows a representative TEM image of CPS-DA which reveals their yolk-shell structure with an outer diameter of

392 ± 7 nm, while the diameter of their inner cores is 258 ± 11 nm. The shell thickness of the CPS-DA is approximately 44 nm. Electrophoretic mobility measurements reveal a positive $\zeta$ potential of CPS-DA equal to 37.4 ± 4.5 mV. These results show that the CPS-DA with deformable and amphoteric characteristics are synthesized.

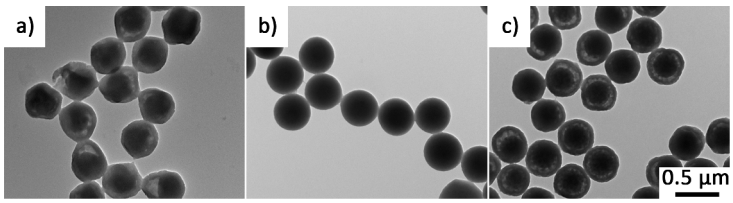


Figure 3.4. TEM images of (a) deformable amphoteric colloids CPS-DA, (b) amphoteric colloids CPS-A, and (c) deformable colloids CPS-D. Scale bars: 0.5 $\mu$m for all images.

#### 3.3.3.2 Synthesis of amphoteric colloids CPS-A

To exclusively reverse the charge of the colloids without etch the colloids, DMF is avoided to use. Van Ravensteijn et al. showed that the colloids charge can also be reversed when the Menschutkin reaction is performed in water with the presence of amines [36]. Therefore CPS-A are synthesized by dispersing CPS-Cl in water and reacting the benzyl chloride groups of CPS-Cl with triethylamine at room temperature for 24 h. Figure 3.4b shows that the colloids CPS-A maintain their morphology, since no yolk-shell structure is observed. This is expected as water is a bad solvent for polystyrene, no etching process would occur. Diameter of 420 ± 7 nm is measured for this type of colloids from TEM images. It has a $\zeta$ potential of 46.9 ± 6 mV obtained by electrophoretic mobility measurements, indicating that charge reversal of the colloids is indeed successful. These results show that the CPS-A with merely amphoteric characteristic are synthesized.

#### 3.3.3.3 Synthesis of deformable colloids CPS-D

To synthesize CPS-D, CPS-Cl are dispersed in THF and magnetically stirred at room temperature for 24 h. Herein THF is used instead of DMF as THF can also etch the linear polystyrene part of CPS-Cl while no reaction occurs between THF and benzyl chloride groups. Indeed colloids with a yolk-shell structure are observed (Figure 3.4c).

The obtained colloids have an outer diameter of 398 ± 7 nm, and the diameter of their inner cores is 257 ± 10 nm. The shell thickness of the CPS-D is approximately 40 nm. Electrophoretic mobility measurements reveal a negative ζ potential of CPS-D equal to -42.8 ± 4.75 mV. These results indicate that the CPS-D with only deformable characteristic are prepared.

#### 3.3.3.4 Synthesis of hydrophobic colloids CPS-H

ATRP reaction is employed to grow a hydrophobic poly(*tert*-butyl acrylate) (PtBA) layer on the surface of CPS-Cl. To avoid both the etching of the colloids and the reversal of their charge, acetonitrile/water mixture (v/v = 8:2) is used as the solvent instead of DMF to synthesize CPS-H. Since acetonitrile is volatile, relatively low reaction temperature is required to limit its evaporation (60 °C in this case instead of 90 °C in DMF). The other parameters are kept constant. Figure 3.5a shows a representative TEM image of CPS-H, as expected, no yolk-shell structure is observed. The CPS-H have a diameter of 434 ± 9 nm. The presence of the hydrophobic layer is confirmed by IR spectroscopy. Figure 3.5b shows the IR spectra of CPS-Cl and CPS-H. Evidently, compared to the spectrum obtained for CPS-Cl, the spectrum of CPS-H contains an additional signal at 1726 $cm^{-1}$ which corresponds to the C=O stretching vibration of the incorporated tBA, indicating a thin hydrophobic PtBA is grew on the colloids. Additionally, its ζ potential remains negative with value of -31 ± 4 mV, which is obtained by electrophoretic mobility measurements. These results show that the CPS-H with only hydrophobic characteristic are prepared.

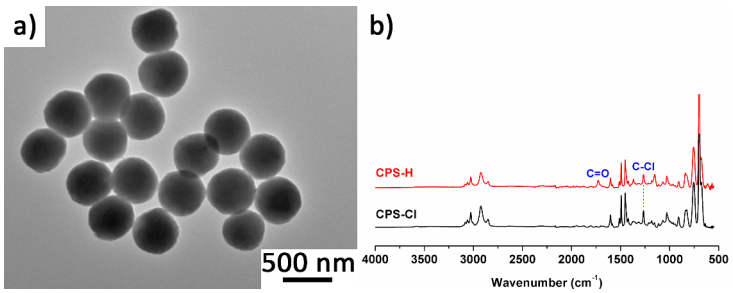


Figure 3.5. (a) TEM image of hydrophobic colloids CPS-H. (b) Infrared spectra of CPS-H (top, red) and CPS-Cl (bottom, black). Scale bar: 500 nm.

#### 3.3.3.5 Synthesis of deformable hydrophobic colloids CPS-DH

We have endeavored to perform ATRP reaction in THF to synthesize the deformable hydrophobic colloids CPS-DH. In principle, we would obtain CPS-DH, since ATRP reaction allows us to grow a hydrophobic PtBA layer and THF etches the colloids. However, in practice, this direct synthesis method becomes problematic, since THF rapidly evaporates during the degassing process due to its high vapor pressure. Therefore, CPS-DH is prepared indirect, which is achieved through the etching of CPS-H by THF. Figure 3.6a shows a representative TEM image of CPS-DH, which reveals that monodisperse colloids with a diameter of 416 ± 8 nm are obtained. The reduced diameter of the CPS-DH compared to that for CPS-H (434 ± 9 nm) confirms that the etching process has taken place. However, the etching process is incomplete as can be seen in Figure 3.6a, less hollow areas are present compared to that for CPS-D (Figure 3.4c), which might due to the presence of the hydrophobic layer that limits the diffusion of the dissolved polystyrene from the colloids interior into the continuous phase. Furthermore, the remaining of the C=O stretching vibration signal at 1726 $cm^{-1}$ in the IR spectrum of CPS-DH verifies that the hydrophobic PtBA layer still exists on the colloids after the etching process (Figure 3.6b). Therefore, these results show that the deformable hydrophobic colloids CPS-DH are synthesized.

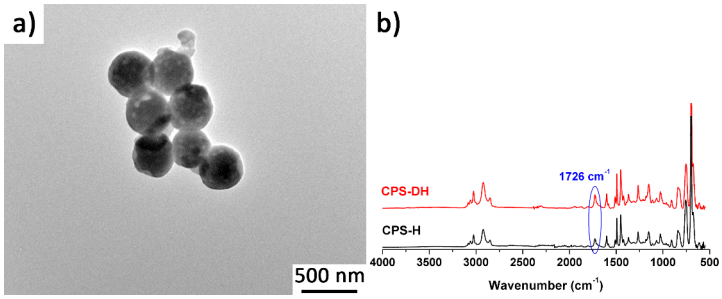


Figure 3.6. (a) TEM image of deformable hydrophobic colloids CPS-DH. (b) Infrared spectra of CPS-DH (top, red) and CPS-H (bottom, black). The blue circle highlighted the signal of the C=O stretching vibration. Scale bar: 500 nm.

### 3.3.3.6 Synthesis of amphoteric hydrophobic colloids CPS-AH

Once more an ATRP reaction is employed to grow a hydrophobic PtBA layer on the surface of CPS-Cl to obtain CPS-AH. In this case, ethanol/water (v/v = 7:3) is used as the solvent instead of DMF to avoid the etching of the colloids. More importantly, *N*,*N*,*N*',*N*'*N*"-pentamethyldiethylenetriamine (PMDETA) is used as the ligand instead of 2,2'-bipyridyl (Bpy), since the catalytic reactivity of the complex of PMDETA with copper ions is higher than that of Bpy with copper ions, such that compromises the relatively low reactivity of ATRP reaction in ethanol/water mixture [40]. Furthermore, PMDETA also serves as the amines source to react with benzyl chloride groups thereby introduce positive charges onto the colloids. Figure 3.7a shows a representative TEM image of CPS-AH, as expected, no yolk-shell structure is observed. The CPS-AH have a diameter of 436 ± 8 nm. The presence of the hydrophobic layer is confirmed by IR spectroscopy. Figure 3.7b shows the IR spectra of CPS-Cl and CPS-AH. Once more, an additional signal at 1726 $cm^{-1}$ which corresponds to the C=O stretching vibration of the incorporated tBA is observed in the spectrum of CPS-AH. Additionally, an extra strong signal at 1093 $cm^{-1}$ is appeared in the spectrum of CPS-AH, which corresponds to the C-N stretching vibration from the PMDETA, indicating the reaction between the benzyl chloride groups on the CPS-Cl and the amine groups of PMDETA takes place[35]. The occurrence of this Menschutkin reaction is further confirmed by electrophoretic mobility measurements. The charge of CPS-AH is indeed reversed, as indicated by its ζ potential of 35.5 ± 4.7 mV. These results show that the CPS-AH with amphoteric and hydrophobic characteristics are prepared.

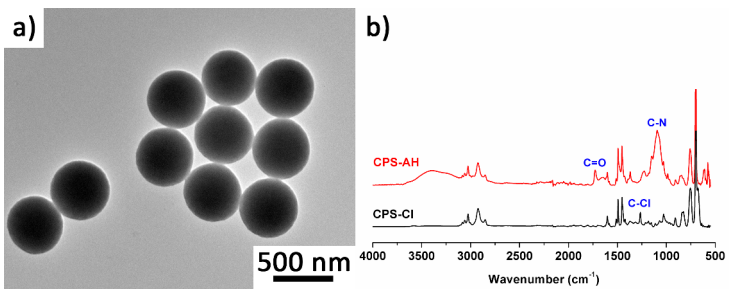


Figure 3.7. (a) TEM image of hydrophobic colloid CPS-AH. (b) Infrared spectra of CPS-AH (top, red) and CPS-Cl (bottom, black). Scale bar: 500 nm.

Table 3.1 summarizes the characteristic properties of the synthesized control colloids.

Table 3.1. Summary of the deformability, amphotericity and hydrophobicity of the synthesized control colloids

| Colloids | Deformability | Amphotericity | Hydrophobility |
|---|---|---|---|
| CPS-DAH | √ | √ | √ |
| CPS-Cl | × | × | × |
| CPS-A | × | √ | × |
| CPS-DA | √ | √ | × |
| CPS-D | √ | × | × |
| CPS-H | × | × | √ |
| CPS-DH | √ | × | √ |
| CPS-AH | × | √ | √ |

### 3.3.4 Assembly of control colloids

In this subsection, we show the assembly results of the above synthesized control colloids. Even though the Bernal spiral-like aggregates formation is a spontaneous process, the centrifugation assembly process is employed in all of the samples here since this process accelerates the Bernal spiral-like aggregates formation. For comparison, the assembly results of CPS-Cl as well as CPS-DAH are also included here. As shown in Figure 3.8, three scenarios of assembly behaviors of the colloids are observed. Firstly, for the cases of CPS-Cl (Figure 3.8a), CPS-A (Figure 3.8b), CPS-D (Figure 3.8c) and CPS-DA (Figure 3.8d), the colloids remain dispersed and no clusters are found. Secondly, for CPS-H (Figure 3.8e) and CPS-DH (Figure 3.8f), the colloids form random aggregates and few individual colloids remain. Lastly, for CPD-AH (Figure 3.8g) and CPS-DAH (Figure 3.8h), Bernal spiral-like aggregates are present regardless of the presence of many individual colloids.

#### 3.3.4.1 Influence of the hydrophobicity

The influence of the hydrophobicity on the formation of the Bernal spiral-like aggregates is firstly studied by comparing Figure 3.8a-3.8d to Figure 3.8e-3.8h. Clearly, the

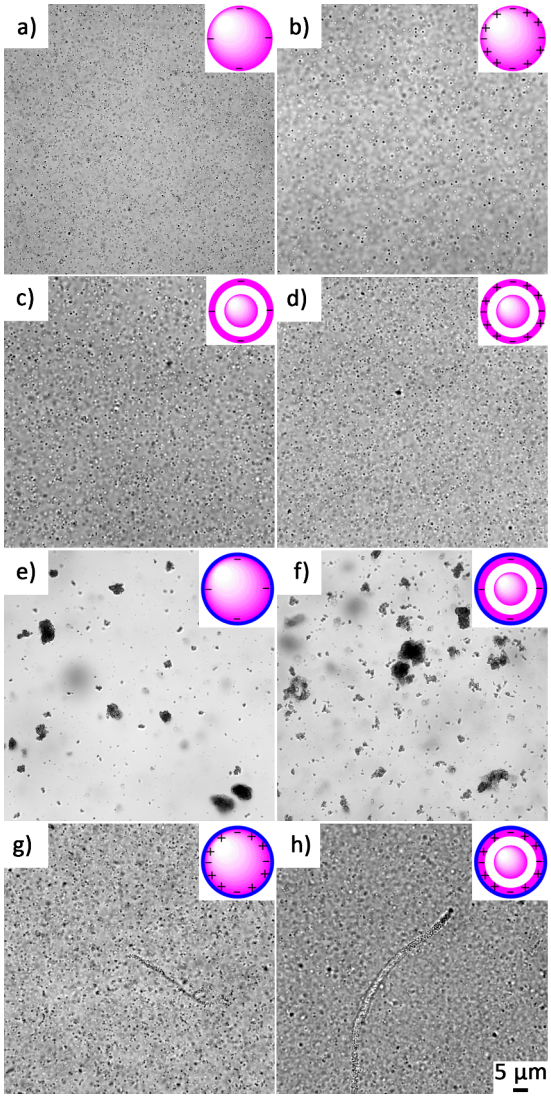


Figure 3.8. Optical micrographs of the assembly results of (a) Seeds CPS-Cl, (b) Amphoteric colloids CPS-A, (c) Deformable colloids CPS-D, (d) Deformable and amphoteric colloids CPS-DA, (e) Hydrophobic colloids CPS-H, (f) Deformable and hydrophobic colloids CPS-DH, (g) Amphoteric and hydrophobic colloids CPS-AH and (h) Deformable, amphoteric and hydrophobic colloids CPS-DAH after the centrifugation assembly process. Scale bars: 5 $\mu$m for all images.

colloids with a hydrophobic layer tend to aggregate in all cases regardless of the final aggregation morphologies (one-dimensional aggregates or random clusters), while the colloids are still well dispersed if the hydrophobic layer is absent. To further confirm that the colloids aggregation is driven by the hydrophobic attraction, CPS-DAH and CPS-H are treated with trifluoroacetic acid (TFA). TFA is commonly used as a strong acid to hydrolyze the ester groups in the PtBA, thereby converting hydrophobic PtBA into hydrophilic polyacrylic acid (PAA) (**Appendix 3.8**) [41]. After hydrolysis, the colloids are subjected to the same centrifugation assembly process as described before. As shown in Figure 3.9, after hydrolysis, for CPS-DAH (Figure 3.9a), the Bernal spiral-like aggregates are still present while the diameter and length of these Bernal spiral-like aggregates are approximately 2 $\mu$m and 5 $\mu$m, respectively, both are much smaller compared to that for the Bernal spiral-like aggregates before hydrolysis (Figure 3.8h). For CPS-H (Figure 3.9b), after hydrolysis, colloids disperse much better compared to that before hydrolysis (Figure 3.8e). However, in both samples, some small aggregates are still observed. The presence of these small aggregates could be ascribed to the incomplete hydrolysis of the ester groups on the colloids (**Appendix 3.8**), i.e., the presence of the hydrophobic patches. Regardless of the presence of small amount of the small clusters, in both systems the colloids disperse much better than before hydrolysis. Based on these results, we conclude that the hydrophobic layer on the colloids is essential for the formation of the Bernal spiral-like aggregates, which acts as a driving force for the colloids to aggregate.

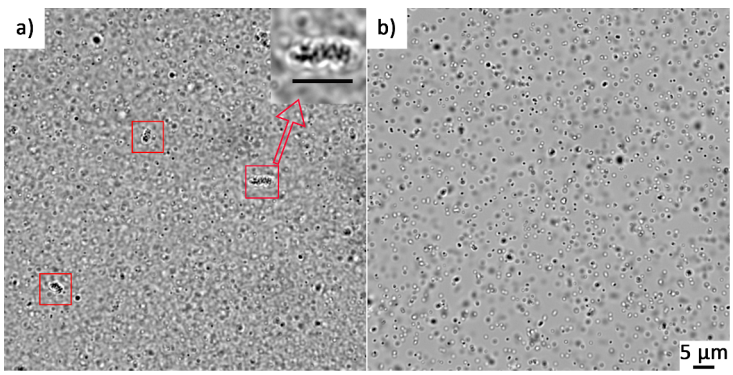


Figure 3.9. Optical micrographs of (a) CPS-DAH and (b) CPS-H after hydrolyzed with trifluoroacetic acid. Scale bars: 5 $\mu$m for all images.

#### 3.3.4.2 Influence of the amphotericity

The influence of the amphotericity on the Bernal spiral-like aggregates formation is studied by comparing Figure 3.8e-3.8f to Figure 3.8g-3.8h. The colloids with amphoteric characteristic can assemble into Bernal spiral-like aggregates, while for negatively charged colloids random clusters are observed. To further investigate the influence of the amphotericity, we design and synthesize a new type of colloids CPS-$C_4$N. These colloids are prepared by reacting benzyl chloride groups on the CPS-Cl with a primary amine *n*-butylamine (Bu-$NH_2$). The synthesized colloids also bear both amphoteric and hydrophobic characteristics as CPS-AH. However, the significant difference between CPS-$C_4$N and CPS-AH is that the CPS-$C_4$N is pH-responsive, it protonates at low pH while deprotonates at high pH ($pKa$, $_{N-\text{methylbutylamine}} \approx 10.9$). Therefore, at low pH, the colloids CPS-$C_4$N are amphoteric and overall positively charged; at high pH, they are non-amphoteric and overall negatively charged. If the amphotericity is prerequisite, we would expect that at high pH where CPS-$C_4$N are non-amphoteric (pH $> pKa$, $_{N-\text{methylbutylamine}}$), no Bernal spiral-like aggregates should be observed. As shown in Figure 3.10, clearly, Bernal spiral-like aggregates are observed both at low (Figure 3.10a) and high (Figure 3.10c) pH, indicating that the amphotericity is not a prerequisite for the formation of the Bernal spiral-like aggregates. While at pH 11, the colloids strongly aggregate (Figure 3.10b). Because of the aggregation, the $\zeta$ potential at pH 11 by electrophoretic mobility measurements cannot be determined accurately. However, a rough estimate is possible. In pure water (pH $\approx 6$), both sulfate groups (pH $>>$ $pKa$, $_{\text{sulfate}} \approx 2$) [42] and amine groups (pH $<<$ $pKa$, $_{N-\text{methylbutylamine}} \approx 10.9$) [43] are highly charged. The $\zeta$ potential of CPS-Cl and CPS-$C_4$N in pure water are -37.9 and 50.1 mV, respectively. Therefore, the total number of positively chargeable groups on the colloids CPS-$C_4$N is approximately twice the total number of negatively chargeable groups. At pH 11 (pH $\approx pKa$, $_{N-\text{methylbutylamine}}$), approximately half of the amine groups are deprotonated while most of the sulfate groups are still charged, therefore the overall charge is approximately zero, suggesting the lack of the effective electrostatic repulsion which results in the random aggregation of the colloids. These results show that it is the overall charge rather than the amphotericity of the colloids finally determines the aggregation behaviors. In other words, the electrostatic interaction plays a significant role in the Bernal spiral-like aggregates formation.

Furthermore, we also notice that in pure water, except the relatively rigid Bernal spiral-like aggregates, flexible colloidal single chains with diameter of only one colloid are also observed (Figure 3.11a). While at pH 11.7, except the relatively rigid Bernal spiral-like aggregates, some spherical aggregates instead of colloidal single chains are observed.

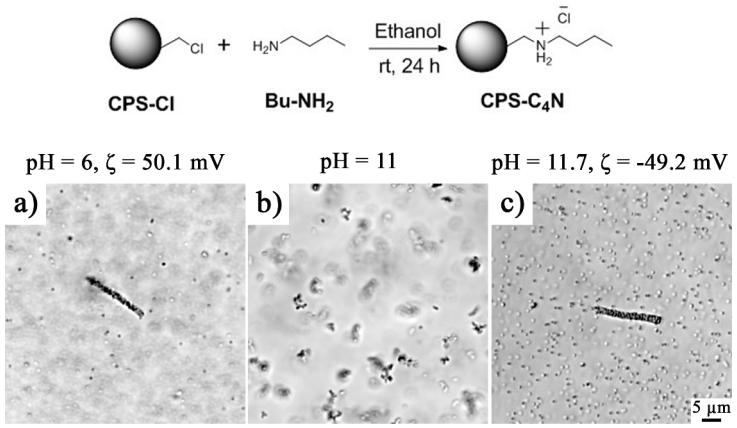


Figure 3.10. Optical micrographs of *n*-butylamine modified CPS-Cl (CPS-$C_4$N) in aqueous solution with pH (a) 6, (b) 11 and (c) 11.7, respectively. Scale bars: 5 $\mu$m for all images.

### 3.3.4.3 Influence of the deformability

While no noticeable differences of aggregation behavior are observed with respect to the deformability of the colloids (Figure 3.8a and 3.8c, 3.8b and 3.8d, 3.8e and 3.8f, or 3.8g and 3.8h). For instance, both CPS-AH (Figure 3.8g) and CPS-DAH (Figure 3.8h) form the one-dimensional aggregates after the assembly process even though the former is not deformable while the latter is. Therefore, we exclude the deformability as the most important characteristic to lead to the formation of the one-dimensional aggregates.

## 3.3.5 Two additional experiments

### 3.3.5.1 Influence of ionic strength on clusters structure

The increase of ionic strength results in the decrease of the electrostatic repulsion with respect to both its range and magnitude. Therefore, if sufficient amount of salt is added, the electrostatic repulsion will not be strong enough to stabilize the formed one-dimensional assemblies, and hydrophobic attraction is expected to dominate. In such conditions it is expected that the one-dimensional assemblies collapse into more compact aggregates. To confirm our hypothesis, the ionic strength of the dispersion with colloidal single chains is tuned to 2 mM by addition of aqueous NaCl solution. As shown in Figure 3.11, after increasing the ionic strength, the colloidal single chains collapse and indeed transform into spherical clusters.

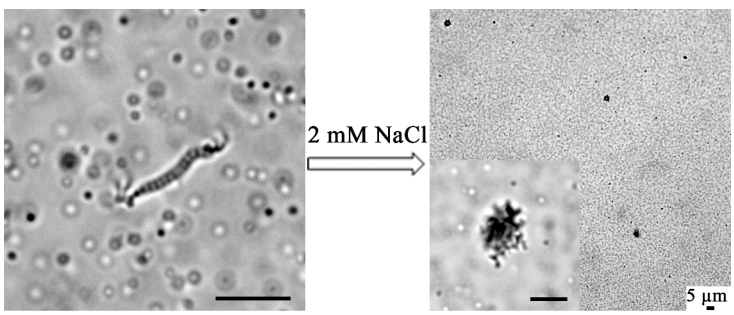


Figure 3.11. Optical micrographs of $n$-butylamine modified CPS-Cl in (left) Pure water and (right) 2 mM aqueous NaCl solution. Scale bars: 5 $\mu$m for all images.

### 3.3.5.2 Influence of magnitude variation of electrostatic repulsion and hydrophobic attraction on clusters structure

The morphology and surface property of the colloids CPS-DAH are complex and not well-defined. Even without the addition of TFA, the ester groups on the grafted PtBA polymers hydrolyze gradually in water (**Appendix 3.9**). The hydrolysis of the ester groups generates carboxylic acids, which results in the decrease of the hydrophobicity and increase of the number of negatively charged carboxylic acid groups. Furthermore, the influence of the yolk-shell structure on the formation of the one-dimensional

aggregates is not fully understood and difficult to investigate. Therefore, we have endeavored to design a new type of colloids: CPS-$C_{12}$N. These colloids are synthesized by the Menschutkin reaction between the benzyl chloride groups on the colloids CPS-Cl and *N*,*N*-Dimethyldodecylamine (DMDA) in ethanol at room temperature. By doing so, there are several advantages. Firstly, the ATRP reaction step is avoided, which makes the synthetic process much easier. Secondly, the hydrophobicity is introduced by the $C_{12}$ moiety of the DMDA, no ester groups are present in the DMDA, and therefore no hydrolysis reaction of ester groups takes place to complicate the surface properties of the colloids. Thirdly, by performing the Menschutkin reaction in ethanol, the morphology of the colloids remains intact, and no yolk-shell structure will be formed. Lastly and most importantly, by withdrawing samples at different time intervals during the reaction, we can obtain colloids with systematically changed $\zeta$ potential and hydrophobicity. That would be prohibitively difficult for CPS-DAH as the ATRP reaction is extremely sensitive towards oxygen, while oxygen is hard to avoid during the withdrawal step. In other words, the electrostatic repulsion and the hydrophobic attraction between the colloids can be systematically regulated by using the Menschutkin reaction. Figure 3.12 summarizes the results. At the very beginning state, the conversion of the Menschutkin reaction is low, the overall charges are still highly negative and the grafting degree of the hydrophobic groups is low, hence the electrostatic repulsion still overwhelms the hydrophobic attraction and van der Waals attraction. Therefore the colloids are well dispersed, and no aggregates are formed (Figure 3.12a and 3.12b). With the Menschutkin reaction proceeding, more positive charges are generated, the overall charges decrease and the $\zeta$ potential approaches to zero after about 60 min, where the magnitude of the electrostatic repulsion is minimal. At the same time, the hydrophobic attraction constantly increases since more hydrophobic groups are grafted onto the colloidal surface. The combination of the reduced electrostatic repulsion and the increased hydrophobic attraction results in the aggregation of the colloids (Figure 3.12c-3.12e). Since in these conditions the electrostatic repulsion is too weak to overcome the hydrophobic attraction and van der Waals attraction, colloids randomly aggregate. As the reaction continues, the charge sign reverses and the overall charges increase again, the increase of the charges results in the increase of the electrostatic repulsion, therefore the colloids start to re-disperse again. At the conditions where the electrostatic repulsion and the

hydrophobic attraction are appropriately balanced, one-dimensional aggregates are formed (Figure 3.12g and 3.12h).

Furthermore, we also study the time-dependent evolution of the aggregation behavior of the CPS-DA (**Appendix 3.10**). In this case, the hydrophobic attraction is absent. After charge reversal, colloids are well dispersed and no one-dimensional aggregates are observed. This set of experiments further confirms the importance of the hydrophobic attraction on the formation of the one-dimensional aggregates.

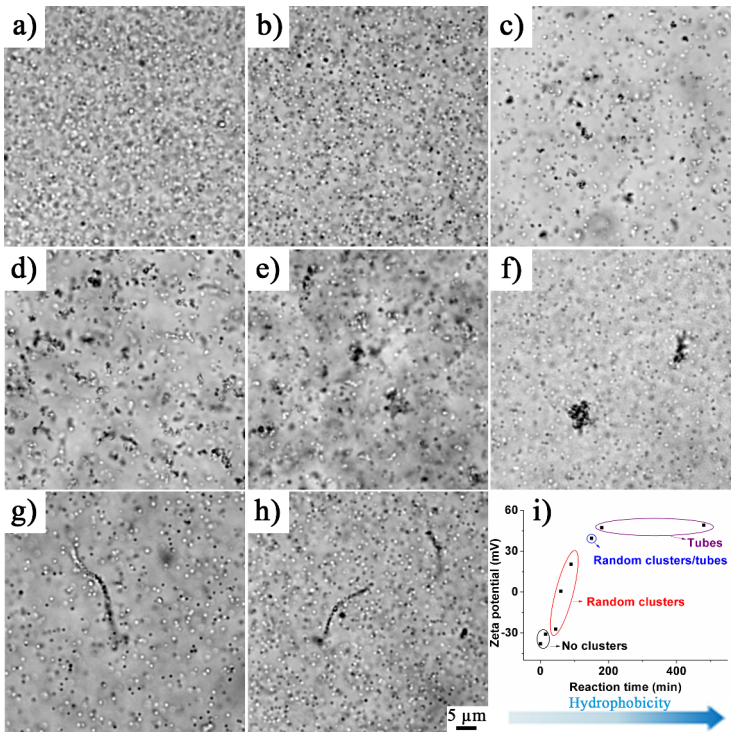


Figure 3.12. (a-h) Optical micrographs of CPS-$C_{12}$N withdrew at different reaction times. (a) 0 min, (b) 5 min, (c) 45 min, (d) 60 min, (e) 90 min, (f) 150 min, (g) 180 min, and (h) 480 min. (i) zeta ($\zeta$) potentials of CPS-$C_{12}$N at different reaction time. The aggregation behaviors of CPS-$C_{12}$N at different reaction times are also shown. Scale bars: 5 $\mu$m for all images.

### 3.3.6 Discussion on a possible mechanism for one-dimensional aggregates formation

Colloids with strong, dominant short-range attraction randomly aggregate to form gels [44]. However, it was found that when the short-range attraction is supplemented by a long-range repulsion, colloids tend to form equilibrium clusters of certain size which can stably disperse in the continuous phase [21, 22, 24, 25, 45]. This can be explained as follows: as the particles are attractive at short range and repulsive at long range, for a cluster with $N$ particles, when $N$ is large enough, addition of an another particle to the cluster non-linearly increases the total repulsion in the cluster, hence further growth is energetically not favored. The shape and size of the clusters are sensitively dependent on the balance between the short-range attraction and the long-range repulsion. By estimation of the ground-state configuration of isolated clusters of different size, Mossa et al. reported that through varying respectively the magnitude and the screening length of the long-range repulsive Yukawa potential, clusters of different morphologies can be formed [45]. In particular, when the clusters diameter exceeds the screening length, and simultaneously the magnitude of the long-range repulsion is sufficiently large, the shape of the aggregates crosses from spherical to linear, i.e., one-dimensional clusters can be generated. Once the one-dimensional clusters are formed, the electrostatic double layers of the individual colloids are rearranged into a uniform double layer surrounding the whole one-dimensional clusters and stabilize them against aggregation [18]. This scenario of the one-dimensional clusters formation that governed by the delicate balance between the short-range attraction and the long-range repulsion has been reported in theory [21], simulation [22, 23] and experiments [24, 25]. More specifically, the formation conditions of the Bernal spiral-like structures in the system of colloids with short-range attraction and long-range repulsion have also been investigated by simulation. Sciortino et al. reported that in the case where the screening length of the repulsion is comparable to the particle radius, particles locally cluster into the Bernal spiral-like structures when the short-range attraction is larger than 15 $kT$, where $kT$ is the thermal energy [22]. Similarly, Mani et al. also obtained the Bernal spiral-like structures when the short-range attraction is in the range of 10 $kT$ to 20 $kT$, while compact clusters were observed when the short-range attraction ranges from 6-8 $kT$. This trend can be

explained by non-equilibrium affect [46].

The control experimental results showed in **subsection 3.3.4** and **3.3.5** strongly indicate the importance of the hydrophobic attraction and the electrostatic repulsion on the formation of the Bernal spiral-like aggregates. As seen in Table 3.2, for CPS-Cl, CPS-H and CPS-DAH, they display quite different aggregation behavior which is ascribed to the different surface hydrophobicity as discussed before. The hydrophobic interaction is a short-range attraction whose effective range is on the order of 10 nm and it decays exponentially with decay length of about 1 nm [47]. The hydrophobic attraction $V_{\mathrm{H}}$ can be expressed as

$$V_{\mathrm{H}} = -2\gamma A \exp(\frac{-h}{D_{\mathrm{H}}}) \tag{3.1}$$

where $\gamma$ is the hydrophobic-water interfacial tension, $A$ is the contact area, $h$ is the particles surface separation, $D_{\mathrm{H}}$ is the decay length which is on the order of 1 nm [47, 48]. The exact value of $\gamma$ is difficult to determine. Kegel et al. estimated that the $\gamma$ of virus capsid proteins is approximately 5 mN/m [48]. In analogy to proteins, the CPS-DAH can also be dispersed in water. Therefore, the $\gamma$ of 5 mN/m is used here to roughly estimate the hydrophobic attraction. According to the equation, we calculate that $V_{\mathrm{H}}$ between the CPS-DAH already reaches to -17 $kT$ when the $h$ is 4 nm, and it becomes stronger with the reduction of the $h$. The particles surface separation of 4 nm is naively selected since the particles possess a rough surface with a typical length scale on the order of a few nanometers. We notice that this attraction strength is comparable to the value of Sciortino and Mani's systems in where Bernal spiral-like structures are also observed [22, 46]. In the case of CPS-Cl, due to the lack of the hydrophobic layer, the particles are well dispersed. While for CPS-H, according to the preparation procedure, we suspect that the hydrophobic layer of CPS-H is much denser than that of CPS-DAH since no etching process and Menschutkin reaction occur during the colloids preparation. Therefore the hydrophobic attraction between CPS-H is expected to be much stronger, which eventually results in the random aggregation of CPS-H.

The concentration of particles at which aggregates start forming can be regarded as a critical micelle concentration (cmc) of a system of surfactants. For a system with aggregates present, this cmc is also the concentration of coexisting monomers. Therefore, another indication of the attraction can be estimated from the fraction of

coexisting monomers in a sample with aggregates *via*

$$\phi_{\text{monomer}} = \frac{V_c}{V_s} \exp(\frac{U}{kT}) \tag{3.2}$$

with $\phi_{\text{monomer}}$ the volume fraction of coexisting monomers, $V_c$ the volume of a colloid, $V_s$ the volume of a solvent molecule, $U$ the average potential per particle at contact [7, 49]. Considering only a few aggregates are formed, the initial volume fraction of colloids ($\approx 0.5\%$) is taken as the $\phi_{\text{monomer}}$. We obtain the average potential a value of $U \approx$ -27 $kT$, acceptable considering the boldness of the estimate of $\gamma$.

Besides the hydrophobic attraction, van der Waals attraction is another candidate driving force for the colloids to aggregate. However, the experimental observation that the colloids restored colloidal stability after charge reversal implies the particles were not trapped in a deep attractive (van der Waals) potential well close to the isoelectric point. Van Ravensteijn ascribed it to the rough surface of the colloids which provides a limit to the minimal inter-particle distance and therefore, to the magnitude of the van der Waals attraction [50]. Therefore, we speculate the van der Waals attraction is not the main driving force for the colloids to aggregate.

To study the influence of the electrostatic repulsion on the Bernal spiral-like aggregates formation, we introduce a parameter $\frac{\Psi^2}{\kappa R}$ which is a measure for the magnitude of the electrostatic repulsion, where $\Psi = \frac{e\zeta}{kT}$, with $e$ the elementary charge, $\zeta$ the zeta potential, $\kappa$ the inverse Debye length and $R$ the radius of the colloids. As shown in Table 3.2, for the cases with medium hydrophobic attraction ($V_H \approx$ -17 $kT$), when $\frac{\Psi^2}{\kappa R}$ is small, for example, in the case of CPS-$C_4$N-B ($\frac{\Psi^2}{\kappa R} = 0.1$), spherical clusters are observed. With increasing value of $\frac{\Psi^2}{\kappa R}$, the morphology of the clusters changes from spherical to linear and the linear clusters become thinner with even higher values of the $\frac{\Psi^2}{\kappa R}$. This tendency of the clusters morphology is consistent with previous report in what Mossa drew the same conclusion by simulation study and a comparable (but not the same) measure for the magnitude of the electrostatic interactions [45]. Therefore, we propose that for the formation of one-dimensional aggregates, the short-range attraction should be on the order of 10 $kT$ and the relatively longer-range repulsion should be sufficiently high. For the formation of the tubes-like aggregates, the mechanism behind it is not so clear, however, from the experimental results, we hypothesize that the combination of centrifugation and the colloids CPS-DAH is responsible for the tubes formation.

Table 3.2. The $\zeta$, $\kappa$, $\frac{\Psi^2}{\kappa R}$, hydrophobicity and aggregation states of several representative colloidal systems

| Colloids | $\zeta$ (mV) | $\kappa^{-1}$ (nm) | $\frac{\Psi^2}{\kappa R}$ | Hydrophobility | states |
|---|---|---|---|---|---|
| CPS-Cl | -38 | $\approx 100^a$ | 1.25 | low | monomers |
| CPS-H | -31 | $\approx 100^a$ | 0.83 | high | random clusters |
| CPS-DAH | 30 | $\approx 100^a$ | 0.78 | medium | Bernal spirals + tubes |
| CPS-$C_4$N-A$^b$ | 50 | $\approx 100^a$ | 2.17 | medium | Bernal spirals + single chains |
| CPS-$C_4$N-B$^c$ | 42 | 6.7 | 0.1 | medium | spherical clusters |

(a) The ionic strength of MQ water used here is approximately $10^{-5}$ M. (b) In MQ water. (c) In water with ionic strength of 2 mM. $\Psi = \frac{e\zeta}{kT}$ , with $e$ the elementary charge, $\zeta$ the zeta potential, $\kappa$ the inverse Debye length and $R$ the radius of the colloids, $kT$ the thermal energy.

### 3.3.7 Ageing of the tube-like aggregates

After two months, we observed the assemblies sample of CPS-DAH made by centrifugation once more (Figure 3.3), surprisingly, we found some interesting structures as shown in **Appendix 3.12**, we are still working on understanding these phenomena. Our first assumption is that these phenomena are related to the gradual self-hydrolysis of the ester groups in water (**Appendix 3.9**), since for the assemblies sample of CPS-$C_{12}$N, we did not observe these structures.

## 3.4 Conclusion

In this chapter, we show that spherical colloids CPS-DAH with isotropic shape and surface functionality can self-assemble into one-dimensional colloidal assemblies in water. The colloids CPS-DAH bear three main characteristics, which are deformability, amphotericity and hydrophobicity. We also synthesize a series of control colloids which only have one or two of the characteristics, and compare the assemblies of the control colloids with the one-dimensional aggregates. We find that deformability is not a prerequisite, that is, colloids which are not deformable can also form one-dimensional aggregates. For amphotericity, we find that the overall charges of the colloids are much more important than the amphotericity. Hydrophobicity is a crucial characteristic, being the main driving force for aggregation. Finally we propose that the formation of the one-dimensional aggregates is the consequence of the delicate balance between the short-range hydrophobic attraction and the relatively longer-range electrostatic

repulsion.

There are three types of one-dimensional aggregates observed: single chains, Bernal spiral-like aggregates, and tube-like aggregates. The single chains are formed at high $\frac{\Psi^2}{\kappa R}$ ($\approx 2$) and they collapse into compact clusters by increasing the ionic strength of the continuous phase. Bernal spiral-like aggregates are observed in the system with the attraction on the order of 10 $kT$ and $\frac{\Psi^2}{\kappa R} \geq 0.78$. For the tube-like aggregates, we hypothesize that the combination of centrifugation and the colloids CPS-DAH is responsible for their formation.

Considering that several proteins can also spontaneously form one-dimensional assemblies, our system could be a model system to study the microscopic mechanism of protein aggregation.

## Acknowledgements

Bas van Ravensteijn and Chris Evers are thanked for their collaboration in designing this research project and discussing the results. Bas van Ravensteijn is also thanked for providing the chlorinated colloids CPS-Cl. Kanvaly Lacina is thanked for taking the scanning electron microscopy images. Hans Meeldijk and Chris Schneijdenberg are thanked for help with freeze-drying samples.

# Appendix

## A3.1 Synthesis of chlorinate colloids CPS-Cl

CPS-Cl are synthesized by seeds emulsion polymerization [51]. First, cross-linked polystyrene colloids CPS as the seeds for the preparation of CPS-Cl are synthesized by emulsion polymerization. Subsequently, a chlorinated, cross-linked thin layer is coated onto the CPS by copolymerizing vinylbenzyl chloride (VBC) and cross-linker divinylbenzene (DVB). The incorporation of VBC is confirmed by infrared (IR) spectroscopy. Figure 3.13a shows IR spectra of CPS and CPS-Cl. A new signal at 1266 $cm^{-1}$ is appeared in the spectrum of CPS-Cl, which corresponds to the stretching vibration of the C-Cl of the incorporated VBC [35]. Electrophoretic mobility measurements reveal a negative $\zeta$ potential of CPS-Cl equal to -37.9 $\pm$ 3.9 mV. The negative charges on the CPS-Cl are originating from the sulfate groups, which are generated from the decomposition of potassium persulfate and sodium bisulfite that act as an initiator system. Figure 3.13b shows a representative TEM image of CPS-Cl which reveals monodisperse colloids with a diameter of 418 $\pm$ 8 nm. Dynamic light scatting (DLS) measurements show a hydrodynamic diameter of 460 $\pm$ 13 nm. These colloids CPS-Cl would be extensively used as seeds for the synthesis of the model colloids as well as the control colloids.

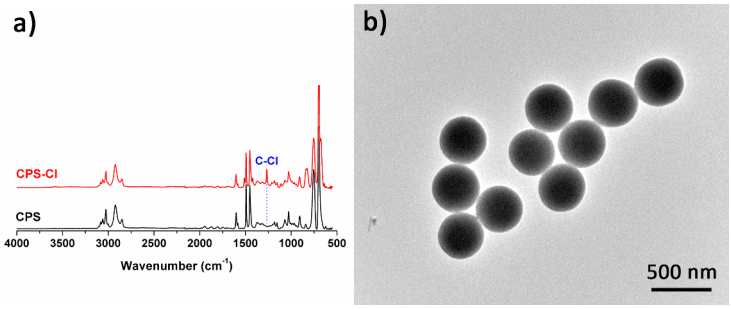


Figure 3.13. (a) Infrared spectra of CPS-Cl (top, red) and CPS (bottom, black). (b) TEM image of chlorinated colloid CPS-Cl. Scale bar: 500 nm.

## A3.2 Controlled growth of hydrophobic layer onto colloids by ATRP reaction

The ATRP reaction is employed to grow a hydrophobic PtBA layer on the surface of chlorinated colloids CPS-Cl. The thickness of the grown layer is regulated using two strategies: by changing the initial monomer concentration or the reaction time. In the first set of experiments, the initial monomer concentration is varied while other parameters are kept constant. Figure 3.14a shows the IR spectra of the obtained colloids with varying initial monomer concentrations. All IR spectra are normalized with respect to the polystyrene signal at 695 $cm^{-1}$ to fairly compare the PtBA content. As can be seen, the signal at 1726 $cm^{-1}$ corresponds to the carbonyl stretching vibration increases as the initial monomer concentration increases. Figure 3.14b and 3.14c quantitatively plot the normalized intensity of the carbonyl signals from IR spectra and hydrodynamic diameters from DLS measurements of the obtained colloids as a function of the initial monomer concentration. A linear relation is obtained for both cases, implying that we can tune the thickness of the PtBA layer by easily adjusting the initial monomer concentration. In the second set of experiments, the initial monomer concentration is kept at 0.25 M, the time-dependent evolution of the IR spectra of the obtained colloids is recorded and plotted in Figure 3.14d. Clearly, the IR spectra show a gradual increase in the normalized intensity of the carbonyl signals in time. The intensity of the carbonyl signals is indicative for the monomer conversion ($p$). Here we assume that full conversion is achieved after 24 h of reaction. Therefore we can plot the normalized intensity of the carbonyl signals as a function of reaction time as shown in Figure 3.14e (black squares). For a typical controlled polymerization, the semi-logarithmic plot should be linear [52]. Therefore we rearrange the data and $\ln(1/(1\text{-}p))$ versus reaction time is plotted. As shown in Figure 3.14e (blue dots), a straight line up to 4 h of reaction is obtained, indicating the reaction is indeed controlled. We also plot the hydrodynamic diameter of the obtained colloids as a function of the reaction time, as expected, the hydrodynamic diameter increases in time and levels off after 4 h of reaction (Figure 3.14f). These results show that we can vary the thickness of the hydrophobic layer grafted from the colloidal surface by changing the initial monomer concentration or the reaction time of ATRP reaction.

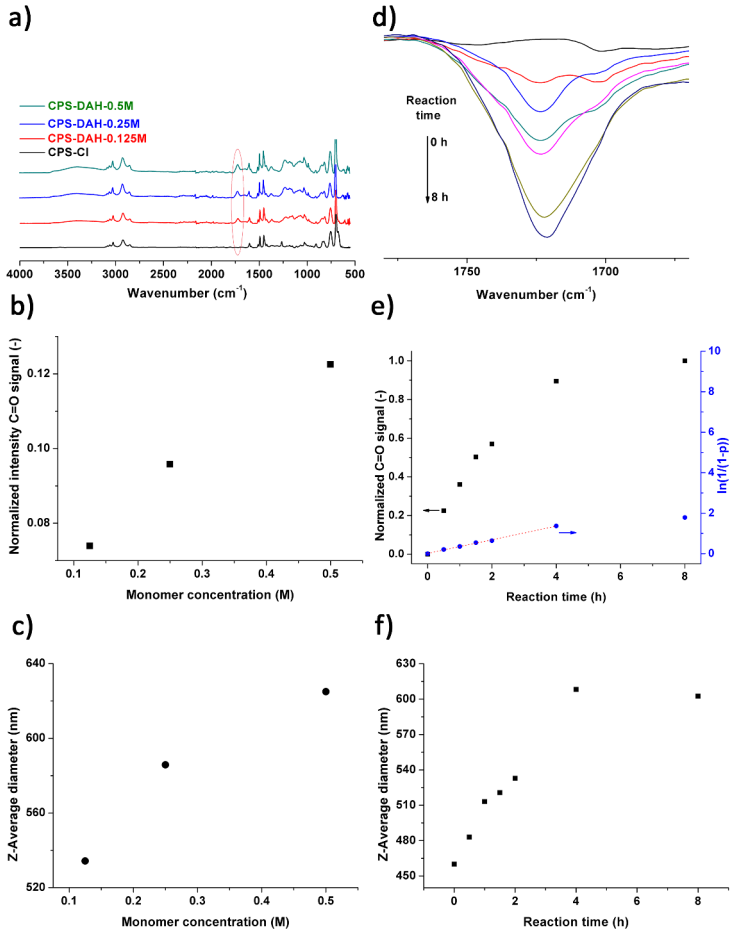


Figure 3.14. (a) IR spectra of colloids after growing PtBA layer on the surface of chlorinated colloid CPS-Cl *via* ATRP reaction with varying initial monomer concentration. (b) Plot of the normalized intensity of the carbonyl signals shown in (a) versus the initial monomer concentration. (c) *Z*-average diameters obtained from DLS measurements versus the initial monomer concentration. (d) Overlay of the carbonyl signals from IR spectra obtained at varying reaction time. (e) Black squares: plot of the normalized intensity of the carbonyl signals shown in (d) versus the reaction time. Blue dots: semi-logarithmic kinetic plot based on monomer conversion ($p$). The straight line indicates the theoretical curve for a controlled radical polymerization. (f) *Z*-average diameters obtained from DLS measurements versus the reaction time.

## A3.3 Investigation of the influence of possible copper ions adsorption on the colloids charge reversal

To determine if the adsorption of copper ions on the colloids also plays a role in the charge reversal of the colloids, energy dispersive X-ray (EDX) measurements are conducted to detect the presence of copper ions on the colloids. Figure 3.15 shows that the signals correspond to copper are absent on both colloids CPS-Cl and CPS-DAH, thereby excluding the adsorption of copper ions on the colloids as a key contribution to the charge reversal of CPS-DAH.

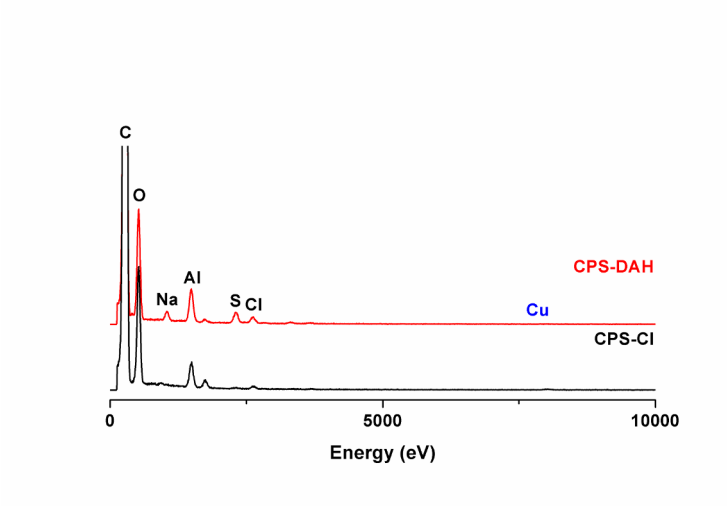


Figure 3.15. Energy dispersive X-ray (EDX) spectra of CPS-DAH (top, red) and CPS-Cl (bottom, black).

## A3.4 Discussion of the formation mechanism of the yolk-shell structure

The CPS-Cl are synthesized by a two-step emulsion polymerization process. For the colloids made by emulsion polymerization method, it is known that the cross-linking density decreases radially from the colloid center [38, 53, 54]. This is not surprising, as the cross-linker has higher reactivity hence a large portion of the cross-linker are incorporated during the initial growth of the colloids, eventually results in high cross-linking density in the center while polymer network with a low fraction or even no chemical cross-linkers are present at the periphery of the colloids. Since the CPS-Cl is synthesized by two-step emulsion polymerization, we speculate the cross-linking density of the CPS-Cl from the center to the periphery is high-low-high-low. This internal structure of the CPS-Cl results in the formation of the yolk-shell structure after the colloids etched by DMF, which is a good solvent for non-cross-linked or even low cross-linked polystyrene but not for high cross-linked polystyrene. If this hypothesis is correct, we would expect that for the seed colloids of the CPS-Cl (CPS), no yolk-shell structure but diminished size should be observed after it is etched by DMF. As shown in Figure 3.16, for CPS, after treated with DMF, no yolk-shell structure is observed, while the diameter decreases from 381 nm to 319 nm. This result confirms that the yolk-shell structure is originating from the inhomogeneous distribution of cross-linking density within the CPS-Cl, or more precisely say, radially decreases from center to periphery.

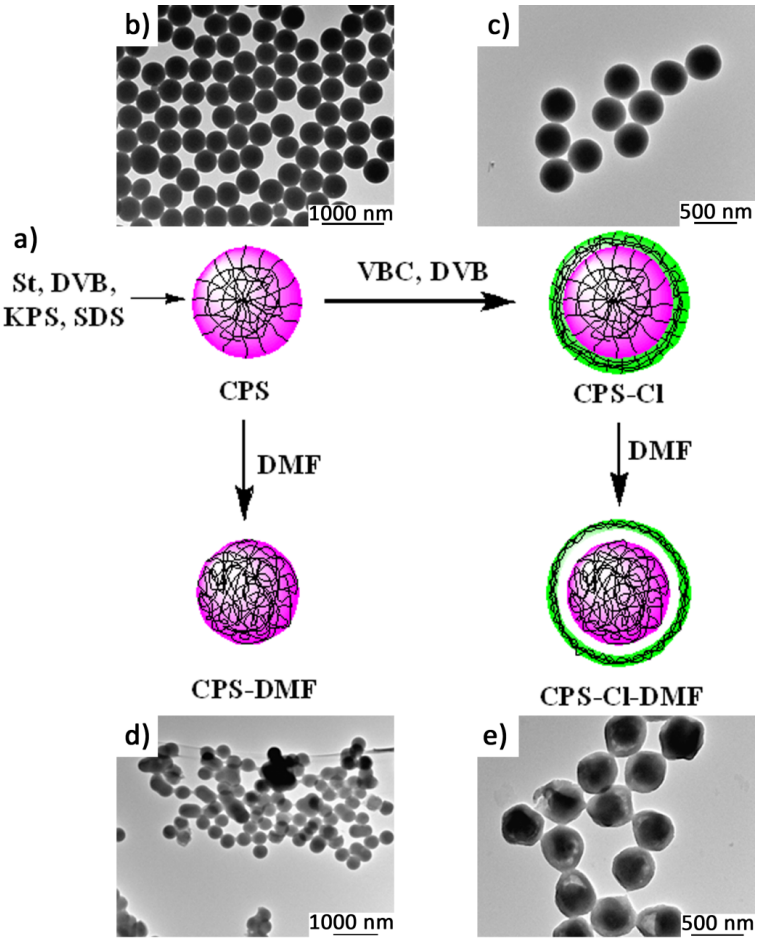


Figure 3.16. (a) Schematic illustration of the etching process. (b-e) TEM images of CPS before (b) and after (d) etching by DMF, TEM images of CPS-Cl before (c) and after (e) etching by DMF. Scale bars: 1 $\mu$m for (b) and (d), 500 nm for (c) and (e).

## A3.5 Additional proof of the spontaneous formation of the Bernal spiral-like structure

After removing the one-dimensional aggregates, the remaining supernatant with individual colloids can self-assemble into one-dimensional aggregates after keeping at rest for one month.

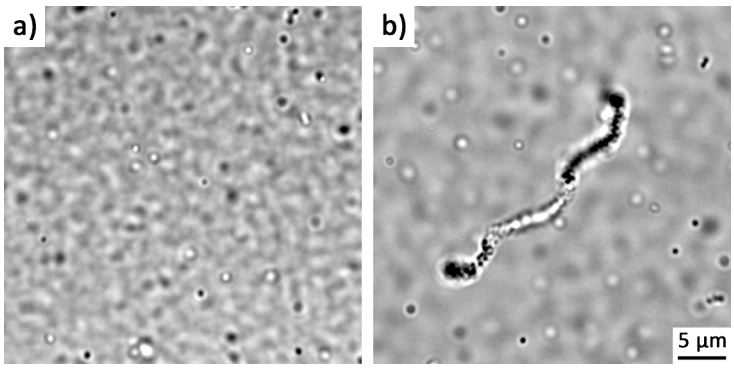


Figure 3.17. (a) the supernatant of the assemblies dispersion. (b) one month aging of the supernatant (a). Scale bars: 5 $\mu$m for both images.

## A3.6 Snapshots of confocal microscope images of the colloidal tubes of CPS-DAH in different $z$-directions

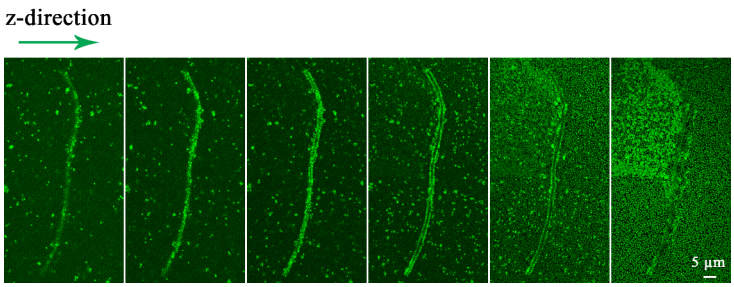


Figure 3.18. Snapshots of confocal microscope images of the colloidal tubes of CPS-DAH in different $z$-directions. Scale bars: 5 $\mu$m for all images.

## A3.7 Several additional colloidal tube examples self-assembled from CPS-DAH with different composition and initial monomer concentrations

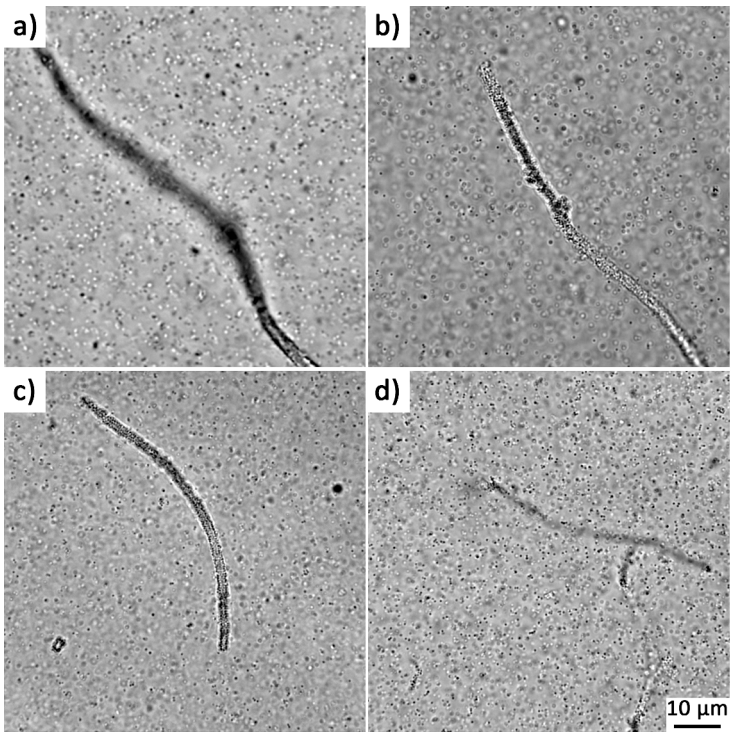


Figure 3.19. Several extra colloidal tube examples self-assembled from CPS-DAH with different monomer and initial monomer concentrations. (a) CPS-DAH-0.25M-0, (B) CPS-DAH-0.5M-0, (c) CPS-DAH-0.25M-0.25M, (d) CPS-DAH-0.5M-0.25M. Note: The first and second number represents the initial concentration of the monomer *tert*-butyl acrylate and styrene, respectively. Scale bars: 10 $\mu$m for all images.

## A3.8 Hydrolysis of CPS-DAH

Figure 3.20a shows a representative TEM image of CPS-DAH after hydrolysis. Instead of yolk-shell structure, the shell of the colloids collapses which might ascribe to the hydrolysis process. Regardless of the collapse of the shell of the colloids, the hydrolysis process is successful as confirmed with IR spectroscopy (Figure 3.20b). The signal at 1726 $cm^{-1}$ which corresponds to the C=O stretching vibration of ester groups of PtBA dramatically decreases, while a new signal at 1688 $cm^{-1}$ which corresponds to the C=O stretching vibration of carboxylic acid groups of PAA appears [35]. However, there is still a small signal presented in the spectrum of CPS-DAH after hydrolysis (marked with blue circle), which indicates that the hydrolysis process is not complete.

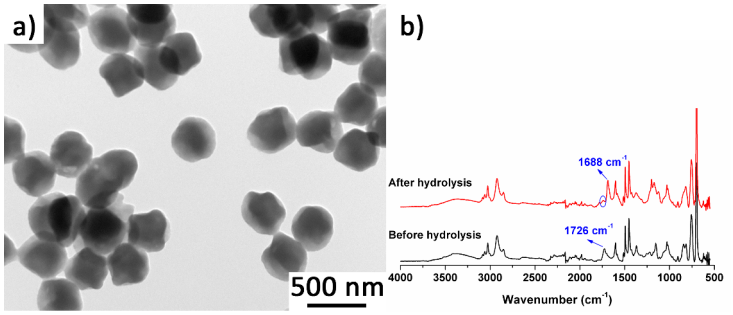


Figure 3.20. (a) TEM image of CPS-DAH after hydrolysis. (b) IR spectra of CPS-DAH before (bottom, black) and after (top, red) hydrolysis. The blue circle highlighted the presence of residual ester groups. Scale bar: 500 nm.

## A3.9 Self-hydrolysis of ester groups of CPS-DAH in water

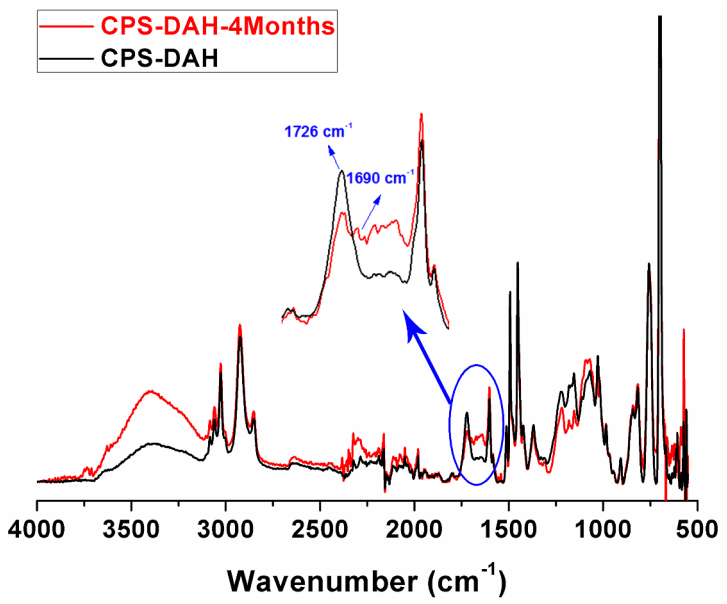


Figure 3.21. IR spectra of CPS-DAH measured immediately after synthesis (black) and measured after stored in water for four months (red). Clearly, after stored in water for four months, the signal at 1726 $cm^{-1}$ corresponds to ester groups decreases while the signal 1690 $cm^{-1}$ corresponds to acid groups generates, indicating the self-hydrolysis of ester groups gradually takes place in water.

## A3.10 Time-dependent evolution of the aggregation behavior of CPS-DA

In this experiment, CPS-Cl are reacted with DMF, the samples are withdrew in time and characterized with optical microscope. In this case, the hydrophobic attraction is absent and the overall surface charges undergo from negative cross the zero point to positive. We study the time-dependent evolution of the aggregation behavior of CPS-DA. The CPS-DA also experience the disperse-aggregate-disperse transformation in time (Figure 3.22). However, due to the lack of the hydrophobicity, after charge reversal, no one-dimensional aggregates are found in this CPS-DA system (Figure 3.22f).

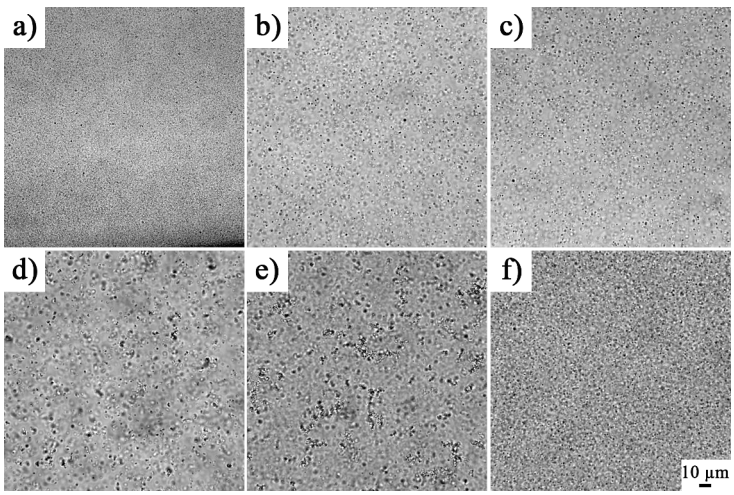


Figure 3.22. Optical micrographs of CPS-DA withdrew at different reaction times. (a) 0 min, (b) 15 min, (c) 45 min, (d) 90 min, (e) 120 min, and (f) 240 min. Scale bars: 10 $\mu$m for all images.

## A3.11 ATRP reaction in DMSO

After we observed that DMF etches the colloids during ATRP reaction and before trying to perform ATRP reaction in acetonitrile/water mixture to synthesize CPS-H, we have also endeavored DMSO as the ATRP solvent. The other parameters are kept the same. Figure 3.23a shows a representative TEM image of the obtained colloids. Indeed, not yolk-shell is observed even though the colloids slightly deformed after ATRP reaction. Additionally, its $\zeta$ potential keeps negative with value of -31 $\pm$ 4 mV which is obtained by electrophoretic mobility measurements. However, compared the IR spectrum of the obtained colloids (Figure 3.23b3, top green) to that for the CPS-Cl (Figure 3.23b1, bottom black), a new signal at 1700 $cm^{-1}$ instead of 1726 $cm^{-1}$ is appeared in the spectrum of the obtained colloids. This new signal is not expected to be corresponding to the C=O stretching vibration of the ester groups of the tBA. On one hand, it shifts away from the region of the C=O stretching vibration signal of the ester groups; on the other hand, the signal intensity is extremely high compared to that for the C=O stretching vibration peak of the ester groups obtained before (Figure 3.1a, top red). This hypothesis is confirmed by the following experiment. We performed the same experiment but without the addition of tBA. Figure 3.23b2 (middle red) shows that the signal at 1700 $cm^{-1}$ is also present even without tBA. Since this signal appears only when DMSO is used, there must be some reactions take place in this system. It was reported that DMSO can react with benzyl chloride groups to yield aldehyde groups [55]. And the peak at 1700 $cm^{-1}$ well fits the C=O stretching vibration signal of the aldehyde groups [35]. Therefore we speculate that in our experimental conditions, the reaction of DMSO and benzyl chloride groups to generate aldehyde groups also takes place, even though the mechanism is not fully understood. These results show that DMSO is not a suitable solvent for ATRP reaction.

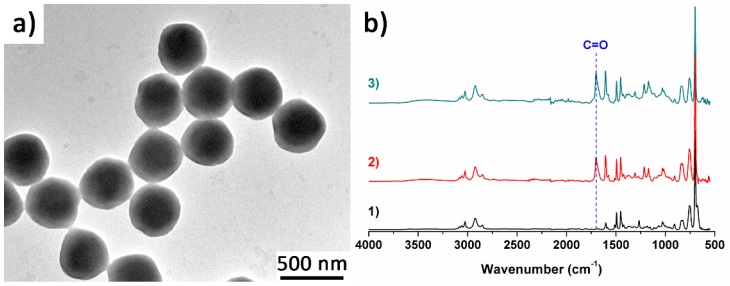


Figure 3.23. (a) TEM image of colloids after ATRP reaction performed in DMSO. (b) IR spectra of (1) CPS-Cl (bottom, black ), (2) CPS-Cl after ATRP reaction performed in DMSO without tBA (middle, red), (3) CPS-Cl after ATRP reaction performed in DMSO with tBA (top, green). Scale bar: 500 nm.

## A3.12 Some new structures of the assemblies of CPS-DAH made by centrifugation after ageing two months

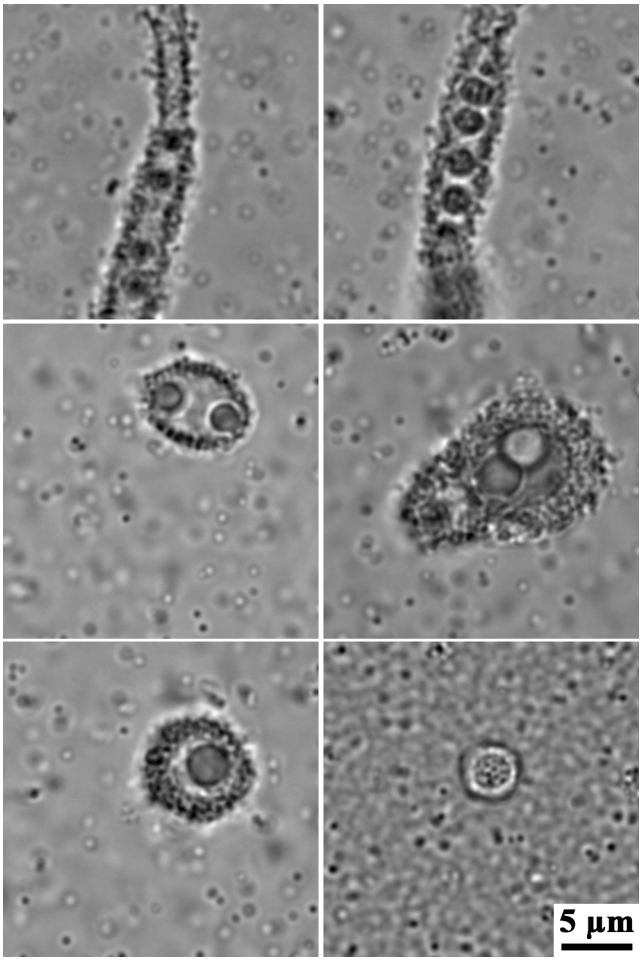


Figure 3.24. Some new structures of the assemblies of CPS-DAH made by centrifugation after ageing two months. Scale bars: 5 $\mu$m for all images.

# Bibliography

[1] O. D. Velev and S. Gupta. Materials fabricated by micro- and nanoparticle assembly the challenging path from science to engineering. *Advanced Materials*, 21:1897–1905, 2009.

[2] F. Li, D. P. Josephson, and A. Stein. Colloidal assembly: The road from particles to colloidal molecules and crystals. *Angewandte Chemie International Edition*, 50:360–388, 2011.

[3] L. Xu, W. Ma, L. Wang, C. Xu, H. Kuang, and N. A. Kotov. Nanoparticle assemblies: dimensional transformation of nanomaterials and scalability. *Chemical Society Reviews*, 42:3114–3126, 2013.

[4] X. Ye and L. Qi. Two-dimensionally patterned nanostructures based on monolayer colloidal crystals: Controllable fabrication, assembly, and applications. *Nano Today*, 6:608–631, 2011.

[5] V. J. Anderson and H. N. W. Lekkerkerker. Insights into phase transition kinetics from colloid science. *Nature*, 416:811–815, 2002.

[6] U. Gasser, E. R. Weeks, A. Schofield, P. N. Pusey, and D. A. Weitz. Real-space imaging of nucleation and growth in colloidal crystallization. *Science*, 292:258–262, 2001.

[7] D. J. Kraft, R. Ni, F. Smallenburg, M. Hermes, K. Yoon, D. A. Weitz, A. van Blaaderen, J. Groenewold, M. Dijkstra, and W. K. Kegel. Surface roughness directed self-assembly of patchy particles into colloidal micelles. *Proceedings of the National Academy of Sciences*, 109:10787–10792, 2012.

[8] C. H. J. Evers, J. A. Luiken, P. G. Bolhuis, and W. K. Kegel. Self-assembly of microcapsules *via* colloidal bond hybridization and anisotropy. *Nature*, 534:364–368, 2016.

[9] Z. Tang, Z. Zhang, Y. Wang, S. C. Glotzer, and N. A. Kotov. Self-assembly of CdTe nanocrystals into free-floating sheets. *Science*, 314:274–278, 2006.

[10] K. Liu, Z. Nie, N. Zhao, W. Li, M. Rubinstein, and E. Kumacheva. Step-growth polymerization of inorganic nanoparticles. *Science*, 329:197–200, 2010.

[11] Q. Chen, S. C. Bae, and S. Granick. Directed self-assembly of a colloidal kagome lattice. *Nature*, 469:381–384, 2011.

[12] Q. Chen, J. K. Whitmer, S. Jiang, S. C. Bae, E. Luijten, and S. Granick. Supracolloidal reaction kinetics of janus spheres. *Science*, 331:199–202, 2011.

[13] R. Guo, J. Mao, X.-M. Xie, and L.-T. Yan. Predictive supracolloidal helices from patchy particles. *Scientific Reports*, 4:7021, 2014.

[14] Y. Wang, Y. Wang, D. R. Breed, V. N. Manoharan, L. Feng, A. D. Hollingsworth, M. Weck, and D. J. Pine. Colloids with valence and specific directional bonding. *Nature*, 491:51–55, 2012.

[15] Z. Tang, N. A. Kotov, and M. Giersig. Spontaneous organization of single CdTe nanoparticles into luminescent nanowires. *Science*, 297:237–240, 2002.

[16] K. Butter, P. H. H. Bomans, P. M. Frederik, G. J. Vroege, and A. P. Philipse. Direct observation of dipolar chains in iron ferrofluids by cryogenic electron microscopy. *Nat Mater*, 2:88–91, 2003.

[17] S. Lin, M. Li, E. Dujardin, C. Girard, and S. Mann. One-dimensional plasmon coupling by facile self-assembly of gold nanoparticles into branched chain networks. *Advanced Materials*, 17:2553–2559, 2005.

[18] H. Zhang and D. Wang. Controlling the growth of charged-nanoparticle chains through interparticle electrostatic repulsion. *Angewandte Chemie*, 120:4048–4051, 2008.

[19] M. S. Nikolic, C. Olsson, A. Salcher, A. Kornowski, A. Rank, R. Schubert, A. Fromsdorf, H. Weller, and S. Forster. Micelle and vesicle formation of amphiphilic nanoparticles. *Angewandte Chemie-International Edition*, 48:2752–2754, 2009.

[20] H. Wang, L. Chen, X. Shen, L. Zhu, J. He, and H. Chen. Unconventional chain-growth mode in the assembly of colloidal gold nanoparticles. *Angewandte Chemie International Edition*, 51:8021–8025, 2012.

[21] J. Groenewold and W. K. Kegel. Anomalously large equilibrium clusters of colloids. *The Journal of Physical Chemistry B*, 105:11702–11709, 2001.

[22] F. Sciortino, P. Tartaglia, and E. Zaccarelli. One-dimensional cluster growth and branching gels in colloidal systems with short-range depletion attraction and screened electrostatic repulsion. *The Journal of Physical Chemistry B*, 109:21942–21953, 2005.

[23] J. A. Luiken and P. G. Bolhuis. Anisotropic aggregation in a simple model of isotropically polymer-coated nanoparticles. *Physical Review E*, 88:012303, 2013.

[24] A. I. Campbell, V. J. Anderson, J. S. van Duijneveldt, and P. Bartlett. Dynamical arrest in attractive colloids: The effect of long-range repulsion. *Physical Review Letters*, 94:208301, 2005.

[25] T. H. Zhang, J. Klok, R. Hans Tromp, J. Groenewold, and W. K. Kegel. Non-equilibrium cluster states in colloids with competing interactions. *Soft Matter*, 8:667–672, 2012.

[26] M. Weijers, R. W. Visschers, and T. Nicolai. Light scattering study of heat-induced aggregation and gelation of Ovalbumin. *Macromolecules*, 35:4753–4762, 2002.

[27] X. Jiang, M. Wang, D. Y. Graham, and M. K. Estes. Expression, self-assembly, and antigenicity of the Norwalk virus capsid protein. *Journal of Virology*, 66:6527–6532, 1992.

[28] M. Raffaele and F. Peter. The self-assembly, aggregation and phase transitions of food protein systems in one, two and three dimensions. *Reports on Progress in Physics*, 76:046601, 2013.

[29] W. H. Roos, R. Bruinsma, and G. J. L. Wuite. Physical virology. *Nat Phys*, 6:733–743, 2010.

[30] S. Jordens, J. Adamcik, I. Amar-Yuli, and R. Mezzenga. Disassembly and reassembly of Amyloid fibrils in waterethanol mixtures. *Biomacromolecules*, 12:187–193, 2011.

[31] R. J. Hunter. *Zeta Potential in Colloid Science*. Academic Press, 1981.

[32] T. von Werne and T. E. Patten. Preparation of structurally well-defined polymernanoparticle hybrids with controlled/living radical polymerizations. *Journal of the American Chemical Society*, 121:7409–7410, 1999.

[33] C. Perruchot, M. A. Khan, A. Kamitsi, S. P. Armes, T. von Werne, and T. E. Patten. Synthesis of well-defined, polymer-grafted silica particles by aqueous ATRP. *Langmuir*, 17:4479–4481, 2001.

[34] B. G. P. van Ravensteijn and W. K. Kegel. Versatile procedure for site-specific grafting of polymer brushes on patchy particles *via* atom transfer radical polymerization (ATRP). *Polymer Chemistry*, 7:2858–2869, 2016.

[35] G. Socrates. *Infrared and Raman Characteristic Group Frequencies, 3rd edition*. John Wiley and Sons Ltd, 2001.

[36] B. G. P. van Ravensteijn and W. K. Kegel. Colloids with continuously tunable surface charge. *Langmuir*, 30:10590–10599, 2014.

[37] R. Purbia and S. Paria. Yolk/shell nanoparticles: classifications, synthesis, properties, and applications. *Nanoscale*, 7:19789–19873, 2015.

[38] B. G. P. van Ravensteijn and W. K. Kegel. Tuning particle geometry of chemically anisotropic dumbbell-shaped colloids. *Journal of Colloid and Interface Science*, 490:462–477, 2017.

[39] W. Abdelwahed, G. Degobert, S. Stainmesse, and H. Fessi. Freeze-drying of nanoparticles: Formulation, process and storage considerations. *Advanced Drug Delivery Reviews*, 58:1688–1713, 2006.

[40] K. Matyjaszewski. Atom Transfer Radical Polymerization (ATRP): Current status and future perspectives. *Macromolecules*, 45:4015–4039, 2012.

[41] Y.-C. Tung, W.-C. Wu, and W.-C. Chen. Morphological transformation and photophysical properties of rod-coil poly[2,7-(9,9-dihexylfluorene)]-block-poly(acrylic acid) in solution. *Macromolecular Rapid Communications*, 27:1838–1844, 2006.

[42] W. M. Haynes. *CRC Handbook of Chemistry and Physics, 97th Edition*. CRC Press, 2016.

[43] D. D. Perrin. *Dissociation Constants of Organic Bases in Aqueous Solution*. Butterworths, London, 1965, Supplement, 1972.

[44] M. Y. Lin, H. M. Lindsay, D. A. Weitz, R. C. Ball, R. Klein, and P. Meakin. Universality in colloid aggregation. *Nature*, 339:360–362, 1989.

[45] S. Mossa, F. Sciortino, P. Tartaglia, and E. Zaccarelli. Ground-state clusters for short-range attractive and long-range repulsive potentials. *Langmuir*, 20:10756–10763, 2004.

[46] E. Mani, W. Lechner, W. K. Kegel, and P. G. Bolhuis. Equilibrium and non-equilibrium cluster phases in colloids with competing interactions. *Soft Matter*, 10:4479–4486, 2014.

[47] E. E. Meyer, K. J. Rosenberg, and J. Israelachvili. Recent progress in understanding hydrophobic interactions. *Proceedings of the National Academy of Sciences*, 103:15739–15746, 2006.

[48] W. K. Kegel and P. van der Schoot. Competing hydrophobic and screened-coulomb interactions in Hepatitis B virus capsid assembly. *Biophysical Journal*, 86:3905–3913, 2004.

[49] J. R. Wolters, G. Avvisati, F. Hagemans, T. Vissers, D. J. Kraft, M. Dijkstra, and W. K. Kegel. Self-assembly of "mickey mouse" shaped colloids into tube-like structures: experiments and simulations. *Soft Matter*, 11:1067–1077, 2015.

[50] B. G. P. van Ravensteijn. *Isotropic and patchy colloids with engineered surface functionality*. Thesis, 2015.

[51] B. G. P. van Ravensteijn, M. Kamp, A. van Blaaderen, and W. K. Kegel. General route toward chemically anisotropic colloids. *Chemistry of Materials*, 25:4348–4353, 2013.

[52] K. Matyjaszewski and J. Xia. Atom transfer radical polymerization. *Chemical Reviews*, 101:2921–2990, 2001.

[53] E. A. Nieuwenhuis and A. Vrij. Light scattering of pmma latex particles in benzene: structural effects. *Journal of Colloid and Interface Science*, 72:321–341, 1979.

[54] W. McPhee, K. C. Tam, and R. Pelton. Poly(*N*-isopropylacrylamide) latices prepared with sodium dodecyl sulfate. *Journal of Colloid and Interface Science*, 156:24–30, 1993.

[55] H. W. Gibson and F. C. Bailey. Chemical modification of polymers. V. oxidation of poly(vinylbenzyl chloride) to poly(vinylbenzaldehyde). *Journal of Polymer Science: Polymer Chemistry Edition*, 13:1951–1955, 1975.

Chapter 4

# Floating Colloidal Crystal Monolayers

ABSTRACT

Well-defined two-dimensional colloidal crystal monolayers (CCM) have numerous applications, such as photonic crystal, sensors, and masks for colloidal lithography. In this chapter we report a facile method to prepare CCM with building blocks with sizes on the order of the wavelength of visible light. A unique feature of this method is that the prepared CCM can freely float in the dispersion. The key to obtain floating CCM is the selection of an appropriate solvent to release the formed CCM from the wall of the centrifugal tube. This solvent is termed extracting solvent. There are two steps involved in the preparation of floating CCM: in the first step, colloids are dispersed in a solvent termed 'dispersing solvent'. Evaporation of the dispersing solvent results in the formation of a meniscus structure of the air-liquid interface between the colloids that are on the wall of the centrifugal tube. The deformation of the meniscus gives rise to capillary attraction, driving the colloids towards each other. Once a crystallization nucleus is formed, a convective flow of further colloids sets in, resulting in the formation of CCM on the wall of the centrifugal tube. In the second step, the remaining bulk dispersion is replaced by an extracting solvent that wets the wall and peels the formed CCM off. During this process, the CCM remains a close-packed layer. The influences of the dispersing solvent, the wall material, the extracting solvent and the types of colloids on the CCM formation are investigated systematically.

## 4.1 Introduction

Colloidal lithography is a powerful tool to prepare two-dimensional (2D) ordered nanostructures, which have potential applications in the areas of photonics, plasmonics, sensing, and solar cells [1–4]. 2D colloidal crystal monolayers (CCM) are the facile, flexible, and efficient templates for colloidal lithography [5–9]. Therefore, numerous effort has been devoted to assemble colloids into CCM. The methods developed up to now include drop casting [10], convective deposition [11], spin coating [12], and electrophoretic deposition [13]. However, the major drawbacks of these methods are the requirement of very hydrophilic substrates onto which colloids assemble, and the difficulty to transfer the formed colloidal crystals to other substrates. Therefore, a variety of approaches have been attempted to prepare so called floating CCM. As the term suggests, floating CCM is not attached to a substrate but can freely float in the continuous phase, allowing easy transfer to desired substrates. The most commonly used approach to prepare floating CCM are the liquid interface mediated methods. Instead of using solid substrates like glass and mica, a liquid interface is used in these methods, such as gas-liquid interface and liquid-liquid interface [14–16]. For example, Kondo et al. [14] prepared floating CCM by spreading monodisperse hydrophobic alkoxyl chains coated silica particles at the air-benzene interface and picking the formed monolayer up with a mica substrate. However, to increase the ordering and packing density in monolayer, the control of the hydrophobicity of colloids [14], the utility of Langmuir-Blodgett trough [17] or the addition of various polymers [18] or surfactants [19] are usually required. Except for the commonly employed liquid interface mediated methods, some other methods are also exploited. Ramos et al. reported a surfactant-mediated method to prepare floating CCM [20]. By mixing aqueous charge-stabilized polystyrene latex particles with a mixture of an oppositely charged and a neutral surfactant which self-assembled into vesicles, 2D colloidal crystal monolayers were formed on the vesicles. In that system, besides 2D colloidal crystal monolayers, there also were many free particles and random clusters present. Furthermore, the requirement of two types of surfactants as well as the formation of vesicles makes the system complicated and difficult to extend. Tang et al. reported the spontaneous formation of floating CCM of CdTe nanoparticles with tetrahedral shape. He ascribed the formation of floating CCM to a combination of electrostatic repulsion

and anisotropic hydrophobic attraction [21]. However, the requirement of anisotropic shape limits the potential applications of this method. Geerts et al. reported that colloids coated with long DNA strands can spontaneously form a crystalline 2D "colloidal carpet" that hovered several microns above the support surface [22]. The formation of these colloidal crystal monolayers was facilitated by the weak, non-specific adsorption of the DNA-coated colloids to a weakly oppositely charged lower surface of the sample cell. However, the "colloidal carpets" were not truly free-floating, they hovered on top of the substrate surface.

In this chapter, we present a new and facile method to prepare floating CCM. As illustrated in Figure 4.1, cross-linked polymer colloids are first dispersed in a volatile dispersing solvent and stored in a centrifugal tube. Subsequently, the centrifugal tube containing the colloidal dispersion is placed in a fume hood with the centrifugal cap opened for approximately 20 minutes. The monolayers are formed onto the inner wall of the centrifugal tube during this period. After removal of the remaining bulk dispersion and addition of an extracting solvent, followed by manual shaking, the formed monolayers are peeled off and dispersed in the extracting solvent. With that procedure, floating CCM are obtained. Firstly, we demonstrate that the formed assemblies are indeed monolayers and these monolayers can freely float in the dispersion. Subsequently, we confirm that these monolayers are formed onto the inner wall of the centrifugal tube due to evaporation of the dispersing solvent. Afterwards, we investigate the influence of the dispersing solvents, the wall materials, the extracting solvents and the types of colloids on the formation of the floating CCM in more detail. Finally, a possible mechanism similar to the mechanism of vertical deposition is proposed, which involves the capillary attraction that originated from the deformation of a meniscus structure of the air-liquid interface between the colloids.

## 4.2 Experimental Section

### 4.2.1 Materials

Styrene (St, 99%), divinylbenzene (DVB, 55% mixture of isomers, tech. grade), 4-vinylbenzyl chloride (VBC, $\geq$ 90%, tech. grade), acrylic acid (AA, 99%), dimethylformamide (DMF, $\geq$ 99%), 1, 4-dioxane (DOX, ACS reagent, $\geq$ 99.0%), *N*-Methyl-

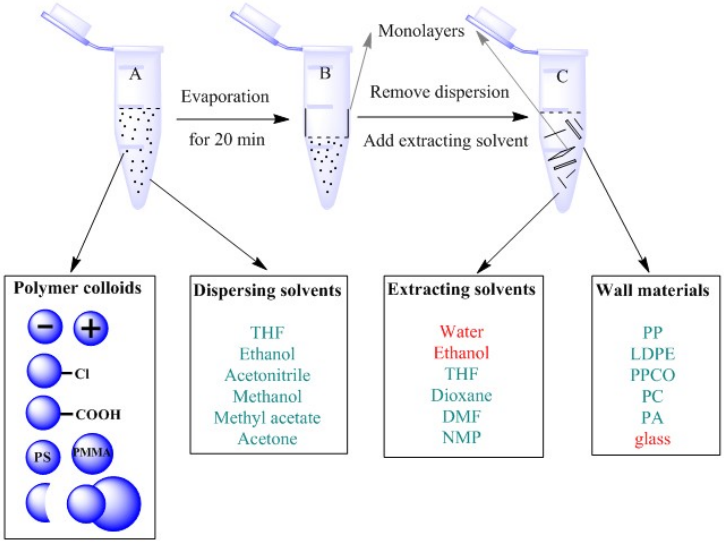


Figure 4.1. Schematic illustration for the proposed method to prepare two-dimensional floating colloidal crystal monolayers (CCM). (A) Colloids disperse in a dispersing solvent. (B) CCM are formed onto the wall of the centrifugal tube after evaporation of the dispersing solvent. (C) CCM are peeled off and freely floated in a extracting solvent after the remaining bulk dispersion is replaced by the extracting solvent. Red terms represent no CCM are observed in those samples.

2-pyrrolidone (NMP, anhydrous, 99.5%), polyvinylpyrrolidone (PVP, K30, $M_w$ = 40 kg/mol), polyvinyl alcohol (PVA, $M_w$ = 85-124 kg/mol, 87-89% hydrolyzed), polyacrylic acid (PAA, Mv $\approx$ 450 kg/mol) were obtained from Sigma-Aldrich. Sodium dodecyl sulfate (SDS) was purchased from BDH. Azobis(isobutyronitrile) (AIBN, 98%), tetrahydrofuran (THF, for analysis, ACS reagent), sodium bisulfite ($NaHSO_3$, ACS reagent) and potassium persulfate (KPS, > 99% for analysis) were purchased from Acros Organics. Ethanol (p.a., ACS reagent) was purchased from Merck. 2,2'-Azobis(2,4-dimethylvaleronitrile) (V65) was purchased from Wako chemicals GmbH. All of the chemicals were used as received. The water used throughout all of the experiments was purified using a Milli-Q water purification system.

### 4.2.2 Synthesis of negatively charged chlorinated polystyrene nanospheres (CPS-Cl)

CPS-Cl colloids were kindly provided by Bas van Ravensteijn and were synthesized by seeds emulsion polymerization. A 500 mL round-bottom flask equipped with a stir bar was placed in an oil bath of 80 °C. 200 mL water was charged into the reactor and allowed to reach the bath temperature. 21.15 g styrene, 0.635 g DVB, and 0.125 g SDS dissolved in 25 mL water were added, followed by 25 mL rinse water. The complete mixture was allowed to heat up to the temperature of the bath. Polymerization was initiated by addition of 0.78 g KPS dissolved in 37.5 mL water. Reaction was allowed to continue for 24 hours. The obtained particles were used as seeds for the preparation of CPS-Cl. 25 mL of the above crude emulsion and 10 mL of water were introduced into a 50 mL three-neck round-bottom flask equipped with a magnetic stir bar. This emulsion was bubbled with nitrogen for 30 minutes at room temperature. Subsequently, 1 mL VBC mixed with 20 $\mu$L DVB was injected while the flask remained under inert atmosphere. The seeds were swollen for 1 hour, after which the temperature was raised to 60 °C. When this temperature was reached, the initiator solution of 0.04 g KPS, 0.03 g sodium bisulfite and 2.5 mL water was injected. After 4 hours the reaction was stopped. The final product was washed with ethanol and water twice respectively. Finally, the particles were stored in water.

### 4.2.3 Synthesis of negatively charged polystyrene nanospheres (CPS)

CPS nanospheres were synthesized by surfactant-free emulsion polymerization. 45 mL water, 4.7 mL St, and 140 $\mu$L DVB were added into a 100 mL three-necked round-bottom flask, followed by 156 mg KPS dissolved in 7.5 mL water. The flask was constantly stirred with a mechanical stirrer under nitrogen flow. Subsequently, the flask was immersed in a 80 °C water bath to initiate the polymerization. The reaction was allowed to proceed for 24 hours under nitrogen atmosphere. The final product was centrifuged at 15000 $g$ for 15 minutes, and washed with ethanol and water sequentially to remove unreacted reagents. Finally, the particles were stored in water.

### 4.2.4 Synthesis of negatively charged PAA decorated polystyrene nanospheres (CPSAA)

CPSAA were prepared using a similar method as described for CPS. The key difference was the presence of AA in the reaction mixture. 45 mL water, 5.5 mL St, 381 $\mu$L AA, and 27.5 $\mu$L DVB were added into a 100 mL three-necked round-bottom flask, followed by 25 mg KPS dissolved in 5 mL water. While being bubbled with nitrogen gas, the mixture was constantly stirred with a mechanical stirrer. After 15 minutes, the nitrogen inlet was raised above the liquid level for another 15 minutes. Subsequently, the flask was immersed in a 70 °C water bath to initiate the polymerization. The reaction was allowed to proceed for 24 hours under nitrogen atmosphere. The final product was centrifuged at 15000 $g$ for 15 minutes, and washed with ethanol and water sequentially to remove unreacted reagents. Finally, the colloids were stored in water.

### 4.2.5 Synthesis of PVP stabilized dimple polystyrene nanospheres (d-CPS)

5 g PVP, 126 mL ethanol, 0.136 g AIBN, and 14 mL water were charged into a 250 mL three-neck round bottom flask. Dissolution of PVP and AIBN was aided by sonication of the mixture for about 1 min. Subsequently, 10 mL St was added. The transparent mixture was constantly stirred with a magnetic stirrer under nitrogen flow, and the flask was immersed in a 70 °C water bath to initiate polymerization. After 1.5 h of polymerization, a premixed solution containing 0.3 mL DVB, 2.5 mL St and 5 mL ethanol was added dropwise, where the total addition time was approximately 30 min. The reaction was allowed to proceed for another 22.5 h. The final product was washed with ethanol and water twice, respectively, and stored in water.

### 4.2.6 Synthesis of dumbbell particles (db-CPS)

Seed particles of db-CPS were synthesized by dispersion polymerization. 2 g PAA, 45 mL ethanol, 0.15 g AIBN, and 5 mL water were charged into a 100 mL three-neck round-bottom flask. Dissolution of PAA and AIBN was facilitated by mechanical stirring. Subsequently, 5 mL St was added and the mixture was constantly stirred

under nitrogen flow. After half hour, the nitrogen flow was stopped and the flask was immersed in a 70 °C water bath to initiate polymerization. 1.5 hours later, a solution containing 0.15 mL DVB, 1.25 mL St and 2.5 mL ethanol was added dropwise (the total addition time was approximately 15 minutes). The reaction was allowed to proceed for another 22.5 hours. The final product was washed with ethanol and water twice respectively. Finally, the seed colloids were stored in water. For preparation of the dumbbell particles db-CPS, 10.2 mg V65, 7.5 $\mu$L DVB, 500 $\mu$L VBC, and 6 mL 1 wt % aqueous PVA solution were added to an elongated 25 mL vial and emulsified at 8000 rpm for 6 minutes by using an IKA T-25 Ultra Turrax with an S25N 10G dispersing tool. Subsequently, 8 mL seeds dispersion (solid content = 4.4 wt %) was added and the vial was placed on a roller-table for 24 hours. After that, the vial was immersed in an oil bath of 70 °C to polymerize for 24 hours. The final product was washed with ethanol and water twice respectively. Finally, the colloids were stored in water.

### 4.2.7 Preparation of 2D floating colloidal crystal monolayers

Figure 4.1 illustrates the formation process of the colloidal crystal monolayers. Typical procedures to form floating colloidal crystal monolayers were as follows: 10 $\mu$L aqueous colloids dispersion (solid content = 5 wt %) and 190 $\mu$L water were added into a 1.5 mL centrifugal tube (Eppendorf Safe-Lock Tubes, colorless) and centrifuged, the supernatant was removed and 200 $\mu$L THF was added to re-disperse the particles. Subsequently, the centrifugal tube with colloidal dispersion was put in a fume hood with the centrifugal cap open for approximately 20 minutes. Afterwards, the remaining bulk dispersion was removed and another 200 $\mu$L THF was added. After manual shaking, the dispersion was filled into a capillary (0.20 mm $\times$ 2.00 mm internal dimensions, Vitrotubes). The filled capillary was placed on a microscope slide (Menzel-Gläser), sealed with high vacuum grease (DOW Corning, Sigma-Aldrich) and fixated using tape. Finally, the sample was observed with optical microscope.

### 4.2.8 Characterization

Transmission electron microscopy (TEM) images were taken with a Philips Tecnai 10 electron microscope typically operating at 100 kV. The samples were prepared by

drying a drop of diluted aqueous dispersion on top of polymer-coated copper grids. For freeze-drying sample, 1 $\mu$L dispersion was brought on a polymer coated copper grid. The grid was vitrified in liquid nitrogen and mounted on a cryo transfer unit which was brought under vacuum of about $10^{-4}$ Pa. Temperature was increased to -90 °C at 5 °C/minute and kept constant for about six hours under vacuum to allow the water to sublimate.

Scanning electron microscopy (SEM) images were taken with a Philips SEM XL FEG 30 typically operating at 5 - 10 kV. The dried samples of particles were sputter coated with 6 nm platinum prior to imaging.

Optical microscopy (OM) images were taken with a Nikon Ti-E inverted microscope. The microscope was equipped with a Nikon TIRF NA 1.49 100× oil immersion objective, intermediate magnification of 1.5×, and a Hamamatsu ORCA Flash camera.

## 4.3 Results and Discussion

### 4.3.1 Experimental proof of the existence of floating CCM

THF is introduced as both the dispersing solvent and the extracting solvent for CPS-Cl colloids, which are kept in a centrifugal tube made of polypropylene. After evaporating THF for approximately 20 minutes in a fume hood, we directly shake the centrifugal tube manually to re-disperse the formed aggregates, since THF itself is a good extracting solvent for CPS-Cl colloids. By following that procedure, floating colloidal crystal monolayers (CCM) are observed. Figure 4.2a and 4.2b show the optical microscopy images of the same two-dimensional colloidal assembly captured at different times. Clearly, the colloidal assembly can freely move and rotate in the continuous medium. In a closer view, the individual particles can clearly be distinguished in Figure 4.2b, revealing the monolayer structure of the formed colloidal assembly. The monolayer feature is further confirmed by scanning electron microscopy measurement (SEM). The SEM sample of the assemblies is prepared by first transferring the assemblies into water, followed by drying under atmospheric condition. As shown in Figure 4.2c, from the curved edge of the colloidal assembly we can clearly see the colloidal assembly is a monolayer. Figure 4.2d shows that a number of CCM can be prepared in one batch. The formed CCM are quite polydisperse in size, with typical dimensions

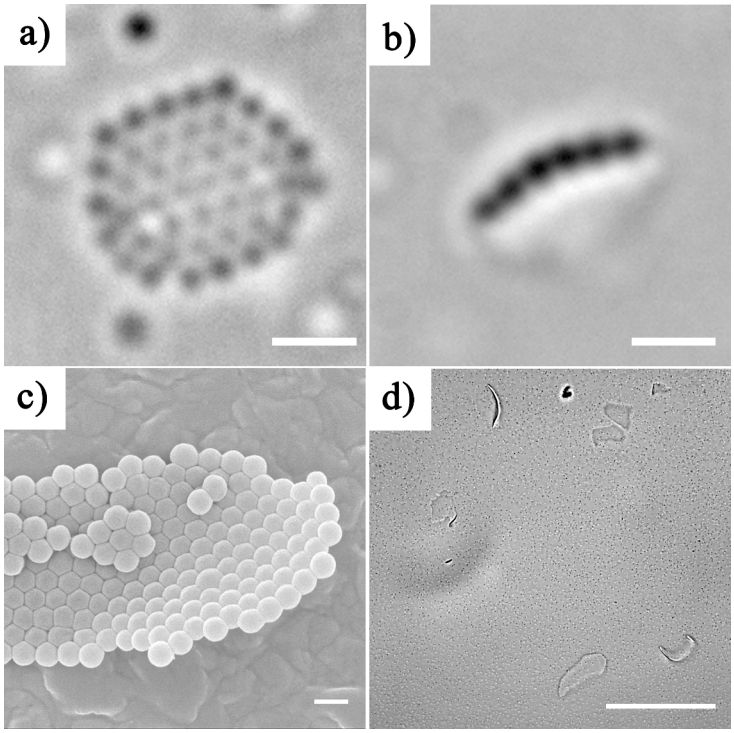


Figure 4.2. (a, b) Optical microscopy images of the same colloidal crystal monolayer (CCM) captured at different times. (c) SEM image of the CCM, sample is dried under atmospheric conditions. (d) Low magnification of optical microscopy image of the CCM. Scale bars: 2 $\mu$m for a, b and c, and 20 $\mu$m for d.

in between roughly 25 $\mu m^2$ and 10000 $\mu m^2$. The shape of these CCM is irregular, sometimes even curved monolayers are observed. Both the size polydispersity and the shape irregularity can be ascribed to the mechanical force generated during the peeling-off process. Additionally, Figure 4.2 also shows that the colloids in the CCM are close-packed mostly in a hexagonal way. These results show that close-packed floating CCM with high yields are prepared.

### 4.3.2 Determination of the location where the CCM form

Before investigating in more details the influences of experimental conditions on the formation of floating CCM and thereafter proposing a possible formation mechanism, it is crucial to find out first the location where the CCM form. In this system, there are roughly three potential locations for monolayers formation, namely on the wall, in the bulk or at the air-liquid interface. Therefore further experiments are conducted to determine where in the sample the monolayers tend to form. In the first experiment, a sample is carefully taken far from the walls and interface, while not shaking the sample. A polypropylene pipette with a very sharp and long tip is used to withdraw the sample to guarantee the accuracy of the sample location. As shown in Figure 4.3a, no monolayer structures appear in this region. In the second experiment, after evaporating THF for approximately 20 minutes in the fume hood, the remaining bulk dispersion is removed carefully and THF is added again, followed by manual shaking. Figure 4.3b (low magnification) and 4.3c (high magnification) show the results. Clearly, floating CCM are found. These results preliminarily indicate that monolayers formed onto the wall of the tube rather than in the bulk.

To eliminate the possibility that the shaking induced monolayer formation, and further demonstrate the importance of the evaporation process on the formation of CCM, another control experiment is conducted. A THF dispersion with colloids is again stored in a centrifugal tube, but this time the tube is closed and firmly sealed by parafilm to prevent evaporation of THF. The sample is left in the fume hood for approximately 20 minutes and subsequently shaken manually. As shown in Figure 4.3d, no monolayers are found in this experiment. Therefore, we conclude that the monolayer is formed on the wall during the evaporation process of the dispersing solvent. Shaking the sample itself does not induce the formation of CCM but only transfers the CCM from the walls into the bulk. Furthermore, this experiment also implies that CCM are not likely formed at the air-liquid interface.

Given the observation that the CCM are formed on the wall due to the evaporation of the dispersing solvent and these CCM are released from the wall into the extracting solvent by manual shaking, it is natural to investigate the influences of the nature of the dispersing solvents as well as the extracting solvents, the vessel wall materials, and the types of colloids. These variables will be investigated systematically in the

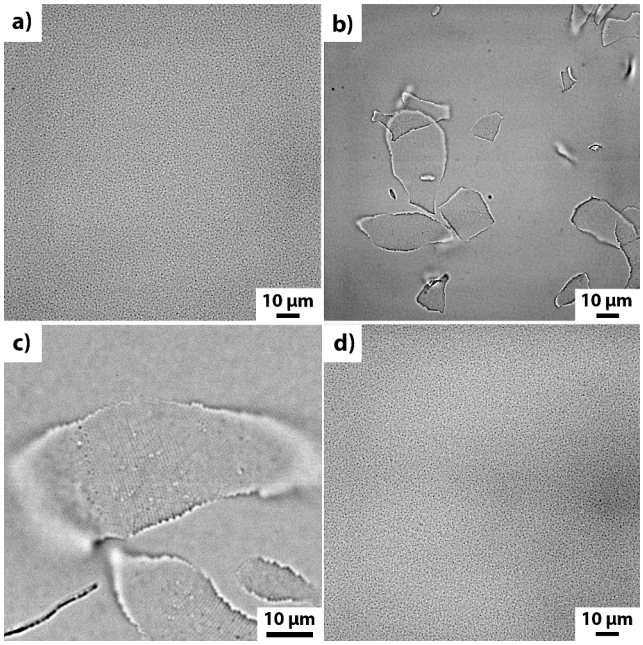


Figure 4.3. Optical microscopy images of the samples. (a) The sample is carefully withdrawn far from the walls and interface after the centrifugal tube with colloidal THF dispersion is placed in the fume hood for approximately 20 minutes with the cap opened, no shaking before withdrawal. (b, c) The sample is prepared by removing the remaining bulk dispersion of (a), refilling the centrifugal tube with THF, following by manual shaking. (b) Low and (c) high magnification. (d) The sample is withdrawn from the centrifugal tube after the centrifugal tube with colloidal THF dispersion is placed in the fume hood for approximately 20 minutes with the cap firmly closed. Shaking is carried out before withdrawal. Conditions: CPS-Cl colloids are used, THF is used as both the dispersing solvent and the extracting solvent. The centrifugal tubes are made of polypropylene. Scale bars: 10 $\mu$m for all images.

following subsections.

### 4.3.3 Influence of the dispersing solvent

The influence of the dispersing solvent on the colloidal crystal monolayers formation is studied in terms of the evaporation rate of the dispersing solvent. The evaporation rate can be characterized by the vapor pressure, which is an intrinsic feature of a solvent

Table 4.1. The dielectric constant, vapor pressure and dipole moment of selected solvents

| Solvent | Dielectric Constant[a] | Vapor Pressure/kPa[b] | Dipole Moment/D[a] |
|---|---|---|---|
| Acetone | 21.01 | 24 | 2.88 |
| Acetonitrile | 36.64 | 9.7 | 3.93 |
| *N*,*N*-Dimethylformamide | 38.25 | 0.35 | 3.83 |
| Dimethyl sulfoxide | 47.24 | 0.061 | 3.96 |
| 1,4-Dioxane | 2.22 | 4.1 | - |
| Ethanol | 25.3 | 5.9 | 1.69 |
| Methanol | 33.0 | 12.8 | 1.7 |
| Methyl acetate | 7.07 | 22 | 1.73 |
| *N*-Methyl-2pyrrolidone | 32.55 | - | 4.1 |
| Tetrahydrofuran | 7.52 | 20 | 1.75 |
| Water | 80 .1 | 1.75 | 1.85 |

a) Obtained from "W. M. Haynes, CRC Handbook of Chemistry and Physics, 97th Edition, CRC Press 2016". b) Obtained from "Christian Reichardt, Solvents and Solvent Effects in Organic Chemistry, Wiley-VCH Publishers, 3rd ed., 2003".

and varies among different solvents. Therefore, various dispersing solvents including ethanol, acetonitrile, methanol, methyl acetate and acetone are tested. The above dispersing solvents are selected for two reasons. On the one hand, all of them disperse CPS-Cl well. On the other hand, they all have relatively high vapor pressures (Table 4.1). The high vapor pressure under atmospheric conditions allows us to perform the experiments in a relatively short time. The other conditions are kept constant: CPS-Cl colloids are used, the centrifugal tubes are made of polypropylene, the evaporation time is approximately 20 minutes and after evaporation, the remaining bulk dispersion is removed and replaced by THF, as shown in Figure 4.4. In all these samples CCM are observed (Figure 4.5). From the observations we draw two conclusions. First, the selected dispersing solvents have significantly different dielectric constant and dipole moment (Table 4.1), while CCM are found in all the selected dispersing solvents, hence we conclude that the variation of the van der Waals interaction, the electrostatic interaction and the dipolar-dipolar interaction is not large enough to lead to significant differences in this system. Second, considering that the vapor pressure of the selected dispersing solvents are quite different, the difference of the vapor pressure can be as large as 4 times, and the vapor pressure is an indication of the evaporation rate of solvent, therefore we conclude that the evaporation rate of the dispersing solvent within that range has only a limited influence on the CCM formation in this system.

However, even though CCM are found in all the samples, the CCM obtained in

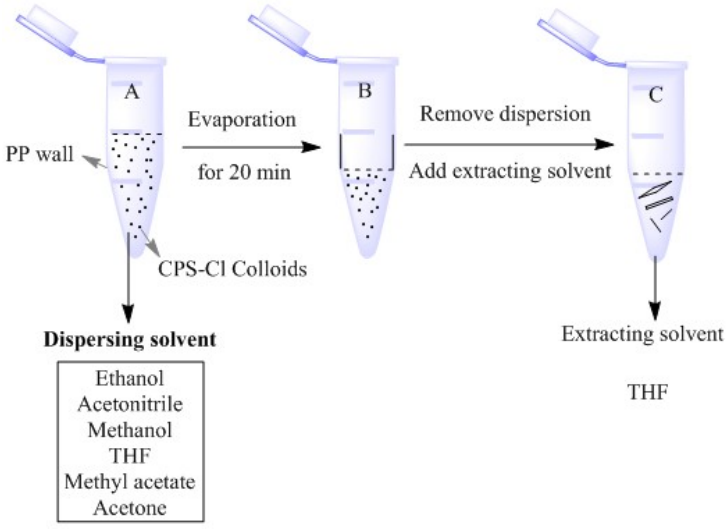


Figure 4.4. Schematic illustration for investigating the influence of the dispersing solvent on the colloidal crystal monolayers formation.

different dispersing solvents are found to have slightly different structures. As shown in Figure 4.5, in ethanol and acetonitrile, CCM with more cracks are formed; in methanol and acetone, relatively smaller CCM are observed; while in THF and methyl acetate, larger CCM with less cracks are obtained. This will be discussed later.

### 4.3.4 Influence of the wall material

Previous results show that CCM form on the wall of the centrifugal tube, herein we investigate the influence of the wall material on the formation of CCM systematically. Therefore centrifugal tubes made of different materials, including polypropylene (PP), low-density polyethylene (LDPE), polypropylene-copolymer (PPCO), polycarbonate (PC), polyallomer (PA, ethylene propylene copolymer) and glass are tested. Since THF is a good solvent for most of the above materials while ethanol is not, ethanol is employed as the dispersing solvent [23]. CPS-Cl dispersed in ethanol is stored in the above centrifugal tubes, after evaporation for approximately 20 minutes in the fume hood, the remaining bulk dispersion is removed and THF used as the extracting solvent is added. After manual shaking, samples are taken and inspected with optical

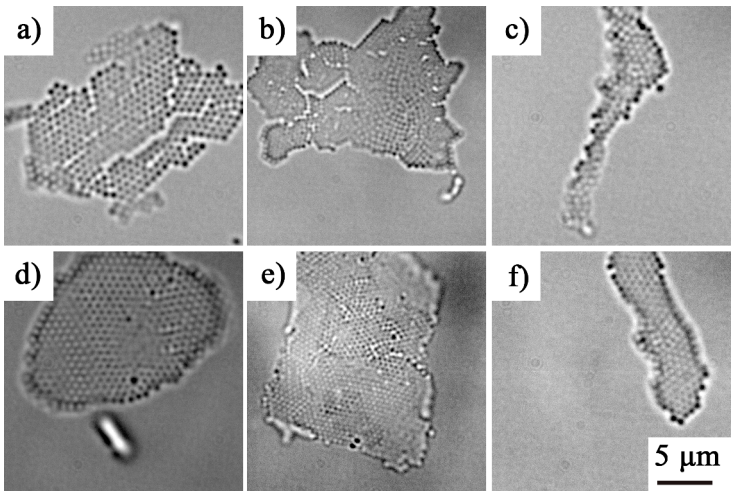


Figure 4.5. Optical microscopy images of the colloidal crystal monolayers obtained in the dispersing solvent of (a) ethanol, (b) acetonitrile, (c) methanol, (d) THF, (e) methyl acetate and (f) acetone. Conditions: CPS-Cl colloids are used, THF is used as the extracting solvent. The centrifugal tubes are made of polypropylene. Scale bars: 5 $\mu$m for all images.

microscope (Figure 4.6). As shown in Figure 4.7, CCM are found in all the samples except for the glass one. Considering that the glass is hydrophilic while most of the polymer materials used here are hydrophobic, the fact that CCM only form on the organic polymer-based substrates while not on the glass implies the importance of the hydrophobicity of wall materials on the CCM formation. The hydrophobicity of a material can be quantified by the contact angle of the material with water. The contact angle of a liquid drop on a solid surface is the angle measured through the liquid, where a liquid-vapor interface meets a solid surface. If the water contact angle of the materials is smaller than 90°, the solid surface is considered hydrophilic while it is hydrophobic if the water contact angle is larger than 90°. The water contact angle of the glass is approximately 10° indicating that glass is quite hydrophilic [24], while the organic polymer-based materials have contact angles in the range from 82° (PC) to 102° (PP) [25]. Therefore, we conclude here that slightly hydrophilic or hydrophobic substrate is required for the formation of the CCM.

Figure 4.7 also shows that all of the formed CCM have cracks, which is consistent

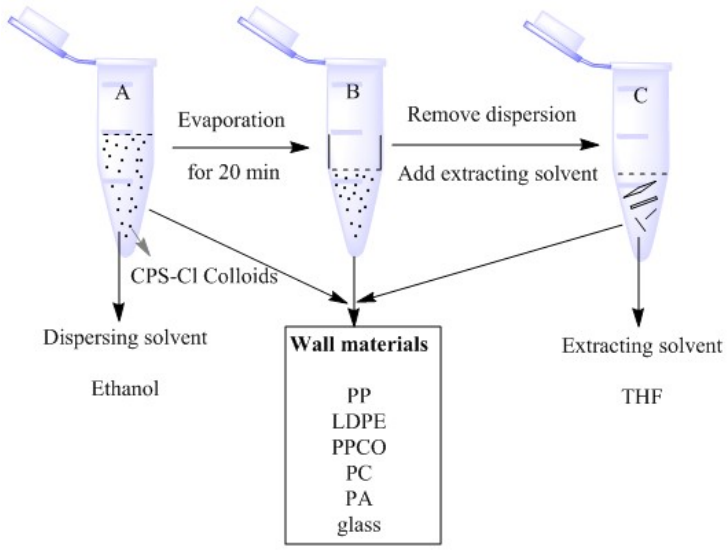


Figure 4.6. Schematic illustration for investigating the influence of the wall material on the colloidal crystal monolayers formation.

with previous observation that CCM with cracks are formed when ethanol is used as the dispersing solvent (Figure 4.5a). Again we will discuss this later.

### 4.3.5 Influence of the extracting solvent

The key difference between the method shown here and the classical vertical deposition reported before [9, 11] is that the formed CCM can readily peel off and freely float in the solvent by using the method described here. Since THF is used as the extracting solvent in our method instead of water being commonly used in classical vertical deposition, we speculate that the properties of the extracting solvent have significant influence on the detachment of the CCM. To study the influence of the extracting solvent, water is employed as the extracting solvent at first. In the experiments conducted here, THF and CPS-Cl are used as the dispersing solvent and the colloids, respectively, and the centrifugal tubes are made of PP. After evaporating colloidal THF dispersion for approximately 20 minutes in the fume hood and removing the remaining bulk dispersion carefully, water as the extracting solvent is refilled and the

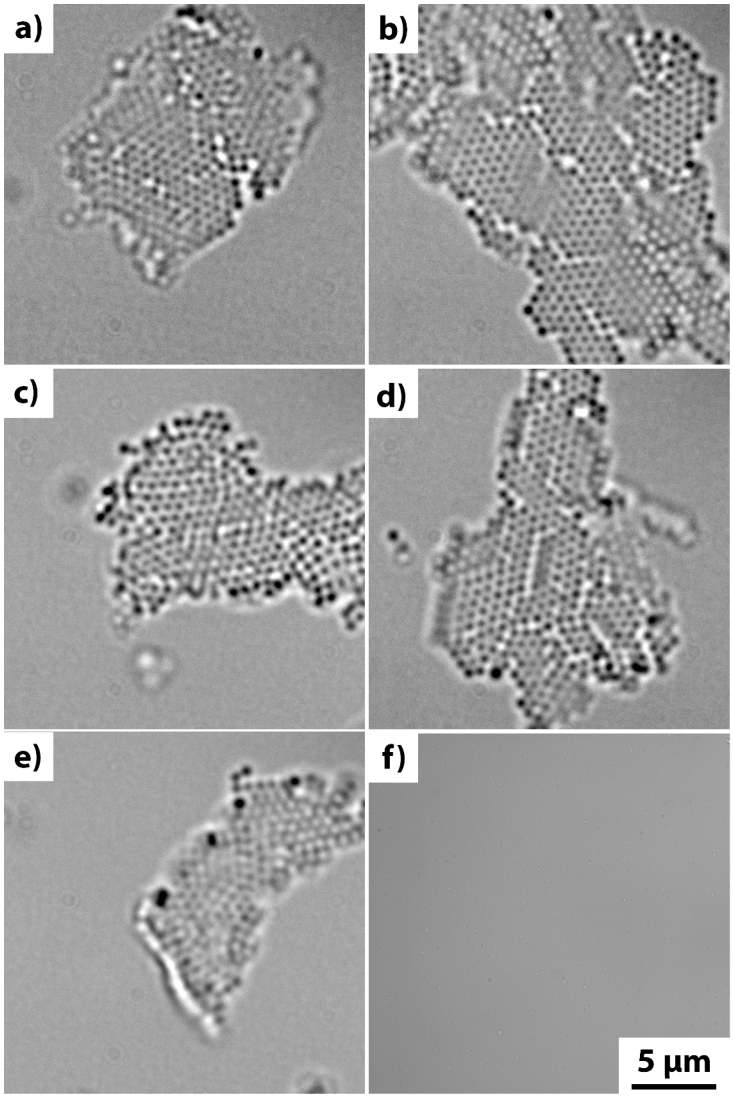


Figure 4.7. Optical microscopy images of samples prepared in the centrifugal tubes made of (a) polypropylene (PP), (b) low-density polyethylene (LDPE), (c) polypropylene-copolymer (PPCO), (d) polycarbonate (PC), (e) polyallomer (PA, ethylene propylene copolymer) and (f) glass. Conditions: CPS-Cl colloids are used, ethanol and THF are used as the dispersing solvent and the extracting solvent, respectively. Scale bars: 5 $\mu$m for all images.

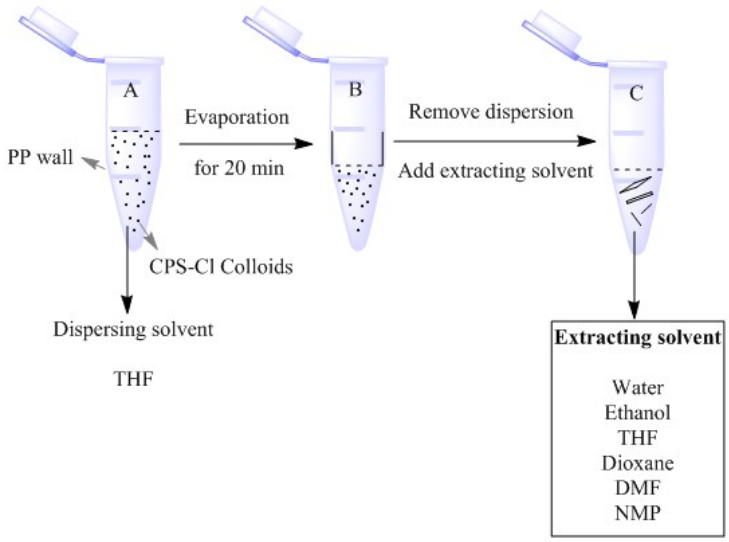


Figure 4.8. Schematic illustration for investigating the influence of the extracting solvent on the colloidal crystal monolayers formation.

sample is manually shaken, as shown in Figure 4.8. Figure 4.9a shows that no CCM are found when water is used as the extracting solvent. There are two possibilities for the absence of CCM in this sample. The first possibility is that the CCM disintegrate into their separate colloidal building blocks. The dielectric constants of THF and water are 7.52 and 80.1 respectively (Table 4.1), in the experimental conditions here, the electrostatic repulsion between particles in water is much higher than that in THF. The dramatically increased repulsion between particles in water may result in the disintegration of CCM. The other possibility is that water is too polar, the solubility of water towards CCM is poor (CCM is made of CPS-Cl which mainly consists of polystyrene), the CCM still stay on the wall and hence no CCM are found in water. To find out, further experiments are conducted. In the first experiment, the water in the above sample is removed, subsequently THF is added, followed by manual shaking. Clearly, CCM are observed as shown in Figure 4.9b, excluding the possibility that water disintegrates the CCM. In the second experiment, ethanol and *N*-Methyl-2pyrrolidone (NMP) are deliberately selected as the extracting solvent for two reasons. On the one hand, they have similar dielectric constant (Table 4.1). On

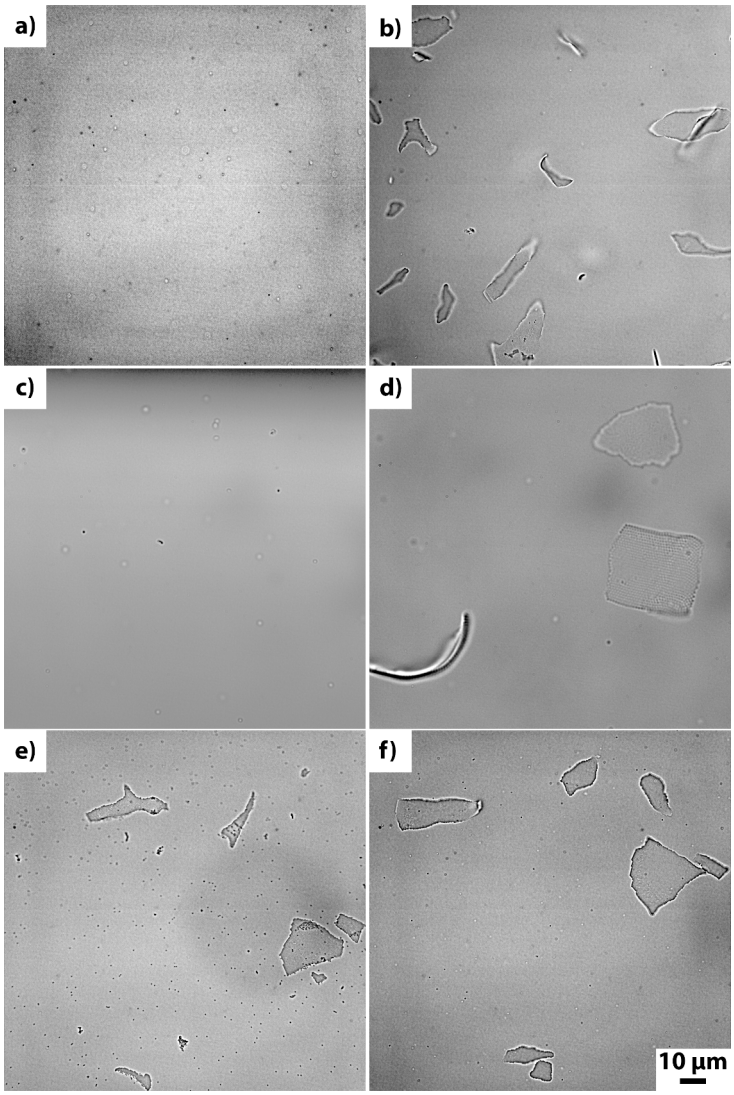


Figure 4.9. Optical microscopy images of samples obtained by using extracting solvent of (a) water, (c) ethanol, (d) *N*-methyl-2-pyrrolidone (NMP), (e) 1, 4-dioxane and (f) DMF. (b) Remove water in (a), then THF is added. Conditions: CPS-Cl and THF are used as the colloids and the dispersing solvent, respectively. The centrifugal tubes are made of polypropylene. Scale bars: 10 $\mu$m for all images.

the other hand, they have different solubility to polystyrene, NMP is a good solvent for polystyrene while ethanol is not [26]. If the absence of CCM in water is due to increased electrostatic repulsion, we would expect that similar results in ethanol and NMP would be observed since they have similar dielectric constant. If the solubility of the extracting solvent is the determining factor, then we would expect that NMP can peel the CCM off while ethanol cannot, hence CCM would be present in NMP but not in ethanol. Clearly, no CCM are found in ethanol (Figure 4.9c) while a number of CCM are present in NMP (Figure 4.9d). Therefore, we can conclude that the solubility of the extracting solvent is more important than the dielectric constant to peel the CCM off. To further confirm this point, 1, 4-dioxane and DMF are selected as the extracting solvent which are both good solvents for polystyrene but with significantly different dielectric constant (Table 4.1) [26]. As show in Figure 4.9e (1, 4-dioxane) and 4.9f (DMF), once more CCM are observed in both solvents.

### 4.3.6 Influence of the types of colloids

To investigate the versatility of the present method, various types of colloids are tested. THF is used as the dispersing solvent as well as the extracting solvent, and the centrifugal tubes used here are made of polypropylene. As shown in Table 4.2 and Figure 4.10, regardless of the materials, the morphologies, the size and the surface chemical functionalities of the colloids, CCM are existed in all cases, indicating the versatility of the present method.

Table 4.2. Materials, morphologies, size and surface chemical functionalities of the colloids CPS-Cl, CPS, CPSAA, CPS-$NH_2$, d-CPS, db-CPS and PMMA

| colloid | Materials | Morphologies | Diameter | Surface chemical functionalities |
|---|---|---|---|---|
| CPS-Cl | PS | sphere | 460 nm[a] | -$OSO_3^-$ / Cl |
| CPS | PS | sphere | 470 nm[a] | -$OSO_3^-$ |
| CPSAA | PS | sphere | 461 nm[a] | -$OSO_3^-$ / -$COO^-$ |
| CPS-$NH_2$ | PS | sphere | 460 nm[a] | -$OSO_3^-$ / -$NH_3^+$ |
| d-CPS | PS | dimple | 871 (400[c]) nm[b] | PVP |
| db-CPS | PS | dumbbell | 820 (476[d]) nm[b] | PAA/Cl |
| PMMA | PMMA | sphere | 1080 nm[b] | PHS[e] |

a) Obtained from DLS. b) Obtained from TEM. c) Diameter of the cavity of the dimple particle. d) Diameter of the small lobe. e) Poly(12-hydroxystearic acid) graft copolymer.

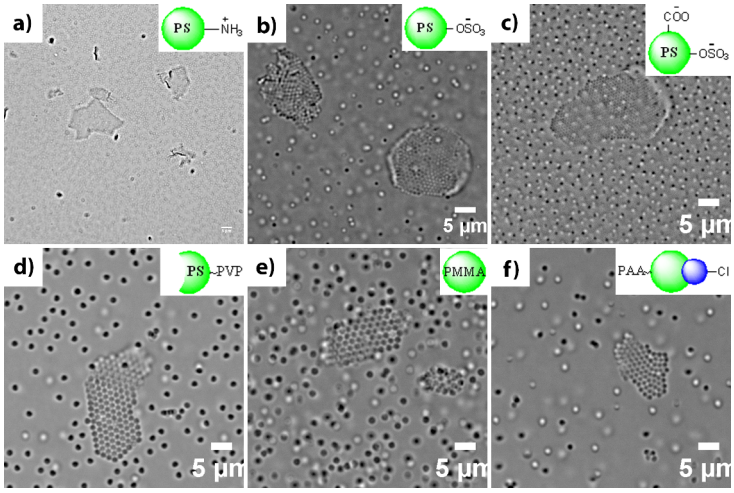


Figure 4.10. Optical microscopy images of the colloidal crystal monolayers made from (a) positively charged PS nanospheres; (b, c) negatively charged PS nanospheres; (d) PVP stabilized PS dimple particles; (e) PMMA nanospheres; (g) dumbbell particles. Conditions: THF is used as both the dispersing solvent and the extracting solvent. The centrifugal tubes are made of polypropylene. Scale bars: 10 $\mu$m for (a), 5 $\mu$m for (b-f).

### 4.3.7 Formation mechanism hypothesis

Based on the experimental results, we now propose a mechanism for the CCM formation, as summarized in Figure 4.11. Firstly, a wetting film of the dispersion arises upward along the wall of the centrifugal tube as the wall is wettable by the dispersing solvent (the contact angle is significantly smaller than 90° as the dispersing solvent can spread over the surface of the centrifugal tube), as shown in Figure 4.11a. With the evaporation of the dispersing solvent, the thickness of the upper part of the wetting film decreases which presses the colloids towards the wall, resulting in a dense layer of colloids onto the wall, as shown in Figure 4.11b [10]. Further evaporation of the dispersing solvent results in the formation of a meniscus structure of air-liquid interface between the colloids on the wall. The deformation of the meniscus structure gives rise to capillary attraction, driving the colloids towards the nucleus, hence a monolayer is formed onto the wall. Simultaneously, more colloids are delivered towards the monolayer growth front by a solvent flux which is built up by the evaporation of

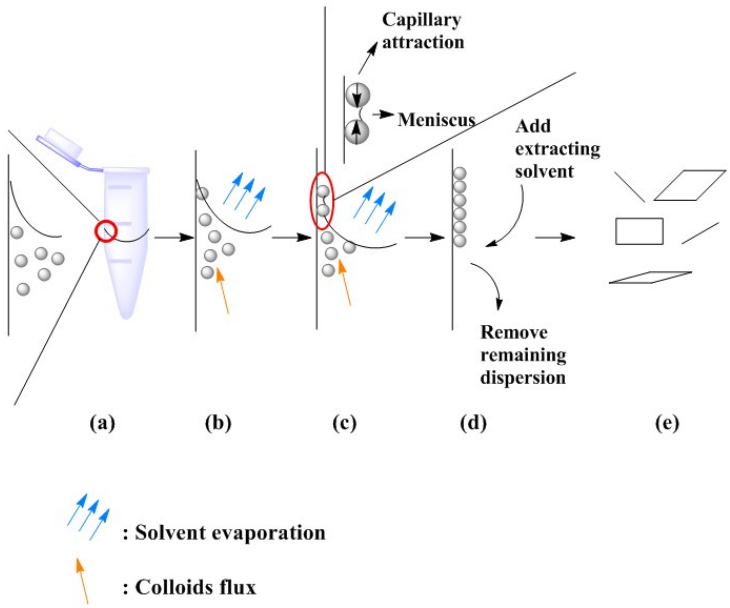


Figure 4.11. Schematic illustration of possible mechanism for the colloidal crystal monolayers formation.

the dispersing solvent, as shown in Figure 4.11c and 4.11d [9, 11]. During this process, the capillary attractions are responsible for pushing the colloidal particles through their stabilizing electrical double layer and steric stabilization layer. Once the particles surface separation is sufficiently close, van der Waals attraction starts dominating and it is probably the attraction that ultimately stabilize the CCM. After replacing the dispersing solvent by a extracting solvent, the extracting solvent penetrates the gap between the colloidal monolayers and the wall surface. Since the attractive forces between the CCM and the wall are weak in the presence of the extracting solvent, the CCM prefer to go to the extracting solvent, therefore the monolayers peel off from the wall and freely float in the extracting solvent, as shown in Figure 4.11e. In this proposed mechanism, there are two main steps: CCM form on the wall and CCM peel off into the extracting solvent. The first step of the proposed mechanism is similar to the classical vertical deposition mechanism. In a classical vertical deposition, (super-)hydrophilic substrate (usually glass or mica after treatment with strong acidic

solution) is inserted into the aqueous colloidal dispersions and withdrawn with a velocity of typical several $\mu$m/s. With that procedure, monolayer or multiple layers colloidal crystals are formed [9, 11]. However, there are three crucial differences between the method reported here and the classical vertical deposition. The first difference is the dispersing solvent. While water is generally being used in the classical vertical deposition, here we use volatile solvents which apparently accelerates the formation of CCM. Second, hydrophobic material (organic polymers) instead of (super-)hydrophilic glass is used as a substrate, and the tedious pretreatment of substrate is avoided. The last and most important distinction is that by using the method present here, CCM can be peeled off easily, and freely float in the dispersion, which is ascribed to the selection of the appropriate extracting solvents.

### 4.3.8 Influence of the solvent on the properties of CCM

As already shown in Figure 4.5 and Figure 4.7, CCM with cracks as well as relatively small size are formed when ethanol, acetonitrile, methanol and acetone are used as the dispersing solvent, while in THF and methyl acetate, larger CCM and with less cracks are obtained. It is well known that the last solvents are good solvent for polystyrene while the first mentioned solvents are not. Therefore, we speculate that the solubility of the dispersing solvent towards polystyrene might contribute to the slightly different CCM structures obtained in different dispersing solvents. Before investigating the influence of the solubility of dispersing solvent on the formed CCM structures, we first look into the morphologies of the colloids CPS-Cl after treatment with different types of dispersing solvents. Ethanol and THF are chosen as representatives for bad solvent and good solvent for polystyrene, respectively. The colloids are first dispersed in either ethanol or THF, and subsequently in water after washing for three times. Afterwards, both samples are placed on the TEM grids and dried by a freeze-drying process so that shrinkage of the CPS-Cl is prevented [27]. Figure 4.12a and 4.12b are the TEM images of CPS-Cl after treatment with ethanol and THF, respectively. Evidently, CPS-Cl remains intact after treatment with ethanol, while a yolk-shell structure is formed when CPS-Cl is treated with THF. The formation of the yolk-shell structure in THF is ascribed to the etching of the linear polystyrene in CPS-Cl by THF (see **Appendix 3.4** of **Chapter 3** for more information).

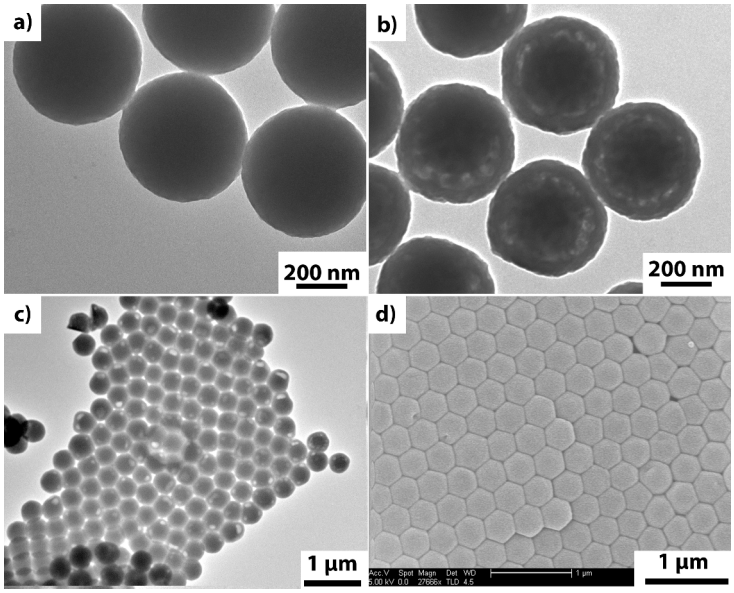


Figure 4.12. TEM images of CPS-Cl after treated with (a) ethanol and (b) THF, the samples are dried by the freeze-drying process. (c) TEM image of the freeze-drying colloidal crystal monolayers (CCM) sample. The CCM are prepared by using THF as both the dispersing solvent and the extracting solvent. (d) SEM image of the CCM sample dried under atmospheric conditions. The CCM are prepared by using THF as both the dispersing solvent and the extracting solvent. Scale bar: (a, b) 200 nm, (c, d) 1 $\mu$m.

Based on these results, we further speculate that the yolk-shell structure formed in THF allows the colloids to pack closer and even interpenetrate upon evaporation. Figure 4.12c shows a TEM image of CCM obtained by using THF as the dispersing solvent. This TEM sample is also prepared by using the freeze-drying method. Compared to the free yolk-shell colloids in Figure 4.12b, the yolk-shell colloids in CCM have hexagonal shapes. The colloids are deformed and compressed by the neighboring colloids, resulting in compression and flattening of the shell at the contact regions. Furthermore, the colloids center-to-center separation in CCM is approximately 343 nm, significantly smaller than the diameter of the free yolk-shell colloids (394 nm), further indicating that the colloids are compressed by the neighboring colloids. Figure 4.12d shows a SEM image of CCM dried under atmospheric conditions, as can be

seen, the spherical colloids are also deformed into hexagonally shaped colloids, further indicating that the shell of the colloids is deformable. These results show that in good solvent, the colloids are etched into yolk-shell structure and the shell is deformable, which allows the colloids to pack closer and interpenetrate during the evaporation process, eventually resulting in the formation of relatively larger CCM with fewer defects. On the other hand, even though CCM can form on the wall when ethanol is used as the dispersing solvent, however, a good solvent such as THF is required to peel off the CCM. The use of THF during the peel off procedure may interfere the structure of the formed CCM. Therefore, we do not have TEM or SEM images of CCM in ethanol.

### 4.3.9 Stability of CCM

Figure 4.13a shows an optical microscopy image of a CCM sample after storing in THF overnight. Clearly, the CCM keep intact, neither aggregation nor disintegration of the CCM is observed. In contrast, sonication of a sample even only for 1 min, CCM completely disintegrate. As shown in Figure 4.13b, free colloids instead of CCM are found. However, the stability of CCM against sonication can be improved to some extent by centrifuging the sample. Before placing the CCM sample in the sonication bath, it is centrifuged at 10600 $g$ for 2.5 minutes. As indicated in Figure 4.13c, CCM are still presented. It is found that after the centrifuge process, the sonication can only break the CCM and make them smaller, instead of completely disintegrate them. Interestingly, no aggregation of the CCM are found, even when the monolayer sample is centrifuged, indicating that the CCM are quite stable. Moreover, the CCM can readily be transferred into water. Figure 4.13d shows a representative optical microscopy image of CCM dispersed in water. The appearance of CCM in water is quite different compared to that in THF (Figure 4.13a), we do not fully understand at this point, one possibility is the difference in refractive index between water and THF. However, from the edge of the CCM, we can clearly distinguish the individual particles, indicating that they are CCM instead of some other materials such as dusts. Considering that water is ubiquitous and environmentally friendly, the fact that the CCM can transfer into water from organic solvents widens the potential applications of the CCM, makes the present method more practical.

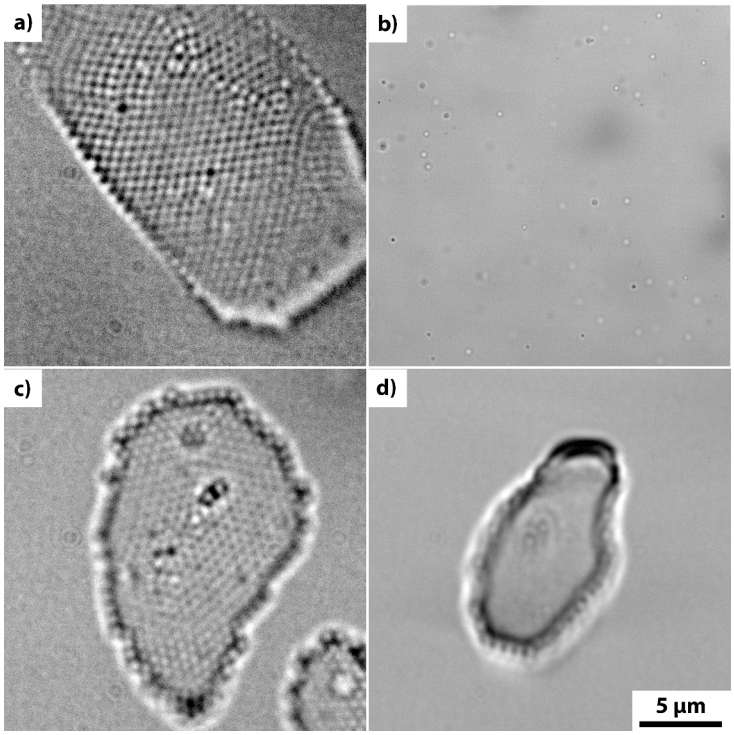


Figure 4.13. Optical microscopy images of CCM samples (a) after storing in THF overnight. (b) after sonication for 1 min. (c) after centrifugation at 10600 $g$ for 2.5 min, followed by sonication for 1min. (d) in water. Scale bars: 5 $\mu$m for all images.

## 4.4 Conclusion

We report a facile and robust method to prepare well-defined, two-dimensional floating colloidal crystal monolayers consisting of building blocks with sizes on the order of the wavelength of visible light. The method involves two steps. In the first step, we make plausible that evaporation of the dispersing solvent results in the formation of a meniscus structure of the air-liquid interface between the colloids on the wall of the centrifugal tube. The deformation of the meniscus gives rise to capillary attraction, driving the colloids towards the crystal zone, therefore monolayers are formed on the wall. The capillary attractions are responsible for pushing particles together

while it is probably the van der Waals attractions that ultimately stabilize the CCM. Subsequently, the remaining bulk dispersion is replaced by an extracting solvent which is a good solvent for polystyrene. Floating CCM are obtained by peeling the colloidal monolayers off from the wall.

The influences of the dispersing solvents, the wall materials, the extracting solvents, and the nature of the colloids on the formation of the CCM are investigated systematically. We find that the evaporation rate of the dispersing solvent indicated by its vapor pressure has negligible influence on the formation of the CCM, while the solubility of CCM in the dispersing solvent has to some extent influence on the structure of the formed CCM. Larger CCM with less cracks can be prepared provided that the dispersing solvent is a good solvent for polystyrene. The key to peel the CCM off from the wall is the selection of the appropriate extracting solvent which is also a good solvent for polystyrene. Furthermore, the CCM formation process is robust in terms of the wall material and the types of the colloids. Eventually, CCM can easily be transferred into water which might broaden potential applications.

## Acknowledgements

I would like to thank Kanvaly Lacina for taking the scanning electron microscopy images. Hans Meeldijk and Chris Schneijdenberg are thanked for help with freeze-drying samples.

## Bibliography

[1] X. Ye and L. Qi. Two-dimensionally patterned nanostructures based on monolayer colloidal crystals: Controllable fabrication, assembly, and applications. *Nano Today*, 6:608–631, 2011.

[2] S. C. Yang, D. J. Yang, J. Kim, J. M. Hong, H. G. Kim, I. D. Kim, and H. Lee. Hollow $TiO_2$ hemispheres obtained by colloidal templating for application in dye-sensitized solar cells. *Advanced Materials*, 20:1059–1064, 2008.

[3] H. Gao, W. Zhou, and T. W. Odom. Plasmonic crystals: A platform to catalog

resonances from ultraviolet to near-infrared wavelengths in a plasmonic library. *Advanced Functional Materials*, 20:529–539, 2010.

[4] J.-T. Zhang, L. Wang, J. Luo, A. Tikhonov, N. Kornienko, and S. A. Asher. 2-D array photonic crystal sensing motif. *Journal of the American Chemical Society*, 133:9152–9155, 2011.

[5] M. E. Abdelsalam, P. N. Bartlett, J. J. Baumberg, and S. Coyle. Preparation of arrays of isolated spherical cavities by self-assembly of polystyrene spheres on self-assembled pre-patterned macroporous films. *Advanced Materials*, 16:90–93, 2004.

[6] P. Jiang. Surface-templated nanostructured films with two-dimensional ordered arrays of voids. *Angewandte Chemie International Edition*, 43:5625–5628, 2004.

[7] F. Sun, W. Cai, Y. Li, B. Cao, Y. Lei, and L. Zhang. Morphology-controlled growth of large-area two-dimensional ordered pore arrays. *Advanced Functional Materials*, 14:283–288, 2004.

[8] J.-T. Chen, D. Chen, and T. P. Russell. Fabrication of hierarchical structures by wetting porous templates with polymer microspheres. *Langmuir*, 25:4331–4335, 2009.

[9] N. Vogel, C. K. Weiss, and K. Landfester. From soft to hard: the generation of functional and complex colloidal monolayers for nanolithography. *Soft Matter*, 8:4044–4061, 2012.

[10] N. Denkov, O. Velev, P. Kralchevski, I. Ivanov, H. Yoshimura, and K. Nagayama. Mechanism of formation of two-dimensional crystals from latex particles on substrates. *Langmuir*, 8:3183–3190, 1992.

[11] A. S. Dimitrov and K. Nagayama. Continuous convective assembling of fine particles into two-dimensional arrays on solid surfaces. *Langmuir*, 12:1303–1311, 1996.

[12] A. Mihi, M. Ocaña, and H. Míguez. Oriented colloidal-crystal thin films by spin-coating microspheres dispersed in volatile media. *Advanced Materials*, 18:2244–2249, 2006.

[13] K.-Q. Zhang and X. Y. Liu. *In situ* observation of colloidal monolayer nucleation driven by an alternating electric field. *Nature*, 429:739–743, 2004.

[14] M. Kondo, K. Shinozaki, L. Bergstroem, and N. Mizutani. Preparation of colloidal monolayers of alkoxylated silica particles at the air-liquid interface. *Langmuir*, 11:394–397, 1995.

[15] F. Reincke, S. G. Hickey, W. K. Kegel, and D. Vanmaekelbergh. Spontaneous assembly of a monolayer of charged gold nanocrystals at the water/oil interface. *Angewandte Chemie International Edition*, 43:458–462, 2004.

[16] J.-T. Zhang, L. Wang, D. N. Lamont, S. S. Velankar, and S. A. Asher. Fabrication of large-area two-dimensional colloidal crystals. *Angewandte Chemie International Edition*, 51:6117–6120, 2012.

[17] B. van Duffel, R. H. A. Ras, F. C. De Schryver, and R. A. Schoonheydt. Langmuir-Blodgett deposition and optical diffraction of two-dimensional opal. *Journal of Materials Chemistry*, 11:3333–3336, 2001.

[18] M. H. Kim, H. K. Choi, O. O. Park, and S. H. Im. Fabrication of robust, high-quality two-dimensional colloidal crystals from aqueous suspensions containing water-soluble polymer. *Applied Physics Letters*, 88:143127, 2006.

[19] Z. Lu and M. Zhou. Fabrication of large scale two-dimensional colloidal crystal of polystyrene particles by an interfacial self-ordering process. *Journal of Colloid and Interface Science*, 361:429–435, 2011.

[20] L. Ramos, T. C. Lubensky, N. Dan, P. Nelson, and D. A. Weitz. Surfactant-mediated two-dimensional crystallization of colloidal crystals. *Science*, 286:2325–2328, 1999.

[21] Z. Tang, Z. Zhang, Y. Wang, S. C. Glotzer, and N. A. Kotov. Self-assembly of CdTe nanocrystals into free-floating sheets. *Science*, 314:274–278, 2006.

[22] N. Geerts and E. Eiser. Flying colloidal carpets. *Soft Matter*, 6:664–669, 2010.

[23] Chemical resistances for beckman coulter centrifugation products. http://www.biophysics.bioc.cam.ac.uk/wp-content/uploads/2011/02/chemres.pdf, 2001.

[24] P. Kumnorkaew, Y.-K. Ee, N. Tansu, and J. F. Gilchrist. Investigation of the deposition of microsphere monolayers for fabrication of microlens arrays. *Langmuir*, 24:12150–12157, 2008.

[25] Critical surface tension and contact angle with water for various polymers. https://www.accudynetest.com/polytable_03.html.

[26] *Polymer Handbook, second edition.* John Wiley and Sons, Inc, 1975.

[27] W. Abdelwahed, G. Degobert, S. Stainmesse, and H. Fessi. Freeze-drying of nanoparticles: Formulation, process and storage considerations. *Advanced Drug Delivery Reviews*, 58:1688–1713, 2006.

Chapter 5

# pH Reversible Encapsulation of Oppositely Charged Colloids Mediated by Polyelectrolytes

ABSTRACT

We report the first example of reversible encapsulation of micron-sized particles by oppositely charged submicron smaller colloids. The reversibility of this encapsulation process is regulated by pH-responsive polyacrylic acid (PAA) present in solution. The competitive adsorption between the small colloids and the polyacrylic acid on the surface of the large colloids plays a key role in the encapsulation behavior of the system. pH offers an experimental knob to tune the electrostatic interactions between the two oppositely charged particle species *via* regulation of the charge density of the polyacrylic acid. This results in an increased surface coverage of the large colloids by the smaller colloids when decreasing pH. Furthermore, the polyacrylic acid also acts as a steric barrier limiting the strength of the attractive forces between the oppositely charged particle species, thereby enabling detachment of the smaller colloids. Finally, based on the pH tunability of the encapsulation behavior and the ability of the small colloids to detach, reversible encapsulation is achieved by cycling pH in the presence of the PAA polyelectrolytes. The role of polyelectrolytes revealed in this work provides a new and facile strategy to control heteroaggregation behavior between oppositely charged colloids, paving the way to prepare sophisticated hierarchical assemblies.

## 5.1 Introduction

Heteroaggregation is a clustering process that occurs between different species of particles and has proven to be a facile strategy for the preparation of a wide variety of (colloidal) clusters/assemblies [1–4]. The shape and structure of the formed clusters depend strongly on the size ratio and volume fractions of the participating particle species. Following this strategy a variety of super-structures have been prepared, including colloidal chains [4] and colloidal crystals [2, 3]. A particularly interesting class of heteroaggregates are so-called raspberry-like composites. These clusters are formed when aggregation is induced between particles with vastly different dimensions (size ratio of $D_{large}/D_{small} > 3$, where $D_{large}$ and $D_{small}$ represent the diameters of large colloid and small colloid respectively). The resulting cluster comprises a central large particle which is encapsulated by the smaller particles [5, 6]. The morphology of these clusters is characterized by large surface areas and high surface roughness. Naturally these parameters are set by the choice of the smaller encapsulation particles. Additionally, by using chemically modified smaller colloids, raspberry-like composites with controllable surface chemistry can be prepared. Owing to these key features, raspberry-like composites have great potential in applications such as catalyst immobilization platforms [7–9], super-hydrophobic films [10, 11], and sensors [12, 13]. To optimize the performance of these rough particles, many efforts have been devoted to precisely control the formation process of raspberry-like composites by using a variety of heteroaggregation strategies. Commonly applied strategies include electrostatics [14, 15], azide-alkyne click reactions [16], colloidal steric stabilization [12, 17], epoxy-amine reactions [10, 18], and non-covalent host-guest interactions [1]. Despite this variety of strategies, the majority of the resulting raspberry-like aggregates are formed irreversibly due to strong attractions compared to the thermal energy between the two particle species. An exception is the work of Yang et al. [1] who reported reversible raspberry-like composites by utilizing photo-responsive host-guest interactions to induce aggregation between the participating particle species. The disadvantage of their method is the requirement of extensive surface functionalization procedures.

Heteroaggregation is obviously not limited to synthetic (colloidal) constructs, but is also frequently exploited in biological systems. For example, the heteroaggregation of negatively charged nucleic acids (DNA or RNA) and net positively charged proteins

is for a large part responsible for the formation of virus capsids. In contrast to the synthetic strategies towards heteroaggregates mentioned above, the formation of virus capsids often is a fully reversible process. The reversibility is governed by a pH-responsive charge density of the individual capsid proteins due to the presence of acidic and basic moieties [19–22].

Inspired by the reversibility of nucleic acid encapsulation displayed by many viruses, we set out to design a reversible encapsulation system consisting of positively charged large polystyrene microspheres and negatively charged small polystyrene nanospheres which were decorated with a pH-responsive polyacrylic acid (PAA) polyelectrolyte outer layer. Since the charge density of the PAA-coated particles can be regulated by adjusting pH of the dispersion, we anticipated to observe pH-dependent encapsulation. At high pH, where the immobilized PAA polyelectrolytes are deprotonated, the particles bear their maximum negative charge, which should result in a high tendency for heteroaggregation. By lowering pH, the surface charge of the PAA-coated particles decreases, which is expected to lead to disintegration of the heteroaggregates. However, although we found a distinct pH-dependence on the encapsulation behavior, interestingly, the trend we observed was completely opposite to our expectation. These initially unexpected results could be rationalized by taking into account the presence of very low concentrations of free PAA-rich polyelectrolytes in the continuous phase that had leached from the PAA-coated particles. By systematically investigating the influence of free PAA on the encapsulation behavior, we were able to identify an experimental window in which the electrostatic mediated encapsulation process was completely reversible.

## 5.2 Experimental Section

### 5.2.1 Materials

Styrene (St, 99%), divinylbenzene (DVB, 55% mixture of isomers, tech. grade), acrylic acid (AA, 99%), [2-(methacryloyloxy)ethyl]trimethylammonium chloride (METMAC, 80 wt.% in water), polyacrylic acid (PAA, $M_w$ = 450 kg/mol), polyvinylpyrrolidone (PVP, $M_w$ = 40 kg/mol), methanol, sodium chloride (NaCl, ACS reagent, $\geq$ 99.5%), and sodium hydroxide (NaOH) were obtained from Sigma-Aldrich. Potassium persulfate

(KPS, > 99% for analysis) and azobis(isobutyronitrile) (AIBN, 98%) were purchased from Acros Organics. Hydrochloric acid (HCl, 36-38%, chem. pure) was obtained from Merck. All chemicals were used as received. The water used throughout all of the experiments was purified using a Milli-Q water purification system.

### 5.2.2 Synthesis of positively charged large polystyrene microspheres (PLPS)

PLPS were synthesized by stabilizer-free dispersion polymerization using METMAC as co-monomer [23, 24]. 37.5 mL methanol, 12.5 mL water, 10 mL styrene, 91 mg AIBN and 123 $\mu$L METMAC were added into a 100 mL three-necked round-bottom flask equipped with a condenser, mechanical stirrer and nitrogen gas inlet. The monomer mixture was purged with nitrogen for 30 min. After degassing, the mixture was mechanically stirred and heated to 75 °C to initiate the polymerization. The reaction was allowed to proceed for 8 h under nitrogen atmosphere. The final product was centrifuged at 500 $g$ for 3 min, and washed with ethanol and water sequentially to remove unreacted reagents as well as secondary nuclei. Finally, the resulting particles were stored in water.

### 5.2.3 Synthesis of negatively charged PAA-decorated small polystyrene nanospheres (CPSAA)

CPSAA were synthesized by surfactant-free emulsion polymerization using acrylic acid as comonomer [25]. 45 mL water, 5.5 mL St, 381 $\mu$L AA, and 27.5 $\mu$L DVB were added into a 100 mL three-necked round-bottom flask, followed by 25 mg KPS dissolved in 5 mL water. While being bubbled with nitrogen gas, the mixture was constantly stirred with a mechanical stirrer. After 15 min, the nitrogen inlet was raised above the liquid level for another 15 min. Subsequently, the flask was immersed in a 70 °C water bath to initiate the polymerization. The reaction was allowed to proceed for 24 h under nitrogen atmosphere. The final product was centrifuged at 15000 $g$ for 15 min, and washed with ethanol and water sequentially to remove unreacted reagents. Finally, the obtained colloids were stored in water.

### 5.2.4 Synthesis of negatively charged small polystyrene nanospheres (CPS)

CPS nanospheres were prepared using a similar method as described for CPSAA. The key difference was the absence of AA in the reaction mixture. 45 mL water, 4.7 mL St, and 140 $\mu$L DVB were added into a 100 mL three-necked round-bottom flask, followed by 156 mg KPS dissolved in 7.5 mL water. The flask was constantly stirred with a mechanical stirrer under nitrogen flow. Subsequently, the flask was immersed in a 80 °C water bath to initiate the polymerization. The reaction was allowed to proceed for 24 h under nitrogen atmosphere. The final product was centrifuged at 15000 $g$ for 15 min, and washed with ethanol and water sequentially to remove unreacted reagents. Finally, the particles were stored in water.

### 5.2.5 Encapsulation process

For all experiments, the small colloids were added in large excess. The number ratio of small colloids over large colloids was approximately 18000. Typical procedures to form clusters of oppositely charged colloids were as follows: 146 $\mu$L 13.7 mM aqueous HCl solution and 4 $\mu$L water were added into a 1.5 mL conical centrifuge tube and mixed *via* shaking by hand. Subsequently, 5 $\mu$L PLPS dispersion (solid content = 0.5 wt% ) was added and mixed. Finally, 45 $\mu$L CPSAA dispersion (solid content = 1 wt% ) was added and homogenized by shaking. The final dispersion was immediately placed on a roller-table and left to equilibrate for 1 h. After this period, 5 $\mu$L of the dispersion was placed on a home-made microscopy cell (for details see the **Characterization section** of **Chapter 3**). The resulting aggregates were directly observed by optical microscopy. Exact quantities and variations on this standard procedure are listed in **Appendix 5.1**.

To investigate the desorption of the smaller colloids and the reversibility of the encapsulation process, 13.7 mM aqueous NaOH solution was added to tune the pH to a desired value. After addition, the sample was equilibrated for 1 h before observation.

To investigate the influence of dissolved PAA on the surface coverage of the large positively charged particles by the smaller negatively charged colloids, commercial PAA was added to the particle dispersion during the heteroaggregation process. A final PAA concentration of $5\times10^{-6}$ g/ml was used. The samples were prepared following an

analogous procedure as described before. Firstly, PAA was dissolved in water followed by the addition of the negatively charged colloids. Lastly, the positively charged colloids were added.

### 5.2.6 Characterization

Transmission electron microscope (TEM) pictures were taken with a Philips Tecnai 10 electron microscope typically operating at 100 kV. The samples were prepared by drying a drop of diluted aqueous dispersion on top of polymer-coated copper grids.

Infrared (IR) spectra were obtained using a PerkinElmer Frontier FT-IR/FIR spectrometer. The attenuated total reflectance (ATR) mode was used. Measurements were carried out on powders obtained by drying the particle dispersion.

Optical microscopy (OM) images were taken with a Nikon Ti-E inverted microscope. The microscope was equipped with a Nikon TIRF NA 1.49 100× oil immersion objective, intermediate magnification of 1.5×, and a Hamamatsu ORCA Flash camera.

The hydrodynamic diameters of the particles were measured using dynamic light scatting (DLS). Measurements were performed on a Malvern Zetasizer Nano instrument. Highly diluted, aqueous samples were prepared at various pH values. The total ionic strength was adjusted to 10 mM for all samples. The measurements were taken in seven runs of 15 individual acquisitions at a scattering angle of 173°. The data was analyzed using the cumulant method.

Zeta potentials were determined by laser Doppler electrophoresis using the same instrument as used for DLS. Highly diluted, aqueous samples were prepared at various pH values. The total ionic strength of these samples was equal to 1 mM. The radii of particles ($R$) were approximately 250 nm, while the Debye length ($\kappa^{-1}$) is on the order of 10 nm under the conditions at which the electrophoresis measurements were conducted. Hence, $\kappa R >> 1$, justifying the use of the Smoluchowski limit of the Henry equation to convert the measured electrophoretic mobilites into the reported zeta potentials [26].

## 5.3 Results and Discussion

### 5.3.1 Synthesis of particles PLPS, CPS and CPSAA

Dispersion polymerization was chosen to synthesize PLPS since it allows for the preparation of particles in the micrometer size regime. The relatively large size of the resulting particles enables us to study the encapsulation behavior *in situ* by optical microscopy. METMAC was used as co-monomer during the dispersion polymerization. The permanently charged quaternary amine functionality of the co-monomer provides a highly hydrophilic character to this monomer, ensuring that the charged moieties will predominantly reside at the outer surface rather than in the hydrophobic interior of the formed colloids. The presence of positive charges also ensures colloidal stability of the particles. Figure 5.1a and 5.1b show an optical micrograph and corresponding size distribution of the prepared PLPS, respectively. The size distribution was obtained by measuring 100 particles in several optical micrographs of as-synthesized PLPS. The PLPS had a broad size distribution with a diameter of 5 $\pm$ 1 $\mu$m. Since the smaller particles used for the encapsulation experiments are significantly smaller than even the smallest PLPS particles, curvature effects are expected to be absent and hence the polydispersity of PLPS has no influence on the encapsulation behavior. Electrophoretic mobility measurements revealed a highly positive zeta potential equal to 55.7 $\pm$ 8.2 mV, indicating successful incorporation of METMAC onto the particle surface.

To synthesize CPS, emulsion polymerization was used, being the method of choice to synthesize submicron, charge stabilized particles. The typical dimensions of colloids obtained using emulsion polymerization procedures guarantee that they are sufficiently large to be observed using optical microscopy, but small enough compared to PLPS. As mentioned before, this large size difference between PLPS and the smaller negatively charged colloids is key in ensuring efficient encapsulation. The emulsion polymerization was performed using KPS as radical initiator. Upon decomposition of KPS, negatively charged sulfate radicals initiate the polymerization. These charged moieties eventually reside at the particle surface generating the desired negatively charged particles. Figure 5.1c shows a typical TEM image of the obtained CPS colloids, revealing relatively monodisperse particles with a diameter of 460 $\pm$ 50 nm. DLS measurements showed a hydrodynamic diameter of 470 $\pm$ 18 nm. As anticipated, the particles were negatively

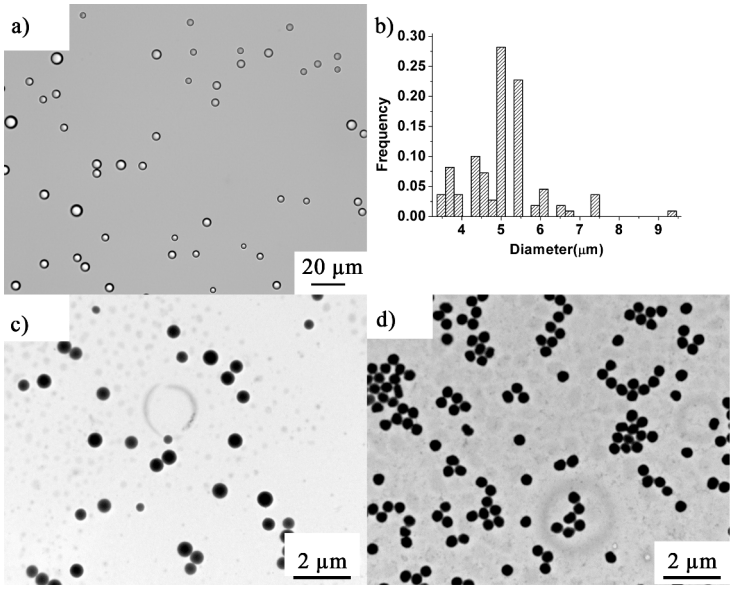


Figure 5.1. (a) Optical micrograph of positively charged large particles (PLPS). (b) The size distribution of PLPS determined from optical micrographs as shown in panel a. The distribution shows a diameter of 5 ± 1 $\mu$m. TEM images of negatively charged small particles (c) CPS (without acrylic acid) and (d) CPSAA (with acrylic acid as co-monomer). Scale bars: 20 $\mu$m for a, 2 $\mu$m for c and d.

charged as reflected by their zeta potential of -61.7 ± 7.0 mV.

CPSAA was synthesized following essentially the same emulsion polymerization procedure as employed for the preparation of CPS. The key difference was that during the CPSAA synthesis, acrylic acid (AA) was present as co-monomer, resulting in particles decorated with a PAA-rich surface shell [25]. Figure 5.1d shows a representative TEM image of CPSAA which reveals monodisperse colloids with a diameter of 400 ± 15 nm. To confirm the incorporation of AA, infrared (IR) spectroscopy was used. Figure 5.2a shows IR spectra of CPS (bottom, red) and CPSAA (top, black). Evidently, compared to the spectrum obtained for CPS, the spectrum of CPSAA contains an additional signal at 1706 $cm^{-1}$. This vibration corresponds to the C=O stretching of the incorporated AA. Successful AA incorporation was further confirmed by measuring the zeta potential and the hydrodynamic diameter of CPSAA as a

function of pH. As depicted in Figure 5.2b, the zeta potential increased from -53 to -33 mV by lowering pH from 6 to 3. The hydrodynamic diameter of CPSAA decreased from 455 nm to 425 nm by tuning pH from 6 to 2. The clear dependence of the zeta potential and the hydrodynamic diameter on pH find their origin in the pH-responsive properties of the PAA-rich outer shell on the CPSAA colloids. The p$K$a of AA is 4.25 without interaction with other carboxyl groups in water [27], at pH = 6, the charge density of the colloids is large due to the deprotonation of the carboxylic acids of the incorporated acrylic acid co-monomers. This increased charge density generates a more pronounced electrostatic repulsion between the PAA-rich segments, resulting in swelling of the particles. The observation that the hydrodynamic diameter keeps increasing, while the zeta potential is fairly constant in a pH range of 4 to 6 might be rationalized by counter ion condensation [28]. While not fully understood at this point, we expect that the high surface density of chargeable groups causes counter ion condensation, leading to a fairly constant surface potential as a function of pH in the pH range from 4 to 6. In contrast, pH has only negligible influence on the hydrodynamic diameter and zeta potential of CPS (see **Appendix 5.2**). pH independent size and zeta potential were anticipated for these non-functionalized polystyrene particles since the surface-immobilized sulfate groups are not pH-responsive within this pH window (p$K$a ≈ 2)[27]. Table 5.1 summarizes all physicochemical properties of the synthesized particles.

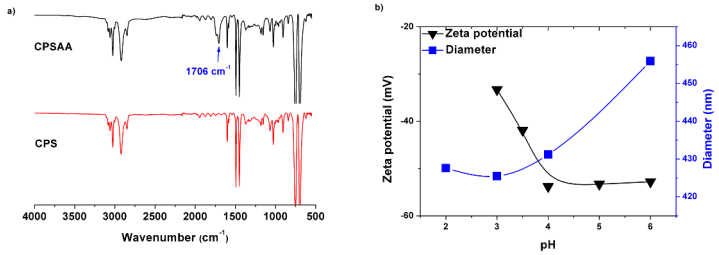


Figure 5.2. (a) Infrared spectra of CPSAA (top, black) and CPS (bottom, red). The highlighted signal at 1706 cm$^{-1}$ is characteristic for the carbonyl stretching vibration of incorporated acrylic acid monomers. (b) Zeta potential (black triangles) and hydrodynamic diameter (blue squares) of CPSAA as a function of pH.

Table 5.1. Charged surface functionalities, size and zeta potentials of as-synthesized particles PLPS, CPS and CPSAA

| Colloid | Charged surface functionalities | Diameter | Zeta potential/mV[c] |
|---|---|---|---|
| PLPS | $-N^+(CH_3)_3$ | $5 \pm 1$ $\mu$m[a] | $55.7 \pm 8.2$ |
| CPS | $-OSO_3^-$ | $470 \pm 18$ nm[b] | $-61.7 \pm 7.0$ |
| CPSAA | $-OSO_3^-/-COO^-$ | $461 \pm 11$ nm[b] | $-62.3 \pm 7.1$ |

Obtained by analyzing 100 particles from optical micrographs; b) hydrodynamic diameter as determined with DLS, measured in Milli-Q water; c) Measured in Milli-Q water.

### 5.3.2 Influence of polyelectrolytes on encapsulation behavior in water

For all encapsulation experiments, the smaller, negatively charged colloids were added in large excess with respect to the larger positively charged spheres to achieve complete encapsulation (see **Appendix 5.3** for the details). As a starting point we investigated the encapsulation behavior of the CPS/PLPS system. Figure 5.3a shows an optical micrograph of a typical aggregate obtained after mixing PLPS and CPS in pure water. As can be seen, only a small fraction of the PLPS surface was covered by CPS. The resulting surface coverage was approximately 6%. Details on calculations of these surface coverages can be found in **Appendix 5.4**. The surface coverage can be increased by addition of salt. As shown in **Appendix 5.5**, the surface coverage reached approximately 20% when particles were mixed in 10 mM aqueous NaCl solution. The fact that the surface coverage increases by addition of salt implies that electrostatic repulsions between the adsorbed CPS plays a role in the encapsulation process. However, in 10 mM aqueous NaCl solution, the Debye length is approximately 3 nm, while the surface separation between the adsorbed CPS is on the order of 100 nm. The remarkable large surface separation between the adsorbed CPS even with small Debye length excludes a direct effect of the electrostatic repulsions. As will be discussed later, the influence of the electrostatic repulsions on the surface coverage may be indirect *via* coupling with hydrodynamics.

Surprisingly, at least at first glance, a distinctly different clustering behavior was observed when PLPS were mixed with CPSAA. In pure water, CPSAA adsorbed to a significantly lesser degree onto PLPS than CPS (Figure 5.3a and 5.3b). This low coverage was measured regardless of the ionic strength of the continuous phase

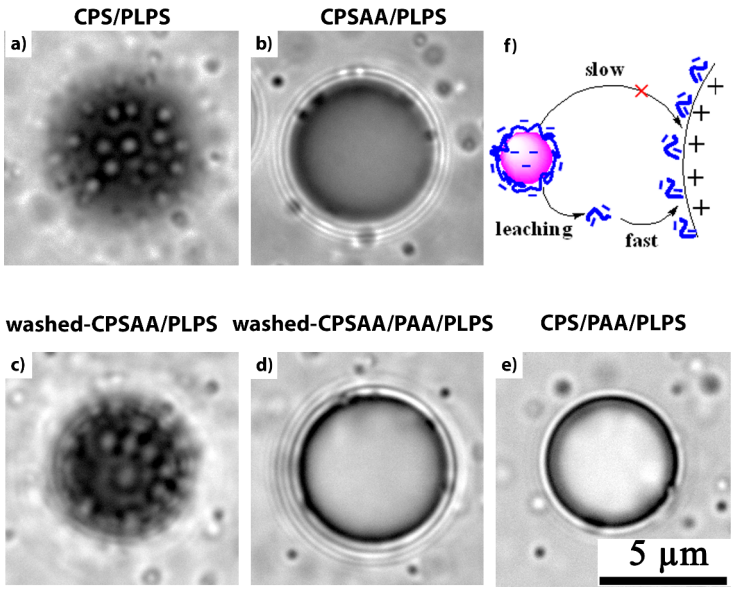


Figure 5.3. Representative optical micrographs of a mixed dispersion containing (a) CPS/PLPS, (b) CPSAA/PLPS, (c) washed-CPSAA/PLPS, (d) washed-CPSAA/PAA/PLPS and (e) CPS/PAA/PLPS in pure water. (f) Schematic illustration of the proposed mechanism in the CPSAA/PLPS system. Scale bar: 5 $\mu$m for all images.

(**Appendix 5.5**, Figure 5.9b). Since both particle species are oppositely charged, we expected to observe encapsulation efficiencies of the CPSAA/PLPS system comparable to those observed for the CPS/PLPS system. The fact that CPSAA hardly adsorb implies the existence of other factors that prevent efficient attachment of CPSAA onto PLPS.

One possible explanation is the steric repulsion caused by the diffusive PAA surface layer of the CPSAA particles. This steric effect was excluded by performing the heteroaggregation experiments of PLPS and PVP stabilized polystyrene particles (PS(PVP)), the results of which are comparable to those observed for the CPS/PLPS system (see **Appendix 5.6** for the details).

In different types of cross-linked particles, it has been observed that cross-linking is incomplete resulting in a (small) fraction of polymers that remains unbound to

the overall cross-linked network. Consequently, these non-cross-linked polymers can migrate from the particle's interior into the continuous phase [29]. If we extend these findings to our systems, we might expect a (very) small fraction of PAA-rich polyelectrolytes to be leaching out from the CPSAA particles. Based on the monomer feeds used to synthesize CPSAA and PLPS, we can roughly estimate the minimal fraction of the initially incorporated acrylic acid moieties that should be expelled in order to neutralize the positive charges on PLPS. If we assume full monomer conversion, 1 g of CPSAA particles contains $10^{-3}$ mol AA, while 1 g of PLPS has $5.6\times10^{-5}$ mol METMAC units. Combining these numbers with the volume fraction ratio of CPSAA to PLPS employed during the encapsulation experiments (Table 5.2), leads to the conclusion that the negatively chargeable groups from incorporated AA are in an approximately 300 times excess compared to the positive METMAC-related charges. This calculation reveals that only 0.3% of PAA leaching from the CPSAA particles would be sufficient to neutralize the charges of PLPS. The fact that only a small fraction of free polymer is required to significantly alter the surface charge of PLPS makes this hypothesis plausible. Moreover, leaching of PAA-rich polyelectrolytes from CPSAA into the aqueous solution is favored by the hydrophilic nature of these polymers.

To experimentally verify if PAA-rich polyelectrolytes were being expelled from CPSAA, a CPSAA dispersion was centrifuged and the top half of the supernatant was carefully collected. PLPS were subsequently dispersed in the collected supernatant and its zeta potential was measured. To be consistent with respect to the encapsulation experiments, the volume fraction ratio of CPSAA to PLPS in this experiment is the same as the one used throughout all encapsulation experiments. The obtained zeta potential of PLPS dispersed in the supernatant was -35 $\pm$ 7.3 mV. Compared to its value of 55.7 $\pm$ 8.2 mV in pure water, the zeta potential clearly reversed, providing experimental evidence of PAA-rich polyelectrolytes leaching into the continuous phase. Evidently, the amount of expelled polymer is sufficient to reverse the charge of PLPS. The leaching of the PAA-rich polyelectrolytes was independently corroborated by measuring the IR spectrum of the dried supernatant. The obtained spectrum revealed the presence of signals at 1706 $cm^{-1}$ and 700 $cm^{-1}$ corresponding to the C=O stretching vibration of the polymerized AA, and the aromatic C-H out-of-plane vibration of incorporated styrene monomers, respectively. These results clearly

indicate that polyelectrolytes composed of AA and styrene monomers are present in the supernatant and have leached out of the colloidal particles (**Appendix 5.7**). As the intensity of the C=O stretching vibration relative to the C-H vibration of styrene is significantly larger in the spectrum of the dried supernatant than it is in the spectrum of the particles CPSAA, we refer to the free polymer as 'PAA-rich'.

Given the fact that free polyelectrolytes are present in our mixed dispersions, we can speculate the effect this has on the heteroaggregation of the two particle species. Kinetically, the free PAA-rich polyelectrolytes are expected to attach onto PLPS faster than CPSAA. The exact molecular weight of expelled PAA-rich polyelectrolytes is unknown, but for a typical soap-free emulsion polymerization reaction, polymers with maximum molecular weights on the order of $10^5$ g/mol are formed [30]. The radii of gyration of these polymers are roughly 15 nm [31]. Based on the Stokes-Einstein equation this translates into diffusion coefficients that are at least an order of magnitude larger than those for CPSAA [32]. Naturally, adsorption of free PAA-rich polyelectrolytes leads to a decreased tendency for the CPSAA particles to aggregate with the partially charge neutralized or even charge reversed PLPS colloids (Figure 5.3f).

With these considerations and experimental evidence in hand, the following experiments were conducted to investigate the influence of free PAA on the encapsulation behavior in more detail. Firstly, we thoroughly washed CPSAA to remove any unbound PAA-rich polyelectrolytes. After washing, we immediately performed the same encapsulation experiment as described before in order to avoid remaining non-cross-linked PAA-rich polyelectrolytes to migrate from the particle's interior to the aqueous phase. As shown in Figure 5.3c, after the additional washing steps, significantly more CPSAA particles attached onto PLPS compared to the unwashed particles (Figure 5.3b).

In the second experiment, we deliberately mixed PLPS and washed-CPSAA with commercial PAA. Before doing this, we mixed PLPS with solutions containing different concentrations of the commercial PAA and measured their zeta potentials. To be consistent with respect to the amount of leached PAA-rich polyelectrolytes in the CPSAA/PLPS system, the concentration of free PAA was chosen such that the resulting zeta potential of PLPS in this experiment (-33.6 $\pm$ 9 mV) closely matched the zeta potential previously measured after dispersing PLPS in the supernatant of CPSAA (-35 $\pm$ 7 mV). As shown in Figure 5.3d, the washed-CPSAA/PAA/PLPS

system showed similar encapsulation behavior as that of the CPSAA/PLPS system, where an extremely low coverage was observed.

The final experiment was conducted by introducing the same amount of commercial PAA as that used in the second experiment into the CPS/PLPS system (the CPS/PAA/PLPS system, Figure 5.3e). Once more the introduction of PAA in the system resulted in similar encapsulation behavior as that observed for the CPSAA/PLPS system.

This set of experiments shows that the low coverage of the CPSAA/PLPS system obtained in pure water can be ascribed to the presence of free PAA-rich polyelectrolytes which leached from the CPSAA colloids. Interestingly, making use of this serendipitous observation, we are able to control the encapsulation behavior of oppositely charged colloids by simply adjusting the solution pH in the presence of polyelectrolytes. We elaborate on this in the next subsections.

### 5.3.3 Influence of polyelectrolytes on encapsulation behavior as a function of pH

As shown in the previous subsection, the competitive adsorption between leached PAA-rich polyelectrolytes and CPSAA results in extremely low coverage of CPSAA onto PLPS in pure water. Since PAA is pH-responsive, one would expect that at low pH, where the PAA chains are partially protonated, a fraction of the positive charges on PLPS will become accessible, promoting adsorption of CPSAA onto PLPS. In other words, the surface coverage of CPSAA on PLPS should be higher at lower pH. Note that CPSAA particles not only contain carboxyl groups, but also approximately 2% sulfate groups relative to the number of carboxyl groups, according to the feed molar ratio between KPS and AA. The sulfate groups are still expected to be negatively charged at low pH, at least as long as pH $\geq$ p$K$a, sulfate group. Therefore, at low pH, significant surface coverage is expected driven by the negatively charged sulfate groups on CPSAA and positively charged quaternary amine moieties on PLPS. To verify this hypothesis, we carried out encapsulation experiments in aqueous solutions with pH values ranging from 2 to 6. As shown in Figure 5.4, for pH $< 4$ (Figure 5.4a and 5.4b), relatively high surface coverages of approximately 30% were indeed observed. The maximum coverage of approximate 30% observed here is in agreement with those

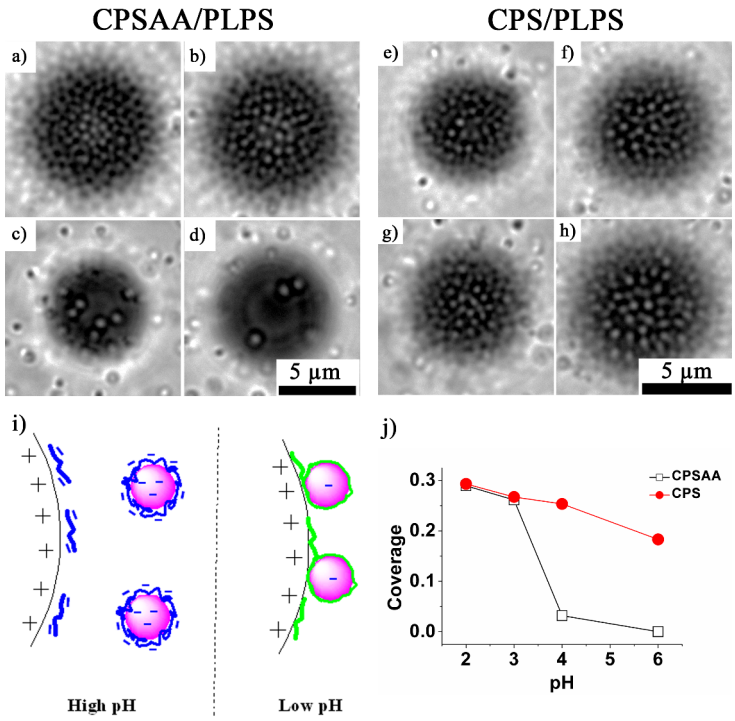


Figure 5.4. (a-h) Representative optical micrographs of coverage as a function of pH for the system of CPSAA/PLPS (left column) and CPS/PLPS (right column). pH = (a, e) 2, (b, f) 3, (c, g) 4, and (d, h) 6. (i) Schematic illustration for the encapsulation process of the CPSAA/PLPS system in dispersions of high and low pH values. Blue and green represent negatively charged PAA and protonated PAA, respectively. (j) Surface coverage as a function of pH for the system of CPSAA/PLPS (black open squares) and CPS/PLPS (red solid dots). Ionic strength = 10 mM. Scale bar: 5 $\mu$m for all images.

reported by Harley who used electron microscopy to analyze the surface coverage after heteroaggregation [33]. The relatively low value of the maximum coverage (i.e., only 30%) is ascribed to random sequential adsorption in combination with hydrodynamic interactions (see **Appendix 5.8** for the details), although the detailed mechanism is not clear [34, 35]. For pH values ranging from 4 to 6 (Figure 5.4c and 5.4d), microscopy analysis of the heteroaggregates revealed a low coverage (less than 5%). The trend in surface coverage within this pH range is in agreement with our expectations. As

depicted in Figure 5.4i, at high pH (Figure 5.4i, left), the PAA-rich polyelectrolytes are highly charged and therefore capable of efficiently reversing the charge of the large particles, which prohibits CPSAA attachment. At low pH (Figure 5.4i, right), the PAA-rich polyelectrolytes are protonated, leading to the situation where sufficient positive charges on the large particles are accessible for CPSAA, resulting in relatively efficient encapsulation with a coverage of approximately 30%. In contrast, for the CPS/PLPS system without polyelectrolytes, the encapsulation efficiency was found to be only weakly dependent on the solution pH (Figure 5.4).

From these experiments we conclude that we can readily tune the surface coverage by adjusting the solution pH and that the aggregation process is largely governed by the charge density of the polyelectrolytes.

### 5.3.4 Reversible encapsulation of CPSAA/PLPS

With experimental evidence that the degree of encapsulation is effectively determined by the charge density of the PAA-rich polyelectrolytes, we proceeded by investigating the influence of polyelectrolytes on the ability of small particles to detach from PLPS. For all the systems we investigated, high coverages of approximately 30% were observed at pH 2 (Figure 5.5). While increasing pH to 7 by addition of aqueous NaOH solution, different degrees of detachment were observed depending on whether or not PAA had been present. pH 7 was chosen as the highest pH in our studies in order to prevent hydrolysis of the ester groups of METMAC, which would result in an irreversible charge reversal of PLPS (see **Appendix 5.9** for more information). In the CPS/PLPS (Figure 5.5b) and washed-CPSAA/PLPS system (Figure 5.5f), no detachment of small particles from PLPS was observed. In contrast, the CPSAA/PLPS (Figure 5.5d) and CPS/PAA/PLPS systems (Figure 5.5h) showed that the majority of the small particles detached after an increase in pH, revealing the essential role of PAA in facilitating particles detachment. Furthermore, comparing the degrees of detachment observed for the CPSAA/PLPS and washed-CPSAA/PLPS systems, again confirms that it is the free PAA leached from CPSAA rather than the PAA chemically bound to CPSAA that dominates the detachment behavior (Figure 5.5d for CPSAA/PLPS system and 5f for washed-CPSAA/PLPS system). Furthermore, we speculate that the free PAA acts as steric barrier restricting the minimal distance that CPSAA and PLPS can approach,

resulting in a weaker Van der Waals attraction, facilitating particle desorption even further.

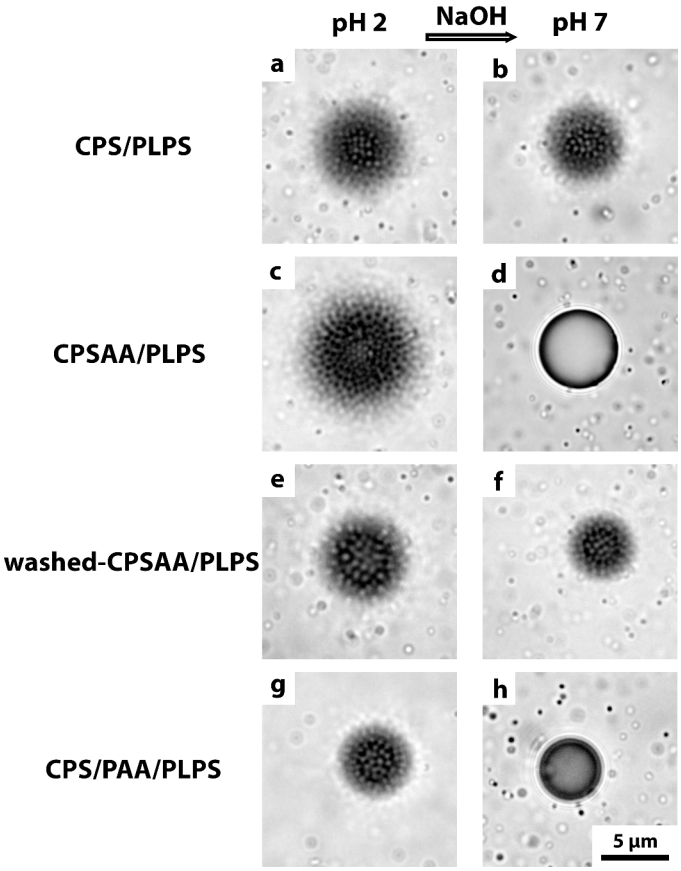


Figure 5.5. Optical micrographs of detachment results of (a, b) CPS/PLPS, (c, d) CPSAA/PLPS, (e, f) washed-CPSAA/PLPS, and (g, h) CPS/PAA/PLPS from pH 2 (a, c, e, g) to pH 7 (b, d, f, h) by addition of aqueous NaOH solution. Scale bar: 5 $\mu$m for all images.

With experimental evidence that the coverage is pH dependent and CPSAA are able to detach from PLPS by raising pH in the CPSAA/PLPS system, we accomplished a fully reversible and repeatable encapsulation of PLPS by CPSAA. We started at pH 2.5 instead of 2 since it yields a dispersion with a lower ionic strength and allows for

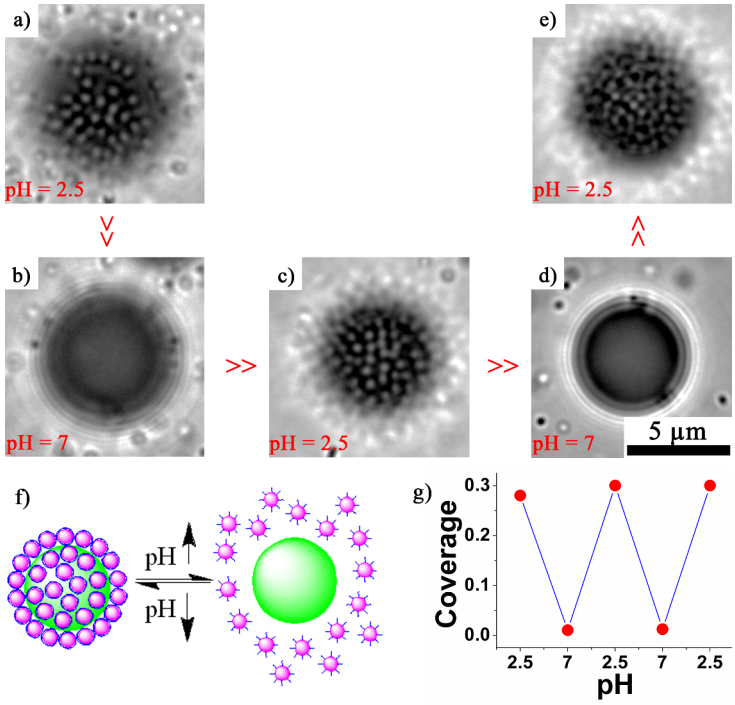


Figure 5.6. Reversible encapsulation of CPSAA/PLPS. (a-e) Optical micrographs of CPSAA/PLPS in pH = 2.5 and pH = 7 repeatedly; (f) Schematic illustration of reversible encapsulation behavior of CPSAA/PLPS. (g) Surface coverage by cycling pH for the CPSAA/PLPS system. Scale bar: 5 $\mu$m for all images.

more reversible encapsulation cycles. As shown in Figure 5.6a, CPSAA significantly covers the PLPS surface under this condition. When we raised pH to 7, most of the CPSAA particles desorbed from PLPS (Figure 5.6b). Encapsulation could be triggered again by lowering pH back to 2.5, as shown in Figure 5.6c. This reversible adsorption and desorption could be repeated 3 times up to the point where the ionic strength of the dispersing medium was too high, causing aggregation of both types of particles. The number of cycles could probably be increased by cycling between closer pH values. Furthermore, as already shown in Figure 5.5g and 5.5h, we expect the system of CPS/PAA/PLPS to show similar reversible encapsulation behavior. The aggregation is dominated by the free polyelectrolytes rather than by the chemical

details of the participating species, making this approach a general strategy to control heteroaggregation processes.

## 5.4 Conclusion

A colloidal model system capable of undergoing reversible encapsulation mediated by polyelectrolytes was developed. The system consists of positively charged large polystyrene microspheres and negatively charged smaller polystyrene particles that were decorated with a pH-responsive PAA outer layer. Reversible encapsulation was observed in the presence of small concentrations of unbound PAA polyelectrolytes in the continuous phase. At high pH, the PAA polyelectrolytes are highly charged, and therefore, when adsorbed, able to reverse the charge of the large positively charged particles. Charging reversal causes an effective electrostatic repulsion between the two particle species, eventually resulting in low coverage of the large particles by the small particles. At low pH, the PAA polyelectrolytes are protonated. Under these conditions, positive charges on the large particles are accessible for the small oppositely charged particles, which leads to relatively high coverage. Furthermore, the presence of the PAA polyelectrolytes also allows small particles to desorb from large particles under appropriate change of pH. Finally, reversible encapsulation of large particles by small particles was achieved by cycling pH between 2.5 and 7 in the presence of polyelectrolytes.

Even under optimal conditions, a relatively low maximum coverage of approximately 30% was observed which is ascribed to a random sequential adsorption mechanism combined with hydrodynamic interactions.

We showed that polyelectrolytes can be used to control heteroaggregation of oppositely charged colloids. Moreover, the tunability of the coverage and reversibility of encapsulation of our system provides a potential platform to prepare sophisticated hierarchical assemblies, such as raspberry-like composites, colloidal molecules and colloidal chains [1, 4, 36].

# Acknowledgments

This chapter is reprinted with kind permission from [37]. Copyright 2017 American Chemical Society


# Appendix

## A5.1 Experimental conditions of encapsulation studies

Table 5.2. Experimental conditions of encapsulation studies

| Entry | $\phi_{PLPS}(10^4)^a$ | $\phi_{CPSAA}(10^4)^a$ | $\phi_{CPSAA}(10^4.washed)^a$ | $\phi_{CPS}(10^4)^a$ | pH | $w_{PAA}(10^6)^b$ |
|---|---|---|---|---|---|---|
| a1 | 1.25 | 0 | 0 | 22.5 | $6^c$ | 0 |
| a2 | 1.25 | 0 | 0 | 22.5 | 2 | 0 |
| a3 | 1.25 | 0 | 0 | 22.5 | $7^d$ | 0 |
| b1 | 1.25 | 22.5 | 0 | 0 | $6^c$ | 0 |
| b2 | 1.25 | 22.5 | 0 | 0 | 2 | 0 |
| b3 | 1.25 | 22.5 | 0 | 0 | $7^d$ | 0 |
| c1 | 1.25 | 0 | 22.5 | 0 | $6^c$ | 0 |
| c2 | 1.25 | 0 | 22.5 | 0 | 2 | 0 |
| c3 | 1.25 | 0 | 22.5 | 0 | $7^d$ | 0 |
| d1 | 1.25 | 0 | 22.5 | 0 | $6^c$ | 5 |
| d2 | 1.25 | 0 | 22.5 | 0 | 2 | 5 |
| d3 | 1.25 | 0 | 22.5 | 0 | $7^d$ | 5 |
| e1 | 1.25 | 0 | 0 | 22.5 | $6^c$ | 5 |
| e2 | 1.25 | 0 | 0 | 22.5 | 2 | 5 |
| e3 | 1.25 | 0 | 0 | 22.5 | $7^d$ | 5 |

a). $\phi$ = volume fraction of particles; b). $w$ = mass fraction of commercial PAA ($M_w$ = 450 kg/mol); c) pure water (pH $\approx$ 6); d) Obtained by adding 13.7 mM aqueous NaOH solution into corresponding dispersion at pH 2.

## A5.2 Zeta potential and hydrodynamic diameter of CPS as a function of pH

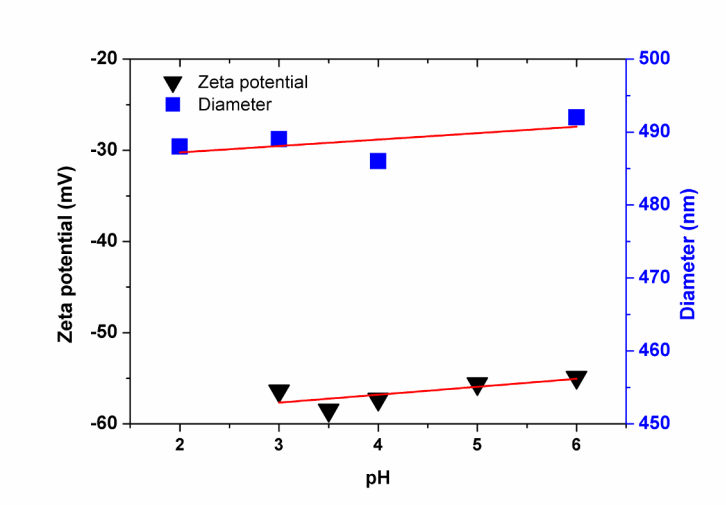


Figure 5.7. Zeta potential (black triangles) and hydrodynamic diameter (blue squares) of CPS as a function of pH.

## A5.3 Theoretical calculation of the maximal number of small particles adsorbing onto a larger central sphere

When larger particles and an excess of small particles with opposite surface charge are mixed, the small particles can adsorb onto the large particles to form raspberry-like heteroaggregates. The theoretical maximum number of small particles that can be accommodated on a single larger central sphere ($\Gamma_{\mathrm{hcp}}$) is obtained when the smaller particles are hexagonally close packed. hcp can be estimated using the following equation [38]:

$$\Gamma_{\mathrm{hcp}} = \frac{2\pi}{\sqrt{3}}\left(\frac{R+r}{r}\right)^2 \tag{5.1}$$

where $R$ and $r$ are the radii of large central particle and small particle, respectively. In our case, $R$ is approximately 2.5 $\mu$m and $r$ is 0.25 $\mu$m, which yields a $\Gamma_{\mathrm{hcp}}$ of 440.

From the volume fraction of the dispersion used throughout the aggregation experiments (Table 5.2) and their radii, the feeding ratio of small particles compared to the larger colloids $N$ was calculated using:

$$N = \left(\frac{\phi_{\mathrm{CPS}}}{\phi_{\mathrm{PLPS}}}\right)\left(\frac{R}{r}\right)^3 \tag{5.2}$$

where $\phi_{\mathrm{PLPS}}$ and $\phi_{\mathrm{CPS}}$ are the volume fraction of particles PLPS and CPS, respectively. In our experiments, $N$ proved to be approximately 18000. Comparing this to the theoretical value of $\Gamma_{\mathrm{hcp}}$, the employed feeding ratio translates into a 40 times excess. Therefore we expect to observe raspberry-like heteroaggregates for all the performed encapsulation experiments.

## A5.4 Calculation of surface coverage

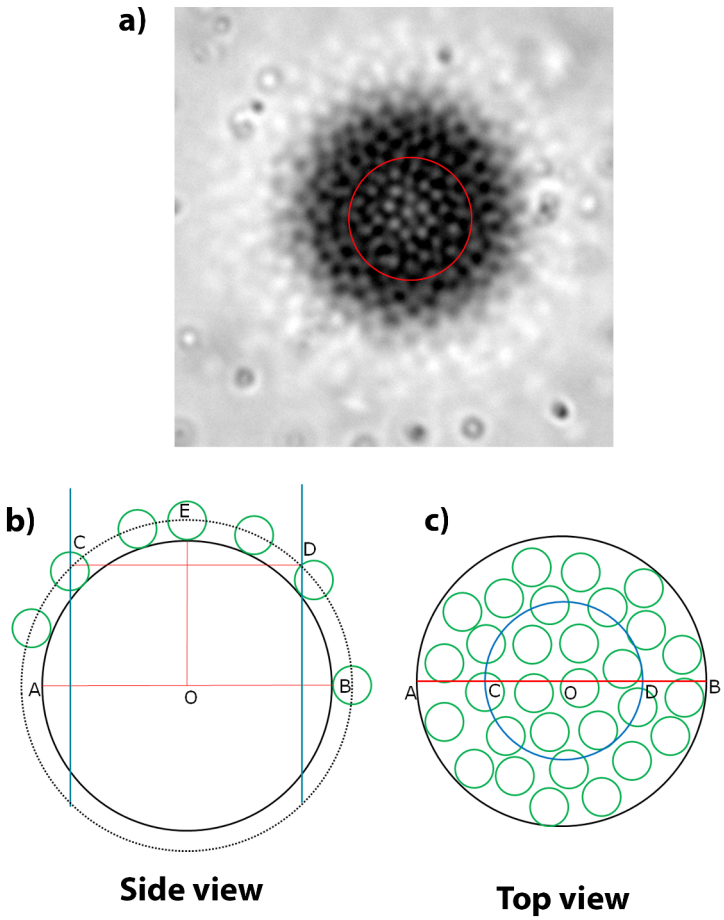


Figure 5.8. Calculation method of surface coverage.

Figure 5.8a shows an optical micrograph of a typical cluster observed after the heteroaggregation process. Clearly, from these images it is very difficult to determine the boundary of cluster and to extract the number of smaller particles. To obtain an estimate of the number of adsorbed smaller colloids, the following procedure was performed. Firstly, a circle is drawn from the center of the aggregate. The dimension

of the circle is chosen such that it encloses a large number of small particles, but does not extend completely to the identifiable edge of the aggregate.

The surface area of the spherical cap of drew circle is

$$S = 2\pi(R+r)[(R+r) - \sqrt{(R+r)^2 - d^2}] \tag{5.3}$$

The total surface area is

$$S_{\text{total}} = 4\pi(R+r)^2 \tag{5.4}$$

Therefore, the total number of small particles adsorbed per large particle is

$$\Gamma = \frac{N_{\text{count}}}{S} S_{\text{total}} = 2(R+r)N_{\text{count}}/[R+r-\sqrt{(R+r)^2 - d^2}] \tag{5.5}$$

In theory, the maximum number of small particles adsorbed per large particle is equal to [38]

$$\Gamma_{\text{hcp}} = \frac{2\pi}{\sqrt{3}}(\frac{R+r}{r})^2 \tag{5.6}$$

So the surface coverage is

$$\theta = \frac{\Gamma}{\Gamma_{\text{hcp}}} \tag{5.7}$$

where $R$ and $r$ are the radii of large particle and small particle, respectively, $d$ is the radii of drew circle. $N_{\text{count}}$ is the number of small particles in the circle.

To eliminate the influence of the size polydispersity of the PLPS, approximately 30 clusters with different size were averaged.

## A5.5 Typical heteroaggregates observed when mixing CPS/PLPS and CPSAA/PLPS in 10 mM aqueous NaCl solution

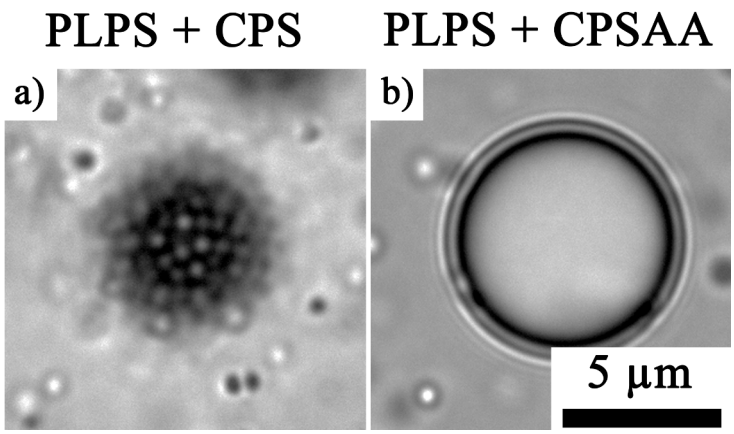


Figure 5.9. Representative optical micrographs of a mixed dispersion containing (a) CPS/PLPS and (b) CPSAA/PLPS in a continuous phase containing 10 mM NaCl. Scale bar: 5 $\mu$m for both images.

## A5.6 Encapsulation behavior of PLPS/PS(PVP) system in pure water and 10 mM aqueous NaCl solution

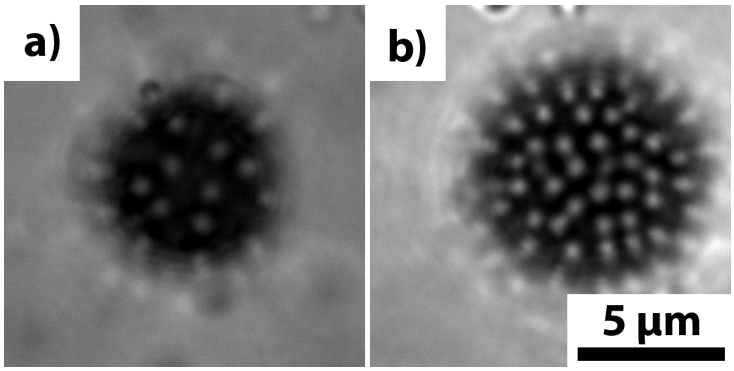


Figure 5.10. Representative optical micrographs of mixed dispersions containing PLPS/PVP stabilized polystyrene particles (PS(PVP)) in (a) pure water, and (b) water containing 10 mM NaCl. Scale bar: 5 $\mu$m for both images.

One possible explanation is the steric repulsion caused by the diffusive PAA surface layer of the CPSAA particles. In pure water (pH $\approx$ 6), the PAA chains are charged (p$K$a of AA is 4.25 without interaction with other carboxyl groups in water) and therefore extend into the solution (Figure 5.2b) [27]. Upon contact of CPSAA and PLPS this charged layer has to be compressed, which is unfavorable. To investigate the influence of this steric effect, we synthesized PVP stabilized polystyrene particles (PS(PVP), **subsection 2.2.2**) by conventional dispersion polymerization. Although not anticipated by the polymerization mechanism and monomer feed, particles with a negative zeta potential of -24 $\pm$ 5.8 mV were obtained. While not understood at this point, the observation that the particles are electrically charged is in agreement with several other reported observations [39, 40]. Performing heteroaggregation experiments using PLPS and PS(PVP) resulted in encapsulation efficiencies of 5% and 20.5% in pure water and in 10 mM aqueous NaCl solution, respectively (Figure 5.10). These efficiencies are comparable to those observed for the CPS/PLPS system, indicating a negligible influence of the steric repulsion of surface-immobilized polymers. Therefore, we can exclude the steric effect as the (most) important contribution to the extremely low coverage of CPSAA on PLPS.

## A5.7 Infrared spectra of pure polyacrylic acid (PAA), the dried supernatant (PS-PAA) and CPSAA

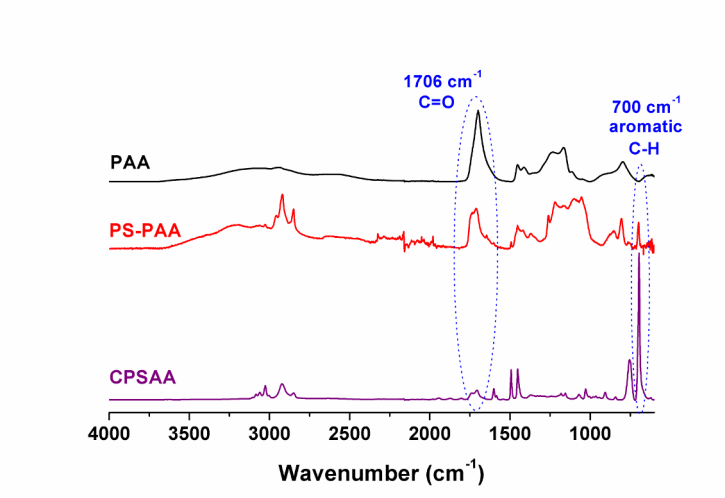


Figure 5.11. Infrared spectra of pure PAA ($M_v \approx 450000$ g/mol, Sigma-Aldrich) (top, black), the dried supernatant (PS-PAA) (middle, red) and CPSAA (bottom, violet). The highlighted signal at 1706 $cm^{-1}$ is characteristic for the carbonyl stretching vibration of incorporated acrylic acid monomers and 700 $cm^{-1}$ corresponds to the aromatic C-H out-of-plane vibration of incorporated styrene monomers.

## A5.8 Discussion of relative low maximum coverage

As shown in Figure 5.4, the maximum coverage can be reached in the system of CPSAA/PLPS is approximately 0.3. This result is in agreement with those reported by Harley who used electron microscopy to analyze the surface coverage after encapsulation [33]. While the theoretical maximum coverage is 0.9, which is obtained by assuming the small particles pack in a close-packed hexagonal array on the surface of a large particle [41]. To investigate the origin of the observed relatively low maximum coverage, the adsorption process was monitored *in situ* with optical microscope. As revealed by Figure 5.12, CPSAA attached onto PLPS in a sequential fashion and once attached, they were unable to detach or move over the PLPS surface, revealing the aggregation process is following a random sequential adsorption mechanism. Feder [34] reported that for random sequential adsorption in a two-dimensional system the theoretical maximum coverage is approximately 0.54. Any inter-particle interaction were neglected in these calculations. To this end, Ko et al. extended the results of Feder and studied the influence of electrostatics and hydrodynamic interactions on the random sequential adsorption of positively charged latex colloids onto packed columns of negatively charged glass beads. They found that the coverage increased with increasing ionic strength or decreasing approach velocity. A theoretical maximum coverage of approximately 0.3 was derived [35].

In our system, the maximum coverage was reached at pH 2. Under these conditions, the Debye screening length is approximately 3 nm, which is much shorter than the average particles separation between CPSAA. Therefore the direct influence of electrostatic double-layer interaction on the low maximum coverage can be excluded. From this we speculated that, the random sequential adsorption mechanism combined with hydrodynamic interaction account for the relative low maximum coverage in this system.

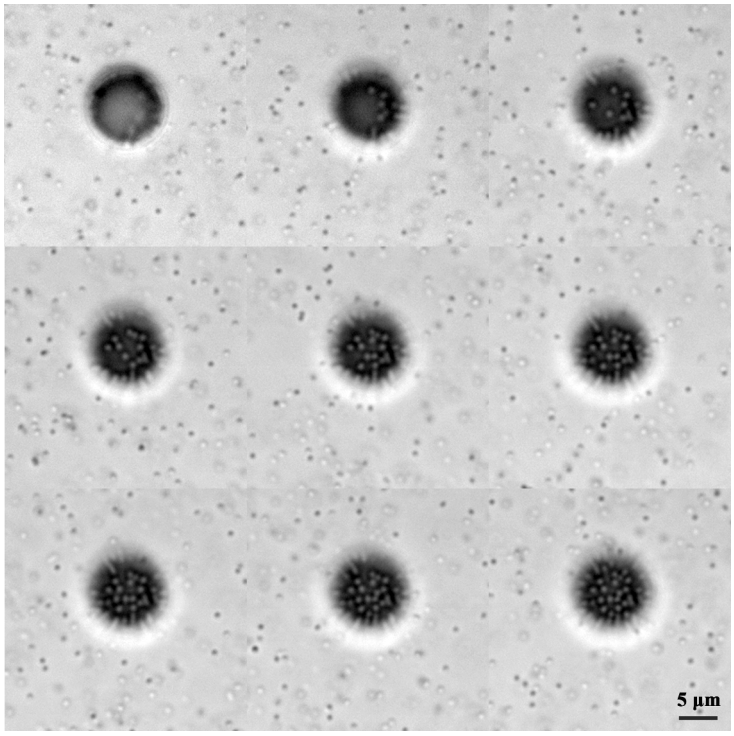


Figure 5.12. Snapshots of optical microscope images of the adsorption process of CPSAA onto PLPS. Interval time: 5 s. The full movie can be found in http://pubs.acs.org/doi/suppl/10.1021/acs.langmuir.7b00845. Scale bars: 5 $\mu$m for all images.

## A5.9 Charge reversal of PLPS *via* base-catalyzed hydrolysis of METMAC ester moieties

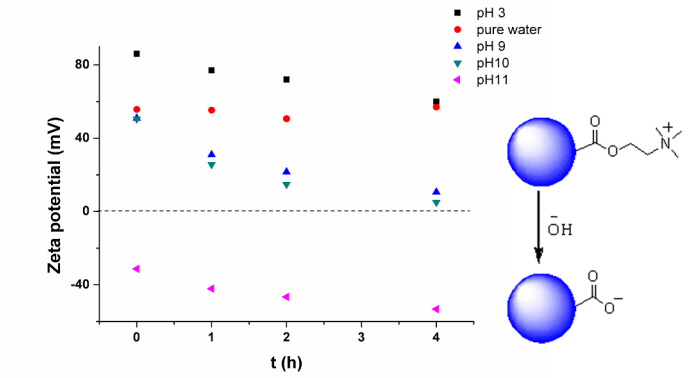


Figure 5.13. Zeta potential of PLPS as functions of time and pH. Under basic conditions (pH = 9 (blue upward triangles) and 10 (green downward triangles)), the ester groups that link the permanently charged quaternary amine functionality to the surface of the particles hydrolyze gradually leading to a decrease in surface charge. This decrease in surface charge originates from the consumption of positively charged quaternary amine and the formation of negatively charged carboxylic acid. At pH = 11 (pink leftward triangles) hydrolysis is sped up significantly, resulting in a charge reversal. Under neutral (pure water, red dots) and acidic (pH 3, black squares) conditions, the ester groups are more stable resulting is a no change or less drastic in zeta potential. Furthermore, the zeta potential of PLPS in pure water has no significant change for months.

# Bibliography

[1] Y. Lan, Y. Wu, A. Karas, and O. A. Scherman. Photoresponsive hybrid raspberry-like colloids based on cucurbit[8]uril hostguest interactions. *Angewandte Chemie International Edition*, 53:2166–2169, 2014.

[2] M. E. Leunissen, C. G. Christova, A.-P. Hynninen, C. P. Royall, A. I. Campbell, A. Imhof, M. Dijkstra, R. van Roij, and A. van Blaaderen. Ionic colloidal crystals of oppositely charged particles. *Nature*, 437:235–240, 2005.

[3] E. V. Shevchenko, D. V. Talapin, N. A. Kotov, S. O'Brien, and C. B. Murray. Structural diversity in binary nanoparticle superlattices. *Nature*, 439:55–59, 2006.

[4] D. R. E. Snoswell, R. K. Brill, and B. Vincent. pH-responsive microrods produced by electric-field-induced aggregation of colloidal particles. *Advanced Materials*, 19:1523–1527, 2007.

[5] K. Furusawa and C. Anzai. Heterocoagulation behaviour of polymer latices with spherical silica. *Colloids and Surfaces*, 63:103–111, 1992.

[6] C. Suwabe, D. Nagao, H. Ishii, and M. Konno. Chemical bonding heterocoagulation of nanoparticles onto polymeric spheres by two-step addition of polymerizable coupling agent. *Colloid and Polymer Science*, 293:2095–2100, 2015.

[7] S. Zhang, Y. Shao, G. Yin, and Y. Lin. Electrostatic self-assembly of a Pt-around-Au nanocomposite with high activity towards formic acid oxidation. *Angewandte Chemie International Edition*, 49:2211–2214, 2010.

[8] Y. Pan, J. Wang, Y. Wang, and Z. Wang. PS microspheres coated by AuNPs *via* thermodynamic driving heterocoagulation and their high catalytic activity. *Macromolecular Rapid Communications*, 35:635–641, 2014.

[9] M. Li, G. Chen, and S. Bhuyain. The induction phenomenon and catalytic deactivation of thiolate-stabilized raspberry-like polymer composites coated with gold nanoparticles. *Nanoscale*, 7:2641–2650, 2015.

[10] W. Ming, D. Wu, R. van Benthem, and G. de With. Superhydrophobic films from raspberry-like particles. *Nano Letters*, 5:2298–2301, 2005.

[11] C. C. M. C. Carcouët, A. C. C. Esteves, M. M. R. M. Hendrix, R. A. T. M. van Benthem, and G. de With. Fine-tuning of superhydrophobicity based on monolayers of well-defined raspberry nanoparticles with variable dual-roughness size and ratio. *Advanced Functional Materials*, 24:5745–5752, 2014.

[12] Y. Li, Y. Pan, L. Zhu, Z. Wang, D. Su, and G. Xue. Facile and controlled fabrication of functional gold nanoparticle-coated polystyrene composite particle. *Macromolecular Rapid Communications*, 32:1741–1747, 2011.

[13] Z. Chao, L. Song, Y. Zhou, W. Nie, and P. Chen. Impact of PS/SiO2 morphologies on the SERS activity of PS/SiO2/Ag nanocomposite particles. *Colloid and Polymer Science*, 292:2841–2848, 2014.

[14] G. Li, X. Yang, and J. Wang. Raspberry-like polymer composite particles *via* electrostatic heterocoagulation. *Colloids and Surfaces A: Physicochemical and Engineering Aspects*, 322:192–198, 2008.

[15] M. Kanahara, M. Shimomura, and H. Yabu. Fabrication of gold nanoparticle-polymer composite particles with raspberry, core-shell and amorphous morphologies at room temperature *via* electrostatic interactions and diffusion. *Soft Matter*, 10:275–280, 2014.

[16] B. Liu, M. Zhou, H. Liu, X. Wang, and X. Yang. Binary colloidal heterocoagulation for raspberry-like particles through azidealkyne click reaction. *Colloids and Surfaces A: Physicochemical and Engineering Aspects*, 436:1027–1033, 2013.

[17] Q. Wu, Z. Wang, X. Kong, X. Gu, and G. Xue. A facile strategy for controlling the self-assembly of nanocomposite particles based on colloidal steric stabilization theory. *Langmuir*, 24:7778–7784, 2008.

[18] T. Song, T. Liu, X. Yang, and F. Bai. Raspberry-like particles *via* the heterocoagulated reaction between reactive epoxy and amino groups. *Colloids and Surfaces A: Physicochemical and Engineering Aspects*, 469:60–65, 2015.

[19] R. F. Garmann, M. Comas-Garcia, C. M. Knobler, and W. M. Gelbart. Physical principles in the self-assembly of a simple spherical virus. *Accounts of Chemical Research*, 49:48–55, 2016.

[20] R. F. Garmann, M. Comas-Garcia, A. Gopal, C. M. Knobler, and W. M. Gelbart. The assembly pathway of an icosahedral single-stranded RNA virus depends on the strength of inter-subunit attractions. *Journal of Molecular Biology*, 426:1050–1060, 2014.

[21] A. Zlotnick, R. Aldrich, J. M. Johnson, P. Ceres, and M. J. Young. Mechanism of capsid assembly for an icosahedral plant virus. *Virology*, 277:450–456, 2000.

[22] W. H. Roos, R. Bruinsma, and G. J. L. Wuite. Physical virology. *Nat Phys*, 6:733–743, 2010.

[23] F. Zhang, Y. Bai, Y. Ma, and W. Yang. Preparing of monodisperse and cation-charged polystyrene particles stabilized with polymerizable quarternary ammonium by dispersion polymerization in a methanolwater medium. *Journal of Colloid and Interface Science*, 334:13–21, 2009.

[24] Q. Liu, Y. Li, S. Shen, Z. Zhou, B. Ou, and S. Tang. Preparation of monodisperse cationic microspheres by dispersion polymerization of styrene and a cation-charged monomer in the absence of a stabilizer. *Journal of Macromolecular Science, Part A*, 48:518–525, 2011.

[25] P. H. Wang and C. Y. Pan. Preparation of styrene/acrylic acid copolymer microspheres: polymerization mechanism and carboxyl group distribution. *Colloid and Polymer Science*, 280:152–159, 2002.

[26] R. J. Hunter. *Zeta Potential in Colloid Science*. Academic Press, 1981.

[27] W. M. Haynes. *CRC Handbook of Chemistry and Physics, 97th Edition*. CRC Press, 2016.

[28] H. Ohshima. Electrophoretic mobility of a spherical colloidal particle in a salt-free medium. *Journal of Colloid and Interface Science*, 248:499–503, 2002.

[29] R. P. A. Dullens, E. M. Claesson, and W. K. Kegel. Preparation and properties of cross-linked fluorescent poly(methyl methacrylate) latex colloids. *Langmuir*, 20:658–664, 2004.

[30] A. R. Goodall, M. C. Wilkinson, and J. Hearn. Mechanism of emulsion polymerization of styrene in soap-free systems. *Journal of Polymer Science: Polymer Chemistry Edition*, 15:2193–2218, 1977.

[31] D. Reith, B. Müller, F. Müller-Plathe, and S. Wiegand. How does the chain extension of poly (acrylic acid) scale in aqueous solution? a combined study with light scattering and computer simulation. *The Journal of Chemical Physics*, 116:9100–9106, 2002.

[32] I. N. Levine. *Physical chemistry, fifth Edition*. McGraw-Hill, 2002.

[33] S. Harley, D. W. Thompson, and B. Vincent. The adsorption of small particles onto larger particles of opposite charge direct electron microscope studies. *Colloids and Surfaces*, 62:163–176, 1992.

[34] J. Feder. Random sequential adsorption. *Journal of Theoretical Biology*, 87:237–254, 1980.

[35] C.-H. Ko, S. Bhattacharjee, and M. Elimelech. Coupled influence of colloidal and hydrodynamic interactions on the RSA dynamic blocking function for particle deposition onto packed spherical collectors. *Journal of Colloid and Interface Science*, 229:554–567, 2000.

[36] D. J. Kraft, W. S. Vlug, C. M. van Kats, A. van Blaaderen, A. Imhof, and W. K. Kegel. Self-assembly of colloids with liquid protrusions. *Journal of the American Chemical Society*, 131:1182–1186, 2009.

[37] Y. Guo, B. G. P. van Ravensteijn, C. H. J. Evers, and W. K. Kegel. pH reversible encapsulation of oppositely charged colloids mediated by polyelectrolytes. *Langmuir*, 33:4551–4558, 2017.

[38] M. Okubo, K. Ichikawa, M. Tsujihiro, and Y. He. Production of anomalous polymer microspheres having uneven surfaces by "stepwise" heterocoagulation technique. *Colloid and Polymer Science*, 268:791–796, 1990.

[39] C.-W. Wu, J.-G. Lee, and W.-C. Lee. Protein and enzyme immobilization on non-porous microspheres of polystyrene. *Biotechnology and Applied Biochemistry*, 27:225–230, 1998.

[40] M. S. Ali, G. Ghosh, and D. Kabir ud. Amphiphilic drug persuaded collapse of polyvinylpyrrolidone and poly(ethylene glycol) chains: A dynamic light scattering study. *Colloids and Surfaces B: Biointerfaces*, 75:590–594, 2010.

[41] B. Vincent, C. A. Young, and T. F. Tadros. Equilibrium aspects of heteroflocculation in mixed sterically-stabilised dispersions. *Faraday Discussions of the Chemical Society*, 65:296–305, 1978.

# Summary

The main goal of this thesis is to increase our understanding of colloidal self-assembly processes and develop new strategies to assemble colloidal building blocks into more sophisticated and well-defined super-structures. The building blocks we are particularly interested in are spherical colloids with isotropic shape and surface functionalities. Self-assembly is a spontaneous process in which a disordered system of pre-existing building blocks forms an ordered structure without human intervention. It is ubiquitous in nature, for example, virus capsid proteins can self-assemble into virus microcapsules. The study of self-assembly processes not only may lead to a better understanding of that aspect of nature, but in principle also enables to develop new functional materials with sophisticated super-structures. However, direct investigation of the self-assembly process of, for examples, proteins and other molecules *in situ*, is difficult since those objects are too small and move too fast to be tracked directly by techniques such as electron and optical microscopy. Therefore, colloids are extensively employed as models of (macro) molecules to study self-assembly.

In China, we have a proverb "even a clever chef cannot cook a meal without a necessary foodstuff". As an experimentalist, the first thing that need to be done is to synthesize necessary building blocks for self-assembly. In **Chapter 2** and part of **Chapter 3**, we synthesize several new colloidal model systems. In **Chapter 2**, we develop a novel method to synthesize monodisperse, micron-sized dimple polystyrene particles with a single cavity based on a facile one-pot dispersion polymerization method. The procedure involves the delayed addition of cross-linker into the reaction mixture. By changing the delayed addition time or the concentration of the cross-linker, the size of cavity can be readily tuned. More importantly, by introducing functional

co-monomers together with cross-linker during the delayed addition step, dimple particles with various surface functionalities are synthesized. We have successfully synthesized dimple particles with chlorine groups, epoxide groups or thermoresponsive groups on their surfaces. The functional groups on the surface of dimple particles allow for further chemical modification. As an example, the chlorine modified dimple particles are selected and reacted with the fluorescent dye fluoresceinamine. The resulting dye-labeled particles show bright fluorescence, indicating the accessibility of the surface functional groups. Furthermore, the dimple particles are used as seeds to prepare hollow dumbbell particles. In **Chapter 3**, we utilize several methods to tune the properties of the colloids. As examples, we introduce an atom transfer radical polymerization (ATRP) reaction to graft a hydrophobic polymer layer onto chlorinated spherical colloids. Moreover, we use the Menschutkin reaction to reverse the colloids charge and make the colloids amphoteric. As a final example, the etching of colloids with dimethylformamide (DMF) or tetrahydrofuran (THF) allows for the preparation of colloids with a yolk-shell structure. In summary, in **Chapter 2** and part of **Chapter 3**, we show various methods to tune the properties of the colloids, including shape (spheres, dimple particles and dumbbell particles), charges (positive, negative and amphoteric), morphology (solid, hollow, yolk-shell), size (ranges from 400 nm up to 5 $\mu$m) and surface properties (hydrophobic, hydrophilic, chlorine groups, epoxide groups). The controllable regulation of these parameters is crucial to better study colloidal self-assembly processes.

**Chapter 3-5** focus on the self-assembly of some of the aforementioned colloids into one, two and three-dimensional colloidal aggregates using different principles. The building blocks mostly used are spherical colloids with isotropic shape and surface functionalities. In **Chapter 3**, we report that the colloids with deformable, amphoteric and hydrophobic characteristics can self-assemble into one-dimensional aggregates in an aqueous colloidal system. To gain insight into the influence of each of these characteristics on the formation of the one-dimensional aggregates, we first design and synthesize a series of control colloids with one or two of these characteristics. Subsequently, we perform the same assembly process as before. By comparing the assemblies of these control colloids with the one-dimensional aggregates, we comprehend the importance of the overall charges and the hydrophobic layer, while deformability is not prerequisite. Thereafter, we propose a possible mechanism for the observed one-

dimensional aggregate formation, which involving the delicate balance of short-range hydrophobic attraction and relatively longer-range electrostatic repulsion. Finally, we confirm our hypothesis by systematically investigating the influence of the electrostatic repulsion and the hydrophobic attraction on the formation of the one-dimensional aggregates.

In **Chapter 4**, we describe a facile method to prepare two-dimensional colloidal crystal monolayers (CCM). A unique feature of this method is that the prepared CCM can freely float in the dispersion. The developed method consists of two main steps: firstly, we make plausible that the evaporation of dispersing solvent (a solvent in which the colloids are initially dispersed) results in the formation of monolayers on the wall of centrifugal tube; secondly, an extracting solvent is used to peel the monolayers off the wall into the continuous phase. We systematically investigate the influences of the dispersing solvent, the wall material, the extracting solvent, and the nature of the colloids on the formation of the CCM. The results show that in the first step, the formation of the CCM on the wall can be described by the vertical deposition mechanism: the evaporation of dispersing solvent results in the formation of a meniscus structure of the air-liquid interface between the colloids that are on the wall of the centrifugal tube. The deformation of the meniscus gives rise to capillary attraction, driving the colloids toward the crystal zone, which leads to the formation of CCM on the wall of centrifugal tube. In the second step, the key to release the CCM from the wall is the selection of an appropriate extracting solvent in which colloids partly dissolve.

In **Chapter 5**, we study the self-assembly behavior of a binary colloidal system. We present an example of pH reversible three-dimensional assembly (encapsulation) of oppositely charged spherical colloids with a vast size difference. The reversibility of this encapsulation process is regulated by pH-responsive polyacrylic acid (PAA) present in solution. The PAA plays two essential roles: firstly, its competitive adsorption with the small colloids on the surface of the large colloids determines the encapsulation behavior of the small colloids onto the larger colloids. By tuning the pH, the charge density of the PAA changes, therefore the surface coverage of the large colloids by the smaller colloids changes. For example, the surface coverage increases by decreasing the pH. The second role of the PAA is as a steric barrier limiting the strength of the attractive forces between the oppositely charged colloids species, thereby enabling detachment

of the smaller colloids. Consequently, based on the pH tunability of the encapsulation behavior and the ability of the small colloids to detach, reversible encapsulation is achieved by cycling pH in the presence of the PAA.

# Samenvatting in het Nederlands

De focus van dit proefschrift is gericht op het verkrijgen van een beter inzicht in de zelf-assemblage van colloïdale systemen en het ontwikkelen van nieuwe strategieën om goed-geordende colloïdale superstructuren te vormen. We zijn met name geïnteresseerd in heb gebruik van bolvormige deeltjes met een isotrope vorm en distributie van oppervlakte functionaliteiten als individuele bouwstenen.

Zelf-assemblage is een spontaan proces waarin een niet-geordende verzameling bouwstenen een geordende structuur vormt zonder enige menselijke interventie. Deze processen komen veelvuldig voor in biologische systemen, bijvoorbeeld virus capside eiwitten die assembleren tot complete virus microcapsules. Het besturen en onderzoeken van zelf-assemblage processen levert niet alleen beter begrip op van deze in de natuur voorkomende voorbeelden, maar levert ook nieuwe routes op naar het verkrijgen van functionele materialen met fascinerende superstructuren. Echter, het direct bestuderen van de zelf-assemblage karakteristieken van bijvoorbeeld eiwitten en moleculen, wordt enorm bemoeilijkt door de extreem kleine dimensies en daaraan gerelateerde snelle dynamica van deze bouwstenen. Dit maakt het vrijwel onmogelijk om de structuur-vormende processen direct te volgen met optische of elektronenmicroscopie. Colloïden zijn significant groter dan typische moleculen en worden daarom veelvuldig gebruikt als model bouwstenen voor het bestuderen van de zelf-assemblage van (macro)moleculen.

In China hebben we het volgende gezegde: zelfs een getalenteerde kok kan geen goede maaltijd bereiden zonder de benodigde ingrediënten. Als een experimenteel colloid chemicus die geïnteresseerd is in het beter begrijpen van zelf-assemblerende systemen, de eerste stap die daarom gezet moet worden is het synthetiseren (maken) van de benodigde bouwstenen. In **Hoofdstuk 2** en een gedeelte van **Hoofdstuk 3**,

beschrijven we enkele nieuwe routes om colloïdale model systemen te verkrijgen. In **Hoofdstuk 2**, ontwikkelen we een methode voor het synthetiseren van polystyreen deeltjes met een goed gedefinieerd kuiltje op hun oppervlak. Deze deeltjes zijn enkele micrometers groot en kunnen verkregen worden via een eenvoudige, op dispersie polymerisatie gebaseerde procedure. De belangrijkste stap in het synthese protocol is de gecontroleerde toevoeging van een netwerk-vormende monomeer enige tijd na de start van de dispersie polymerisatie. Het systematisch variëren van de concentratie en de periode waarna het netwerk-vormende monomeer werd toegevoegd maakt het mogelijk om de afmetingen van het gevormde kuiltje te controleren. Daarnaast waren we in staat om de deeltjes van chemische functionaliteiten te voorzien door samen met de netwerk-vormer functionele co-monomeren toe te voegen. Deze strategie leverde deeltjes op met chloride, epoxide of temperatuurgevoelige functionaliteiten. De aanwezigheid van de chemisch reactieve groepen maakt het mogelijk om de oppervlakte eigenschappen van de deeltjes met een kuiltje verder te modificeren met een grote variëteit aan moleculen. Om dit te illustreren, immobiliseren we een fluorescent label met amine functionaliteit op het oppervlak van gechloreerd deeltjes. De intense fluorescente eigenschappen van de resulterende deeltjes bevestigde de reactiviteit en toegankelijkheid van de oppervlakte chloride groepen. **Hoofdstuk 2** wordt afgesloten met het beschrijven van een experimentele methode om de deeltjes met kuiltjes te gebruiken als startpunt voor de synthese van holle sneeuwpop-vormige deeltjes.

In **Hoofdstuk 3**, passen we een variëteit aan methodes toe om de oppervlakte eigenschappen van colloïdale deeltjes te controleren en te beïnvloeden. Een van deze voorbeelden is gebaseerd op Atom Transfer Radical Polymerization (ATRP) reacties en stelt ons in staat om op gecontroleerde wijze hydrofobe polymeren te groeien op oppervlakken van colloïdale deeltjes. Daarnaast kunnen we gebruik maken van de zogenaamde Menschutkin reactie om permanente positieve ladingen te introduceren op initieel negatief geladen deeltjes. De effectieve oppervlaktelading te controleren van deze deeltjes wordt in dit geval bepaald door de verhouding van negatief en positief geladen groepen. Als laatste voorbeeld laten we zien dat we polystyreen colloïden chemisch kunnen etsen met dimethylformamide (DMF) of tetrahydrofuran (THF), resulterend in colloïden met een massief centraal deeltje opgesloten in een holle schil.

Samenvattend, in **Hoofdstuk 2** and een gedeelte van **Hoofdstuk 3** presenteren we een aantal experimentele protocollen om eigenschappen, zoals geometrie (bolvormig,

colloïden met een kuiltje op het oppervlak en sneeuwpop-vormig), oppervlaktelading (positief, negatief en een combinatie van beide), morfologie (gevuld/massief, hol, massief mobiel deeltje in een holle schil), afmeting (400 nm - 5 $\mu$m) en oppervlakte functionaliteit (hydrofoob, hydrofiel, gechloreerd, ge-epoxideerd) van colloïdale systemen te controleren. Controle over deze parameters is cruciaal en bevordert het systematisch bestuderen van colloïdale zelf-assemblage.

In **Hoofdstuk 3 - 5** richten zich op de zelf-assemblage van de eerder genoemde colloïden in één-, twee- en drie-dimensionale aggregaten. De focus ligt hierbij op het gebruik van bolvormige deeltjes met een isotrope vorm en verdeling van oppervlakte functionaliteiten. In **Hoofdstuk 3** laten we zien dat colloïdale deeltjes die vervormbaar zijn, zowel positieve als negative oppervlakte ladingen bezitten en hydrofobe oppervlakte eigenschappen hebben een-dimensionale clusters vormen in waterige media. Om beter inzicht te krijgen in de invloed van deze deeltjes eigenschappen op de formatie van de geobserveerde één-dimensionale aggregaten, een serie colloïdale deeltjes met slechts één of twee van deze eigenschappen werd gesynthetiseerd. Deze referentie colloïden werden vervolgens geassembleerd volgens de zelfde procedure als toegepast voor de deeltje die over alle drie de eigenschappen beschikken. De referentie experimenten lieten overtuigend zien dat de netto lading en een colloïdaal oppervlak met een hydrofoob karakter essentieel zijn voor de formatie van één-dimensionale aggregatie. Vervormbaarheid van de individuele bouwstenen bleek niet vereist te zijn. Op basis van deze experimentele observaties nemen we aan dat de formatie van de één-dimensionale structuren gereguleerd wordt door een samenspel van korte dracht hydrofobe interacties en langere dracht elektrostatische repulsie tussen de individuele deeltjes. Deze hypothese werd vervolgens experimenteel bevestigt door het effect van elektrostatica en hydrofobe attracties op de zelf-assemblage systematisch te onderzoeken.

In **Hoofdstuk 4** beschrijven we een methode voor de vorming van twee-dimensionale collodale kristallen. Deze kristallen bestaan uit slechts een monolaag van deeltjes. Een unieke eigenschap van de gevormde kristallen is dat deze vrij is dispersie kunnen bewegen. De formatie procedure bestaat uit twee essentiële stappen: allereerst maken we aannemelijk dat de verdamping van de continue fase waarin de individuele deeltje gedispergeerd zijn leidt tot de formatie van monolagen van deeltjes aan de wand van de centrifuge buizen; na de formatie gebruik we een ‘extractie’ solvent om

de monolagen los te weken van de wand. De invloed van de dispergerende continue fase, de chemische eigenschappen van de wand waaraan de monolagen vormen, het 'extractie' solvent en de fysisch-chemische eigenschappen van de deeltjes werd vervolgens systematisch onderzocht. Uit deze set van experimenten bleek dat monolagen vormen via de verticale depositie van colloïdale deeltjes. De verdamping van het dispergerende solvent resulteert in de vorming van een meniscus aan het lucht-solvent grensvlak. Deformatie van deze meniscus geeft aanleiding tot attractieve capillaire krachten die de gedispergeerde deeltjes naar de kristallisatie zone drijft. De gevormde kristallijne monolagen konden vervolgens van de wand losgeweekt worden door een 'extractie' solvent toe te voegen waarin de collodale deeltjes gedeeltelijk oplosbaar zijn.

In **Hoofdstuk 5** bestuderen we de zelf-assemblage van een binair colloïdaal systeem. We presenteren de pH-reversibele, drie-dimensionale assemblage van tegengesteld geladen deeltjes. De positief geladen deeltjes zijn significant groter dan de negatieve geladen deeltjes, wat resulteert in superstructuren waarin de grotere, positief geladen deeltjes bedekt zijn met de negatief geladen deeltjes. In de aanwezigheid van moleculair opgelost, vrij poly(acrylzuur) (PAZ) dit assemblage proces bleek reversibel te zijn. De competitieve adsorptie van PAZ en de kleinere negatief geladen deeltjes op het oppervlak van de grotere positief geladen colloïden dicteert het assemblage proces. De ladingsdichtheid van de PAZ polymeren kan gereguleerd met de pH van de dispersie. Omdat PAZ adsorbeert op de positief geladen deeltjes biedt de pH een experimentele knop om de effectieve lading van de positief geladen deeltjes en daarmee de oppervlaktebedekking van de kleinere deeltjes, te controleren. Experimenteel werd aangetoond dat de oppervlaktebedekking toeneemt met afnemende pH. Naast het reguleren van de oppervlakte lading van de positief geladen deeltjes, genereren de geadsorbeerde PAZ polymeren een sterische barrière voor de adsorberende negatief geladen deeltjes. Dit zorgt ervoor dat de elektrostatische attractie tussen de tegengesteld geladen deeltjes beperkt blijft, wat desorptie van de geadsorbeerde deeltjes bevorderd. De experimentele data laat daarom duidelijk zien dat we in staat zijn on grotere positief geladen deeltjes reversible in te kapselen met kleinere negatief geladen deeltjes in de aanwezigheid van PAZ polymeren.

# Acknowledgments

There are many people who have helped me and directly or indirectly contributed to the work described in this thesis. I would like to take this opportunity to express my sincere gratitude to all of them.

First of all I would like to thank my promotor and daily supervisor, Willem Kegel. Willem, thank you for giving me the opportunity to conduct my PhD project with you. I really enjoyed performing research under your supervision, with your endless support and enough freedom. The door of your office was always open for me to have a discussion. Every time I knocked on your door and asked "Hi, Willem, do you have some time, I would like to discuss with you", the answer always was " Yes, of course". Discussions with you have broadened my knowledge in both science and life. Not only your office door, but also your mind is open. When I showed you some unexpected results, you were always excited, encouraged and inspired me to do further research. I am also grateful for your patience while correcting my thesis even though you were tormented by my horrible English. Thank you for everything.

Next, I would like to thank Bas van Ravensteijn. You were involved in most of my projects, you gave me a lot of assistance and also inspired me a lot. Even after you graduated and went to the USA, you still helped me correct my manuscripts and provided fruitful suggestions, and also translated my summary into dutch. Furthermore, it is my pleasure to have shared the lab with you, where our "team rocket" photo still reside.

To make four years of PhD research a success, a good support crew is a necessity. Marina is thanked for taking care of lots of administrative affairs. Thanks to Dominique and Kanvaly for the support in the lab . Also thanks Dominique for giving me a

lot of furniture and Kanvaly for transporting them to my house. Bert is thanked for supporting me to conduct catalysis experiments in his group and Henk and Emma are thanked for teaching me how to conduct the catalysis experiments. Ben is thanked for guiding me in how to supervise second-year bachelor students and for useful discussions. Jan is thanked for fruitful discussions. Bonny is thanked for the nice workshops including DLS, SLS and Zetasizer. Chris and Mark are thanked for teaching me the use of the optical microscopes. Hans and Chris are thanked for the nice TEM introduction and technical support. Stefan is thanked for computer related technical support. And Albert, sorry for breaking your chair, I did not expect that I am so heavy.

Besides being supervised myself, I also had the opportunity to supervise some students. I would like to thank you all for working with me and for the good time we had together: my master student Ellen and my second-year bachelor students, the HEMA group (Harm, Eva, Mark and Alexander), Laurens and Wolfer. An additional thanks to the HEMA group for the nice T-shirt you gave me.

I would like to thank Frans for sharing the lab, the office and also the room during conferences. I like the "cold jokes" you made, especially for the one "I am too tired". Mark, Jasper and Nina are also thanked for sharing the office.

Many thanks to Frans and Fuqiang for being my paranimfen.

I would also like to thank Ping, Chris, Jasper and Samia for the Latex. Without your help, this thesis could not look such nice.

Many thanks to all my other colleagues at FCC for providing the perfect scientific and relaxed atmosphere: Anke, Sonja, Samia, Ping, Laura, Andrei, Albert, Gert-Jan, Remco, Henk, Hans, Chris, Joost, Jos, Pepijn, Alex, Roel, Fuqiang, Faranaaz, Burak, Susanne, Rob, Janne-Mieke, Antara, Alvaro, Ivan, Daniel and all the students.

I would like to thank all of my Chinese friends that I met in the Netherlands. With your company, I felt less homesick: Da Wang, Yang Liu, Yumao Zhang, Meng Li, Xin Yang, Bo Lou, Fang Liu, Feilong Sun, Hongkai Wang, Yuan Ji, Yulong Zhao, Haili Shi, Zenghui Liu, Dingyu Liu, Hao Zhang, Wenjing Lu, Yipu Wei, Zidan Mao, Chen Chen, Chen Chen, Ruixue Yuan, Yang Liu, Tiansong Deng, Haoran Yang, Jinyang Liu and Wang Xuewei.

I also owe special gratitude to my bachelor and master supervisor Prof. Tianying Guo in Nankai University with whom I started my scientific research. The research

experience there motivated me to pursue a PhD.

Lastly and most importantly, I would like to thank my father, mother, brother, sister-inlaw, niece and families in China for endless supports.

Utrecht
July 2017

# List of Publications

**This thesis is based on the following publications**:

• **Yong Guo**, Bas G. P. van Ravensteijn, Chris H. J. Evers, Willem K. Kegel. *pH Reversible Encapsulation of Oppositely Charged Colloids Mediated by Polyelectrolytes.* Langmuir, **2017**, 33 (18): 4551-4558. (Chapter 5)

**Manuscripts in preparation**:

• **Yong Guo**, Bas G. P. van Ravensteijn, Willem K. Kegel. *Cavity size control, surface functionalization and applications of dimple particle.* (Chapter 2)

• **Yong Guo**, Bas G. P. van Ravensteijn, Chris H. J. Evers, Willem K. Kegel. *Self-assembly of one-dimensional aggregates from spherical colloids with hydrophobic attraction and electrostatic repulsion.* (Chapter 3)

• **Yong Guo**, Willem K. Kegel. *Floating Colloidal Crystal Monolayers.* (Chapter 4)

**Other papers by the author**:

• **Yong Guo**, Ruiyu Wang, Wenhao Chi, Shuai Liu, Heguang Shi and Tianying Guo. *One-step synthesis of reactant-product-dual-template imprinted capsules as phosphotriesterase mimetic enzymes for pesticide elimination.* RSC Adv., **2014**, 4, 7881-7884.

• **Yong Guo**, Tian Ying Guo. *A dual-templates imprinted capsule with remarkably enhanced catalytic activity for pesticides degradation and elimination simultaneously.* Chem. Commun., **2013**, 49 (11): 1073-1075.

• **Yong Guo**, Tian Ying Guo. *Application of imprinted polymer in environmental governance.* Polym. Bull., **2013**,1: 113-127. (Review in Chinese)

• Wenhao Chi, Heguang Shi, Wang Shi, **Yong Guo**, Tianying Guo. *4-Nitrophenol surface molecularly imprinted polymers based on multiwalled carbon nanotubes for the elimination of paraoxon pollution*. Journal of Hazard. Mater., **2012**, 227228 (0): 243-249.

• **Yong Guo**, Ying Yang, Lei Zhang, Tian Ying Guo. *Core/shell molecular imprinting microparticles prepared using RAFT technology for degradation of paraoxon*. Macromol. Res., **2011**, 19 (11): 1202-1209.

• **Yong Guo**, Ying Yang, Tian Ying Guo. *Preparation of a PTE simulacrum based on surface molecular imprinting*. Chin. Chem. Lett., **2011**, 22(4): 493-396.

• Kuichang Hua, Lei Zhang, Zhenhui Zhang, **Yong Guo**, Tianying Guo. *Surface hydrophilic modification with a sugar moiety for a uniform-sized polymer molecularly imprinted for phenobarbital in serum*. Acta Biomaterialia, **2011**, 7(8): 30863093.

• Tian Ying Guo, **Yong Guo**, Ying Yang. *A preparation method of surface imprinting polymer for catalyzing degradation of paraoxon*. CN101942062A. **2011**.

# Curriculum Vitae

Yong Guo was born on the $6^{th}$ of April 1987 in Jinhua, Zhejiang Province, China. After graduation from Lanxi No 5 Middle school in 2006, he started studying Chemistry at Nankai University, where he received his bachelor's degree *cum laude* in June 2010. In the same year, he was recommended for the master study at the same university without taking entrance examinations. Under the supervision of Prof. Tianying Guo, he worked on molecular imprinted polymers for pesticide degradation and elimination, and received his master's degree cum laude in June 2013. In September 2013, he started his PhD study at Van 't Hoff Laboratory for Physical and Colloid Chemistry in Utrecht University, the Netherlands, under supervision of Prof. Willem K. Kegel with scholarship from China Scholarship Council (CSC). During his PhD study, he worked on the synthesis of anisotropic colloids and the self-assembly of isotropic colloids. This thesis is the ultimate result of his PhD research. Parts of his work are published in scientific journals and have been presented at national and international conferences, as described in this thesis.